IVAN FRANCISCO DE SOUZA

ASSESSING THE ROLE OF TEXTURE AND MINERALOGY ON ORGANIC MATTER PROTECTION AND CYCLING IN OXISOLS

Tese apresentada à Universidade Federal de Viçosa, como parte das exigências do Programa de Pós-Graduação em Solos e Nutrição de Plantas, para obtenção do título de *Doctor Scientiae*.

VIÇOSA

MINAS GERAIS – BRASIL

2016

Ficha catalográfica preparada pela Biblioteca Central da Universidade Federal de Viçosa - Câmpus Viçosa

T
S719a
2016

Souza, Ivan Francisco de, 1984-
Assessing the role of texture and mineralogy on organic matter protection and cycling in oxisols / Ivan Francisco de Souza. – Viçosa, MG, 2016.
viii, 106f. : il. (algumas color.) ; 29 cm.

Inclui anexo.
Inclui apêndices.
Orientador: Ivo Ribeiro da Silva.
Tese (doutorado) - Universidade Federal de Viçosa.
Inclui bibliografia.

1. Química do solo. 2. Solos - Teor de compostos orgânicos. 3. Latossolo. 4. Carbono. 5. Mineralogia do solo. I. Universidade Federal de Viçosa. Departamento de Solos. Programa de Pós-graduação em Solos e Nutrição de Plantas. II. Título.

CDD 22. ed.

IVAN FRANCISCO DE SOUZA

ASSESSING THE ROLE OF TEXTURE AND MINERALOGY ON ORGANIC MATTER PROTECTION AND CYCLING IN OXISOLS

Tese apresentada à Universidade Federal de Viçosa, como parte das exigências do Programa de Pós-Graduação em Solos e Nutrição de Plantas, para obtenção do título de *Doctor Scientiae*.

APROVADA: 20 de abril de 2016.

Maurício Dutra Costa

João Carlos Ker

Leonardus Vergütz
(Coorientador)

Carlos Alberto Silva

Ivo Ribeiro da Silva
(Orientador)

AGRADECIMENTOS

A toda minha família, especialmente aos meus pais *Luiz* e *Célia*, e meus queridos avós, *José Sérvulo* e *Maria Honorata*.

A *Junia*, pelo amor incondicional e por sua presença tão importante em tantos momentos ao longo destes últimos 4 anos.

Aos professores e funcionários que dedicam suas vidas ao ensino, pesquisa e extensão na *Universidade Federal de Viçosa* e no *Departamento de Solos*, o meu muito obrigado!

Aos professores *Ivo* e *Nairam*, pela oportunidade de trabalhar em seu grupo desde 2006...

Ao prof. *Markus Kleber* pelo incentivo e apoio durante o período do Doutorado Sanduiche na Oregon State University, Oregon, EUA.

Ao *Conselho Nacional de Desenvolvimento Científico e Tecnológico (CNPq)* e à *Coordenação de Aperfeiçoamento de Pessoal de Nível Superior (CAPES)*, pelas bolsas de estudo.

Aos funcionários do DPS: *João Milagres, Humberto, Júlio e Giovani, seu Cardoso, Beto, Poliana, Geraldo Vitor, Zé Luiz*, e especialmente *Luciana Freitas*.

Aos meus queridos colegas do Laboratório de Isótopos Estáveis: *Gabriel, Nanda, Bola, Ricardo, Luisito, Chico Bento, Croc, Baiano, BBT, Ana, Thalles* e *Aline*.

A *Adelina, Rafa, Marcelo, Kleber, Heider, Eduardo, Fernandinho, Luciano* e *Vinicius* pela convivência tão prazerosa.

Aos meus novos amigos de Corvallis, Oregon: *Tom, Stephany, Sharon* e em especial *Trang*, por ajudar a melhorar meu Inglês tão rudimentar, além dos passeios para a coleta de blackberries!

Por último, mas não menos importante, aos meus antigos amigos ainda dos tempos da graduação, que ainda estão em Viçosa ou que retornam eventualmente para dividir comigo bons momentos: *Áian, Tarcísio, Mônica, Bruna, Lívio* e *Adriana*...

Minha vida faz muito mais sentido porque eu conheci cada uma de vocês. Serei eternamente grato pelos momentos que compartilhamos, alguns dos dias mais felizes da minha vida até agora. Muito obrigado!

BIOGRAFIA

Ivan Francisco de Souza, filho de Luiz Donato de Souza e Célia Maria F. Souza, nasceu em Ponte Nova Minas Gerais, em 19 de novembro 1984.

Em março de 2005 mudou-se de Ponte Nova para Viçosa para cursar Agronomia pela Universidade Federal de Viçosa (UFV). Concluiu a graduação em dezembro de 2009 e em março do ano seguinte iniciou o Mestrado em Solos e Nutrição de Plantas, pela UFV. Em fevereiro de 2012 concluiu o Mestrado, e em março deste mesmo ano iniciou o Doutorado em Solos e Nutrição de Plantas, também pela UFV. Entre janeiro e dezembro de 2015, cursou o Doutorado Sanduíche pela Oregon State University.

Concluiu o Doutorado em Solos e Nutrição de Plantas em 20 de abril de 2016.

SUMÁRIO

RESUMO

SOUZA, Ivan Francisco de, D.Sc., Universidade Federal de Viçosa, abril de 2016. **Assessing the role of texture and mineralogy on organic matter protection and cycling in Oxisols.** Orientador: Ivo Ribeiro da Silva. Coorientadores: Emanuelle M. B. Soares, Raphael B. A. Fernandes e Leonardus Vergütz.

Em escala global, os estoques de carbono orgânico do solo (COS) preservados na forma de matéria orgânica (MOS), representam valores superiores à soma de todo o C presente na forma de CO_2 na atmosfera e na vegetação. Portanto, em um cenário de aumentos dos níveis de CO_2 atmosférico e seus possíveis efeitos na temperatura média global, o entendimento dos fatores que regulam os estoques de COS se faz essencial. Apesar do grande número de fatores que regulam os estoques da MOS no solo, promover o sequestro de C tem sido considerado fator chave para a mitigação dos níveis de CO_2 atmosférico. Por outro lado, os solos também podem contribuir para elevar ainda mais os níveis de CO_2 atmosférico, caso ocorra aumento significativo nas taxas de decomposição da MOS em resposta ao aumento da temperatura média global (feedback positivo). Até então, a comunidade científica não tem respostas completas para estas questões fundamentais. Apesar disso, importantes avanços conceituais e tecnológicos nos últimos 20 anos, contribuíram de modo significativo para o entendimento da dinâmica da MOS. Consequentemente, ao invés de assumir que a MOS pode resistir a decomposição apenas por sua composição química, existem indícios significativos que mecanismos físicos e químicos que operam na interface mineral-orgânica, exerce papel fundamental na persistência de compostos orgânicos em solos. Além disso, estes mecanismos podem ser considerados solo-específicos e por isso, nosso estudo foi baseado na investigação destes processos em Latossolos. Estes solos predominam em ecossistemas tropicais e sua mineralogia é dominada por argilas de baixa atividade. Os objetivos específicos deste trabalho foram (i) inferir a capacidade para o acumulo de COS em função da textura e saturação por C (i.e. redução da eficiência de conversão de litter-C em MOS associada aos minerais da fração <53 µm, com o aumento das doses de C aplicadas); (ii) inferir a influência dos minerais na fração <53 µm na

formação e persistência da MOS associada aos minerais em Latossolos. Neste estudo, avaliou-se a incorporação de C e N fração <53 µm em adicionados via litter de plantas de eucalipto duplamente marcadas com os isótopos estáveis ^{13}C e ^{15}N, em experimento de incubação conduzidos por 12 meses. No capitulo 1, avaliou-se a incorporação do ^{13}C na fração <53 µm em função da textura e saturação por C. Nesta etapa do trabalho, ficou demonstrado o efeito da textura na capacidade de acúmulo de C e a saturação por C da fração <53 µm. Além disso, a textura do solo afeta os mecanismos de proteção da MOS, com possível aumento da proteção física de compostos em função da agregação de partículas com o aumento do teor da fração <53 µm. No segundo capitulo, avaliou-se a incorporação dos isótopos (^{13}C e ^{15}N) em função da mineralogia da fração <53 µm. Nesta etapa, demonstrou-se que os óxi-hidróxidos de Al e Fe de baixa cristalinidade são os principais componentes da matriz mineral envolvidos na formação de associações organo-mineral em Latossolos. Devido à baixa concentração dos óxi-hidróxidos de Al e Fe de baixa cristalinidade na fração <53 µm e sua importância para proteção da MOS, sugere que os estoques de C nestas regiões podem ser muito sensíveis a alterações ambientais. Portanto, pesquisas adicionais são necessárias para avaliar a ocorrência destas associações organo-mineral em solos tropicais, bem como sua sensibilidade frente a mudanças climáticas e possíveis impactos na taxa de ciclagem da MOS em Latossolos. No terceiro capítulo, utilizou-se scanning transmission eléctron microscopy (STEM) para a avaliar a composição elementar das associações organo-mineral em um Latossolo húmico. Neste estudo, demonstrou-se boa correlação espacial entre a MOS e os óxi-hidróxidos de Al e Fe. Além disso, ao se submeter amostras da fração <53 µm ao tratamento térmico, observou-se que as reações de desidroxilação dos óxi-hidróxidos de Al e Fe foi acompanhada de reações de oxidação da MOS. Estes dados corroboram os dados da distribuição espacial da MOS e confirma existência de associações entre os óxi-hidróxidos de Al e Fe e compostos orgânicos em Latossolos. Portanto, estes trabalhos contribuem para melhorar o atual entendimento acerca dos fatores que controlam a formação e persistência de associações organo-mineral em Latossolos.

ABSTRACT

SOUZA, Ivan Francisco de, D.Sc., Universidade Federal de Viçosa, April, 2016. **Assessing the role of texture and mineralogy on organic matter protection and cycling in Oxisols.** Adviser: Ivo Ribeiro da Silva. Co-advisers: Emanuelle M. B. Soares, Raphael B. A. Fernandes and Leonardus Vergütz.

Worldwide, the soil organic carbon (SOC) stock accounts for more C in the form of organic matter (SOM) than the total C in the atmosphere and in the biomass combined. Therefore, in a context of increasing levels of atmospheric CO_2 and its possible impacts on the average global temperature, understanding the factors controlling SOC stocks is key. Despite the large number of factors regulating SOM stocks, managing soil C sequestration is thought to be critical for offsetting the excess of atmospheric CO_2. Otherwise, soils also could further contribute to increase the concentration of CO_2 in the atmosphere if faster decomposition rates of SOM is to become an important climate feedback. Up to now, the scientific community has not complete answers for these questions. However, important conceptual and technological developments over the last 20 years have boosted our understanding on SOM dynamics. As a result, rather than relying on intrinsic resistance of SOM against decomposers, it seems that physical occlusion and chemical reactions within the mineral matrix play a much more significant role on the persistence of reduced C in soils. In addition, these mechanisms can be soil-specific and as such, we addressed the occurrence of these processes in Oxisols. These are the predominant soils in tropical ecosystems and are dominated by low-activity clays. The specific objectives of this research were to infer (i) the capacity for SOC storage as a function of soil texture and C-saturation (i.e. lower conversion efficiency of plant litter-C into mineral-organic associations with increasing C additions; (ii) infer the influence of reactive minerals within the clay+silt fraction of Oxisols on the formation and persistence of mineral-organic associations in these soils. We assessed the incorporation of a labeled plant litter (containing ^{13}C and ^{15}N) into mineral-organic associations in Oxisols by performing incubation experiments conducted throughout 12 months. In the first chapter, we

address the incorporation of the ^{13}C label into mineral-organic associations as related to soil texture and C-saturation. In this chapter, we deomontrate that soil texture has a strong influence on the capacity for SOC storage and the C-saturation of the fraction <53 μm. Additionally, we observed evidence of higher the contribution of physical protection of SOM within microaggregates pore-space area, with increasing content of the fine fraction. In the second chapter, we address the incorporation of the labeled plant litter (^{13}C and ^{15}N) into mineral-organic associations as affected by the mineralogy of the mineral matrix. In this chapter, we demonstrate that amorphous Al-/Fe-(hydr)oxides are the main components within the fine fraction of Oxisols involved in the formation and the persistence of SOM. Given the relatively low concentration of amorphous Al-/Fe-(hydr)oxides within the fine fraction and their contribution for the protection of SOM, suggests that SOC stocks in the tropics could be very sensitive to environmental changes. Therefore, further research on this subject would evaluate the composition of mineral-organic associations in tropical soils. This would help to predict the possible impacts of climate change on SOM cycling in tropical ecosystems. In the third chapter, we used scanning transmission electron microscopy (STEM) and thermal analysis to probe the chemical composition of mineral-organic associations in a C-rich Oxisol (not included in the incubation experiment). In this chapter, we used elemental mapping to demonstrate that SOM is closely associated to Al-/Fe-(hydr)oxides. Furthermore, we submitted the sample to thermal analysis to relate mineral dehydroxylation to the oxidation of SOM. Indeed, we observed strong oxidation reactions to overlap with dehydroxylation of gibbsite, short-range order Al species and goethite. Our results contribute to improve the current understanding on the minerals and the mechanisms by which these components interact and ultimately protect SOM against decomposition in Oxisols.

INTRODUCTION

Over the last 15 years, several conceptual and technological advances have contributed significantly to improve the characterization of soil organic matter (SOM) and the implications for C storage and cycling in terrestrial ecosystems (Lehmann and Kleber, 2015). Since the soil C pool surpasses the total amount of C in the atmosphere and in the vegetation combined (Ciais et al., 2013), SOM dynamics may affect the size of the other compartments, either by sequestering C or by increasing the release of CO_2 to the atmosphere. The prospect of faster decomposition rates of SOM is critical because this C pool is thought to be sensitive to higher temperatures (Heimann and Reichstein, 2008). As a result, faster decomposition rates of SOM could contribute to increase the emissions of CO_2 from soils, that is, a positive climate feedback (Heimann and Reichstein, 2008; Schmidt et al., 2011). For this reason, there is ongoing debate on the mechanisms controlling the potential and limitations for SOM storage and C dynamics in soils (Schmidt et al., 2011).

Managing soil C sequestration is intrinsically complex because it involves many environmental factors including physical processes, chemical reactions, and necessarily biological activity both autotrophs and heterotrophs. Invariably, the C content stored as SOM in a given ecosystem would include interactions among all of these factors (Schmidt et al., 2011). Generally, the C cycle can be affected by nutrient cycling (e.g., P and N) and it is also intimately related to the hydrological cycle and temperature (Feng et al., 2015b; Wieder et al., 2015), which add substantial challenges for understanding the dynamics of the soil C pool. Consequently, the research on C cycling and storage in terrestrial ecosystems has been directed particularly to (i) quantifying the potential and limitations for soil organic carbon (SOC) sequestration; (ii) linking plant litter decomposition to the formation of mineral-organic associations; (iii) connecting the formation of protective associations between the mineral matrix and SOM and therefore, its impact on soil C sequestration in the long-term.

Limitations and potential for promoting SOC sequestration has been associated to the amount of the clay and silt-sized particles in soils (Hassink, 1996; Six et al., 2002a). Additionally, these authors proposed that the degree of "C-saturation" of the clay+silt fraction has important implications for promoting soil C sequestration. These propositions are based on the premise that protective mechanisms operate mostly within the clay+silt fraction (Six et al., 2002a). Once the reactive sites within the mineral matrix reach their C-saturation level, further addition of organic matter would not cause a proportional increment within the SOC content associated to the clay+silt fraction (Castellano et al., 2015). In this context, the parameterization of the potential for SOM protection and its degree of C-saturation should be among the main factors to determine the extent by the strategies aiming at promoting SOC sequestration will succeed.

Another important aspect concerning SOC sequestration is the relative complexity to link plant litter decomposition to the formation of mineral-organic associations. It has been increasingly recognized that soil microbial biomass acts as a bottleneck in the conversion of plant litter into these mineral-organic associations (Miltner et al., 2012; Hatton et al., 2012; Bradford et al., 2013; Cotrufo et al., 2015). The main implication of such reasoning is that biotic conversion of the plant material into mineral-organic associations should be much more relevant than abiotic processes in terrestrial ecosystems (Cotrufo et al., 2015). Therefore, the type of association (physical and/or chemical interactions) developed between the microbial-processed residues and the mineral matrix would have a huge impact on the persistence of SOM in the ecosystem (Dungait et al., 2012). This is mainly because the microbial residues would include relatively labile organic compounds, rather than intrinsically recalcitrant organic material (Kleber et al., 2011).

The preservation of labile organic compounds as the main constituents of SOC however, would depend mainly on the reactivity of the components within the mineral matrix (Baldock and Skjemstad, 2000). For this reason, restricting the decomposition and consequently

allowing the accumulation of labile organic compounds as SOC, would depend upon the mineral matrix acting as a barrier separating the potential substrate from the decomposers (Dungait et al., 2012). Because of the inherent complex nature of soils, physical and chemical mechanisms often overlap, which limits quantitative inference on the contribution of each of these interactions for SOC storage. Despite some limitation for inferring on these mechanisms separately, identifying the structures responsible for SOC preservation is critical for two main reasons: First, quantitative assessment on these factors is essential for modeling SOM storage and cycling in terrestrial ecosystems. Second, identifying the drivers of SOM persistence is also important because these components also may be sensitive to environmental changes (Doetterl et al., 2015). Such considerations indicate that the development of mineral-organic associations should be soil-specific, and could be affected by local conditions (e.g., land-use change) and/or by long-term environmental changes (e.g., positive feedbacks to global warming).

In this research, we address the potential and limitations for SOC storage and link plant litter decomposition to the development of mineral-organic associations in Oxisols. The main reasons stressing the needs for such research in these soils are (i) In tropical regions, approximately 25-30% of the land surface is dominated by Oxisols, which can occur as clayey, medium and even coarse-textured soils. This would limit the size of the clay+silt fraction in coarse-textured soils and could probably affect their capacity for SOC storage; (ii) these soils are highly weathered, implying the existence of low-activity clays such as kaolinite, gibbsite (the most common crystalline Al-(hydr)oxide in Oxisols), Fe-(hydr)oxides, mainly in the form of goethite and hematite, and also amorphous Al-/Fe-(hydr)oxides; (iii) most of the reactive surfaces that could interact with SOM in these soils would be provided by amorphous Al-/Fe-(hydr)oxides, a small fraction of the whole clay+silt fraction; (iv) despite the predominance of low-activity clays in tropical regions, soils in these areas account for more than 25% of the global SOC stock, and (v) given the general low fertility of Oxisols, SOM plays a central role on nutrient cycling in tropical ecosystems.

We assessed the incorporation of a labeled plant litter (containing ^{13}C and ^{15}N) into mineral-organic associations in Oxisols by performing incubation experiments conducted throughout 12 months. In the first chapter, we address the incorporation of the ^{13}C label into mineral-organic associations as related to soil texture and C-saturation (i.e., reduced conversion efficiency of plant litter into mineral-organic associations with with increasing C inputs). We tested the hypotheses that the capacity of soils to promote C sequestration is limited by the amount of the fraction <53 µm, while the overall increment within the protected C pool depends on the degree of C-saturation of clay+silt fraction. The specific objectives were to assess the extent by which mineral protection to SOC and C-saturation are affected by texture.

In the second chapter, we address the incorporation of the labeled plant litter (^{13}C and ^{15}N) into mineral-organic associations as affected by the mineralogy of the mineral matrix. We tested the hypothesis that litter-derived C forms preferential associations with Al- and Fe-(hydr)oxides, particularly with the amorphous types. The objectives were to compare the transference of both C and N into the fraction <53 µm, infer the influence of microbial activity on the process and identify the components within the mineral matrix involved in the formation of mineral-organic associations throughout the incubation experiment.

In the third chapter, we used scanning transmission electron microscopy (STEM) and thermal analysis to probe the chemical composition of mineral-organic associations in a C-rich Oxisol (not included in the incubation experiment). We expected SOM spatial distribution to be better correlated with Al- and Fe-(hydr)oxides than with kaolinite, the predominant phyllosilicate in Oxisols. We also tested the hypothesis that SOM oxidation would overlap with dehydroxylation reactions of Al- and Fe-(hydr)oxides under thermal treatment. The specific objective of this research was to infer the mechanisms by which SOM interacts with the mineral matrix in Oxisols.

References

Baldock, J.A., and J.O. Skjemstad. 2000. Role of the soil matrix and

minerals in protecting natural organic materials against biological attack. Org. Geochem. 31(7-8): 697–710.

Bradford, M.A., A.D. Keiser, C.A. Davies, C.A. Mersmann, and M.S. Strickland. 2013. Empirical evidence that soil carbon formation from plant inputs is positively related to microbial growth. Biogeochemistry 113(1-3): 271–281.

Castellano, M.J., K.E. Mueller, D.C. Olk, J.E. Sawyer, and J. Six. 2015. Integrating plant litter quality, soil organic matter stabilization, and the carbon saturation concept. Glob. Chang. Biol. 21(9): 3200–3209.

Ciais, P., C. Sabine, G. Bala, L. Bopp, V. Brovkin, J. Canadell, A. Chhabra, R. DeFries, J. Galloway, M. Heimann, C. Jones, C. Le Quéré, R.B. Myneni, S. Piao, P. Thornton, P.C. France, J. Willem, P. Friedlingstein, and G. Munhoven. 2013. Carbon and other biogeochemical cycles. Clim. Chang. 2013 - Phys. Sci. Basis: 465–570.

Cotrufo, M.F., J.L. Soong, A.J. Horton, E.E. Campbell, M.L. Haddix, D.H. Wall, and W.J. Parton. 2015. Formation of soil organic matter via biochemical and physical pathways of litter mass loss. Nat. Geosci. 8(10): 776–779.

Doetterl, S., A. Stevens, J. Six, R. Merckx, K. Van Oost, M. Casanova Pinto, A. Casanova-Katny, C. Muñoz, M. Boudin, E. Zagal Venegas, and P. Boeckx. 2015. Soil carbon storage controlled by interactions between geochemistry and climate. Nat. Geosci. 8(10): 780-783.

Dungait, J.A.J., D.W. Hopkins, A.S. Gregory, and A.P. Whitmore. 2012. Soil organic matter turnover is governed by accessibility not recalcitrance. Glob. Chang. Biol. 18(6): 1781–1796.

Feng, Z., T. Rütting, H. Pleijel, G. Wallin, P.B. Reich, C.I. Kammann, P.C.D. Newton, K. Kobayashi, Y. Luo, and J. Uddling. 2015. Constraints to nitrogen acquisition of terrestrial plants under elevated CO_2. Glob. Chang. Biol.: 21(8): 3152-3168.

Hassink, J. 1996. Preservation of plant residues in soils differing in unsaturated protective capacity. Soil Sci. Soc. Am. J. 60(2): 487–

491.

Hatton, P., M. Kleber, B. Zeller, C. Moni, A.F. Plante, K. Townsend, L. Gelhaye, K. Lajtha, and D. Derrien. 2012. Transfer of litter-derived N to soil mineral–organic associations: Evidence from decadal 15N tracer experiments. Org. Geochem. 42(12): 1489–1501.

Heimann, M., and M. Reichstein. 2008. Terrestrial ecosystem carbon dynamics and climate feedbacks. Nature 451(7176): 289–292.

Kleber, M., P.S. Nico, A. Plante, T. Filley, M. Kramer, C. Swanston, and P. Sollins. 2011. Old and stable soil organic matter is not necessarily chemically recalcitrant: Implications for modeling concepts and temperature sensitivity. Glob. Chang. Biol. 17(2): 1097–1107.

Lehmann, J., and M. Kleber. 2015. The contentious nature of soil organic matter. Nature 528(7580): 60–68.

Miltner, A., P. Bombach, B. Schmidt-Brücken, and M. Kästner. 2012. SOM genesis: Microbial biomass as a significant source. Biogeochemistry 111(1-3): 41–55.

Schmidt, M.W.I., M.S. Torn, S. Abiven, T. Dittmar, G. Guggenberger, I.A. Janssens, M. Kleber, I. Kögel-Knabner, J. Lehmann, D.A.C. Manning, P. Nannipieri, D.P. Rasse, S. Weiner, and S.E. Trumbore. 2011. Persistence of soil organic matter as an ecosystem property. Nature 478(7367): 49–56.

Six, J., R. Conant, E. Paul, and K. Paustian. 2002. Stabilization mechanisms of soil organic matter: implications for C-saturation of soils. Plant Soil 241: 155–176.

Wieder, W.R., C.C. Cleveland, W.K. Smith, and K. Todd-Brown. 2015. Future productivity and carbon storage limited by terrestrial nutrient availability. Nat. Geosci. 8(6): 441-444.

Organic matter storage and Carbon-saturation as related to texture in Oxisols – evidence from long-term incubation experiments (chapter one)

1. Abstract

Rationale: Soil organic carbon (SOC) storage and C-saturation are presumably restrained by texture, although the mechanisms underlying such patterns are unknown. ***Objectives***: The objectives of this research were to assess SOC storage and the mechanisms underlying C-saturation in Oxisols. ***Methods***: We performed a long-term incubation experiment, including C inputs at 0, 4.5, 9.0 and 18.0 mg g^{-1} soil to samples of six Brazilian Oxisols, collected at 0-10, 10-20, 20-40 and 60-100 cm in areas under native vegetation. The difference between their original SOC content and that estimated as a function of their clay+silt content, was set as the C-saturation deficits. We assessed the effect of texture on C-saturation by diluting the mass of clay+silt at 0, 20, 40 and 80% by adding fine sand to the fine earth fraction. ***Results***: After the incubation, the litter-C within the fraction <53 µm increased exponentially with C-saturation deficits, with low increments in the mineral-associated SOC content in fine-textured soils. Otherwise, the conversion of litter-C into the clay+silt fraction, increased asymptotically with C additions, irrespective of texture. ***Conclusions***: In fine-textured Oxisols, C-saturation of microaggregates-associated pore space network seems predominant. Otherwise, in coarse-textured Oxisols, C-saturation of isolated or less aggregated silt- and clay-sized particles seems the prevalent mechanism.

2. Introduction

Carbon sequestration in soils has been regarded as a key strategy to help counteract the rising atmospheric CO_2 by increasing SOC stocks (Paustian et al., 2000; Lal, 2004). However, increasing the C content in soil is rather difficult to accomplish because the SOC pool is determined by interactions among many environmental factors and physical, chemical and biological processes (Schmidt et al., 2011). Consequently, management practices that are supposed to promote soil C sequestration (e.g., no-tillage) do not always increase the SOC stock (Luo et al., 2010). Contemporarily, there is growing awareness of a limited capacity of soils to protect organic matter against decomposition (Six et al., 2002a; Stewart et al., 2007; Powlson et al., 2011). Such protected C pool is typically parameterized as the SOC associated to minerals exhibiting particle-size <53 µm (Castellano et al., 2015), further referred to in this text as the "fine fraction". Presumably, the potential for increasing the SOC within the protected pool is mainly affected by how far a given soil is from reaching its C-saturation level (CSL) (Hassink, 1996). Therefore, the CSL is defined as the point where an increase in C inputs does no longer lead to a proportional increment in the mineral-associated SOC at steady-state, i.e. the system has reached equilibrium with respect to C input and output from the soil (Castellano et al., 2015).

In terrestrial ecosystems, C enters in the soil as plant litter, both above or belowground (Cotrufo et al., 2013). As as the decomposition progresses, the plant litter is fragmented and incorporated into the particle-size fraction smaller than 2 mm, which is referred to as particulate organic matter (POM) (Castellano et al., 2015). Furthermore, as the microbial biomass assimilates the decomposing plant material, part of the microbial-resynthesized compounds can form associations with reactive components within the mineral matrix (Cotrufo et al., 2013). It is widely accepted that the fine fraction includes the soil components most important for the protection of SOC against microbial decomposition (Kögel-Knabner et al., 2008; Mikutta and Kaiser, 2011; Cotrufo et al., 2013). This is because relative to larger particle-size fractions, the fine particles exhibit comparatively larger specific surface

area and greater surface charge density, both of which promote the formation of protective mineral-organic associations (Kleber et al., 2015). Therefore, since mineral-organic associations would ultimately depend upon interactions among organic compounds with silt- and clay-sized minerals, the total amount of these particles has been used to estimate the CSL (Hassink, 1997; Six et al., 2002a). Consequently, estimating the CSL would allow the calculation of the C-saturation deficit (CSD), which has been suggested as a quantitative assessment of the potential for further increasing SOC stocks (Hassink, 1996).

CSL estimates based to the content of fine particles are build on the premise that the amount of silt- and clay-sized fractions would account for both chemical and physical mechanisms that allow mineral-associated organic matter to persist in soils (Baldock and Skjemstad, 2000). According to Stewart et al. (2007) the magnitude of the increment on the protected SOC content in response to C inputs is directly proportional to the CSD. Hence, in soils with high CSD, its protected SOC content should increase steeply with respect to C additions. Presumably, after the fine fraction and the aggregates pore-space network reaching their specific CSL, further additions of organic matter would cause a large amount of C to accumulate within unprotected pools (Castellano et al., 2015). Therefore, in soils where SOC protection can be assumed to be dominated by interactions with the mineral matrix (i.e. adsorption and aggregation), the protected C pool can be mathematically expressed as an asymptote that rises towards a maximum of SOC content in response to C inputs (Six et al., 2002a; Stewart et al., 2007; Castellano et al., 2015). Despite the mechanisms leading to the formation of protective mineral-organic associations being reasonably well-understood, there remains considerable uncertainty with respect to soil carbon-saturation and its occurrence in different ecosystems worldwide (West and Six, 2007).

Carbon-saturation seems to be soil-specific and should vary with physical and chemical properties of the mineral matrix (Stewart et al., 2007; Castellano et al., 2015). However, the majority of the research on C-saturation has been conducted in temperate zones (Kong et al., 2005;

West and Six, 2007; Chung et al., 2008; Stewart et al., 2008, 2009). This is relevant because in the tropics, the soils present some specific features remarkably different from those occurring in temperate regions. For instance, the predominant soils in tropical regions are Oxisols (Lal, 2004), in which the minerals within the fine fraction are strongly aggregated, giving rise to a specific microstrucure (Beinroth, 1982; Schaefer, 2001; Schaefer et al., 2004; Buol, 2009). In addition, the mineralogy of Oxisols is mainly composed by kaolinite, a non-expansive phyllosilicate (Schaefer et al., 2008). The fine fraction in these soils also have variable amounts of gibbsite, which is the most stable Al-(hydr)oxide), and also Fe-(hydr)oxides, mainly in the form of goethite and hematite (Schaefer et al., 2008). Moreover, Oxisols can occur in a range of textures and as such, the amount of the fine fraction varies substantially (Schaefer et al., 2004). However, it is not yet known to what extent the strong microaggregation of the fine fraction and the variable texture can exert on SOC storage and C-saturation in Oxisols.

We tested the hypothesis that the mechanisms underlying C-saturation in Oxisols vary as a function of their texture. Thus, C-saturation would be caused by the clogging of microaggregates pore-space area by SOC as the clay+silt content increases. Otherwise, in coarse-textured soils, C-saturation would be a function of limited availability of mineral surfaces to interact with SOC. To test our hypothesis, sampled six representative Oxisols with contrasting natural textures, which were further modified by diluting the mass of their fine fraction through the addition fine sand to the samples to the fine earth fraction. Because we collected samples at different depths, this would provide an increasing CSD from the topsoil towards de bottom layers. Accordingly, we used a ^{13}C-labeled plant litter to track down its incorporation into the fine fraction by performing a relatively long-term incubation experiment (12 months). The objectives of this research were to assess SOC storage capacity and the mechanisms underlying C-saturation by measuring the increment on the C content within the fine fraction as a function of texture, and infer the conversion of plant litter into mineral-organic associations in Oxisols.

3. Material and methods

3.1. Soils collection

Briefly, the soils were collected in a transect ranging from 40 to 51° W and 18 to 20° S, but despite being relatively close to each other, these are very representative Oxisols, particularly in terms of texture. The selected Oxisols were either under native vegetation on forests remnants of the Mata Atlântica (Atlantic Rainforest) or in the Cerrado (savanna-like) biomes. The Typic Hapludox (THD), the Humic Hapludox (HHD) and Xanthic Hapludox (XHD) were collected within the Atlantic Rainforest biome, while the Xanthic Haplustox (XHT), the Rhodic Haplustox (RHT) and the Typic Haplustox (THT) were collected within the Cerrado. Further details on the vegetation traits and overall distribution of both biomes on the Brazilian territory can be found elsewhere (Ratter et al. 1997; Morellato et al. 2000). According to the Koppen classification, the climate within the Atlantic Rainforest is predominantly Aw, tropical with dry winter and within the Cerrado is predominantly Cwa, temperate moist with dry winter and warm summer (Alvares et al. 2013). The annual precipitation is practically the same for both climate types, ranging from 1300 to 1600 mm per year (Alvares et al., 2013), although the rain season for the area under the Cwa climate type is mostly concentrated in the period from October to March. The sampling consisted on collecting the soil material at different depths (0-10, 10-20, 20-40, and 60-100 cm) and after collection, the samples were kept on plastic bags and transported to the laboratory.

3.2. Physical analyses

The samples were air-dried and sieved to pass a 2-mm screen to yield the fine earth fraction. The water holding capacity (WHC) of the soils was estimated by saturating 20 g of the fine earth fraction with deionized water into a 25.4 mm diameter steel ring and submitted to a tension equivalent to -30 kPa. After reaching equilibrium, the samples were weighted before and after being dried at 105 °C for 48 hours.

The texture analysis was preceded by chemical dispersion 5 g of the fine earth fraction using 5 mL of sodium hydroxide (NaOH) 0.1 mol

L^{-1} and 25 mL of deionized water into a 50 mL centrifuge tube under continuous stirring for 16 hours at 120 rpm. After dispersion, the samples were wet-sieved through a 53-µm mesh screen in to separate de sand- from the silt- and clay-sized fractions. The fraction <53 µm was used for quantifying clay and silt content by using the pipette method and by applying the Stoke's Law. The mass of the fractions obtained were dried at 105 °C during 48 hours and weighted.

3.3. ^{13}C isotope labeling

Briefly, the plant material used as the source of C for our incubation experiment was produced by growing eucalypt hybrid seedlings (*Eucalyptus urophylla* x *Eucalyptus grandis*) under controlled conditions. As such, three seedlings (120-days old) were grown into a 10 L vase on a nutrient solution (pH 5.5) for 18 weeks with continuous oxygen supply. For the isotope labeling, the seedlings were kept into a 448 dm^3 chamber in which the ^{13}C added by acidifying $Na_2{}^{13}CO_3$ (^{13}C at 99 atom%, Isotec Inc. Miamisburg, Ohio) with H_2SO_4. The $^{13}CO_2$ was added into the chamber by preparing a $Na_2{}^{13}CO_3$ solution at 0.18 mol L^{-1} that was mixed with 50 mL of H_2SO_4 3.8 mol L^{-1}. The CO_2 concentration within the chamber was kept at 500 mg dm^{-3} throughout the labeling experiment, which was repeated 3 three times a week. At the end of the isotope labeling, the seedlings were collected and separated into leaves, twigs, stem and roots (predominantly fine roots, diameter <2 mm), and dried under forced air circulation at 45 °C until constant weight. After drying, the plant material was milled on a Wiley mill in order to achieve a particle-size <500 µm. For further homogenization (prior to the chemical analysis), the milled plant material was finely ground using a ball-mill after which the final particle-size achieved was <149 µm. The samples were analyzed using an Isotopic Ratio Mass Spectrometer (IRMS) with continuous flux (20-20, ANCA-GLS, Sercon, Crewe, UK). The C and N content, and their respective stable isotope abundance ($\delta^{13}C$) for each of the components (leaves, twigs, stem and roots) are shown in Table 1.

Table 1. Components of the plant litter, their C and N content, and their respective stable isotopes concentration

Component	Mass, g[†]	C, g kg^{-1}	δ^{13}C, ‰
Bark	21.9	425.0	318.6
Leaves	135.9	455.0	508.5
Twiggs	40.5	427.0	423.1
Stem	52.3	452.0	210.4
Roots	58.5	457.0	358.4
Corrected mean[‡]	-	**449.0**	**405.5**

[†]Dry matter of each component produced in grams per plant. The plant litter was added to the soils as a mixture, for which the amount of each component was proportional to their content on the plant grown for the ^{13}C labeling.

3.4. Incubation experiment

The incubation was carried out during 12 months under controlled conditions with temperature kept fixed at 25 ± 1 °C. The experimental units consisted on air tight vials (150 mL) containing 20 grams of the fine earth fraction (<2mm). The moisture content of the samples was kept at approximately 60-70% of the WHC of each soil. The plant litter additions rates were 0, 10, 20, and 40 mg g^{-1} soil, which were equivalent to C additions at 0, 4.5, 9, and 18 mg g^{-1} soil, respectively. For each treatment, we had 3 replicates. The characterization of each component of plant litter is shown in Table 1. However, for the incubation experiment, the litter-C was added to the soils in a mixture that contained each component in the exact proportion they occurred on the ^{13}C-labeled plants, from which they derived.

During the first 4 weeks the vials were opened 3 times a week during 1 hour to avoid O_2 limitation for the decomposers. After the first month, the vials were opened only once a week and the weight of the experimental units were monitored to avoid water limitation. The moisture content was controlled by weighting each experimental unit after every 2 weeks and compared to the total weight measured at the first day of the incubation. When necessary, deionized water was added using a pipette in to assure the moisture content was kept between 60 and 70% of the WHC.

We modified the natural texture of the soils by adding fine sand (150 to 250 µm-size) to dilute the clay- and silt-sized fractions by 0, 20,

40 and 80%, thus yielding 4 textures for each Oxisol (Table 2). For example, to dilute the clay- and silt-sized fractions by 20%, we used 16.0 g of soil (fine earth fraction) mixed to 4.0 g of fine sand and so forth. This procedure was repeated systematically for all Oxisols, irrespective of their original texture, given that the objective of the experiment was not to produce soils presenting the same amount of clay+silt after their dilution. Given that we added fine sand to the fine earth to dilute the mass of the clay+silt fraction, we based our results/discussion on the variation of the SOC associated to this fraction after the incubation. Accordingly, when the C associated to the clay+silt fraction was expressed relative to fine earth fraction mass (whole soil), we proceeded as follows:

$$\text{SOC, g kg}^{-1}\text{ soil} = C_{(C+S)} * M_{(C+S)} \div M_{FEF}$$

where $C_{(C+S)}$ is the C content within the fine fraction, g C kg^{-1} clay+silt; $M_{(C+S)}$ is the mass of the clay+silt fraction, g; and M_{FEF} is the mass of the fine earth fraction, which was set at 20 grams. Irrespective of the dilution, the final mass of the samples incubated was 20 grams.

We justify the dilution because had we collected soils with different natural textures, we would no longer keep the mineralogy or the C content within the fraction <53 µm, as its mass varied. Thus, by diluting the silt- and clay-sized fractions we would avoid potential confounding effects due to either direct or indirect effects of texture on SOC (Parton et al., 1987; Oades, 1988; Baldock and Skjemstad, 2000). The dataset describing the dilution of the fine fraction is presented in Table 2).

Table 2. Oxisols texture (sand, silt and clay content), extractable Al and Fe by ammonium oxalate (AO) and dithionite-citrate-bicarbonate (DC) and kaolinite and gibbsite content within the clay fraction

Oxisol	Depth	Sand	Silt	Clay	Al_{AO}†	Fe_{AO}†	Al_{DC}†	Fe_{DC}†	Kaolinite‡	Gibbsite‡	Texture Class
	cm	g kg^{-1} soil									
Typic Hapludox-THD	0-10	363.8	33.1	603.2	0.8	0.7	12.2	49.1	439.5	32.1	Clay
	10-20	289.8	33.7	676.7	0.9	0.9	15.1	54.3	493.1	36.1	Clay
	20-40	249.3	31.6	719.2	1.0	0.8	13.2	54.8	524.1	38.3	Clay
	60-100	234.4	31.1	734.6	1.1	0.5	14.0	56.9	535.2	39.1	Clay
Humic Hapludox-HHD	0-10	324.9	78.4	596.8	4.1	2.2	14.5	36.2	354.4	136.3	Clay
	10-20	355.3	55.4	589.4	3.9	2.2	13.6	37.9	350.0	134.6	Clay
	20-40	316.0	51.4	632.7	4.4	2.5	15.2	40.2	375.8	144.5	Clay
	60-100	307.9	34.7	657.5	3.3	1.7	15.2	47.7	390.5	150.2	Clay
Xanthic Hapludox-XHD	0-10	752.8	24.2	223.1	0.4	0.2	1.6	4.9	200.9	1.2	Sand clay loam
	10-20	629.0	38.2	332.9	0.6	0.3	2.7	7.6	299.8	1.8	Sandy clay
	20-40	622.8	38.0	339.3	0.5	0.3	2.5	7.9	305.5	1.8	Sandy clay
	60-100	606.8	35.7	357.6	0.7	0.2	2.8	9.2	322.0	1.9	Sandy clay
Xanthic Haplustox-XHT	0-10	395.9	86.6	517.6	2.5	0.6	4.2	11.7	176.3	303.8	Clay
	10-20	388.6	80.0	531.5	1.8	0.5	3.6	10.7	181.3	311.9	Clay
	20-40	378.6	59.4	562.1	2.4	0.7	3.9	11.8	191.5	329.9	Clay
	60-100	393.0	44.4	562.6	2.3	0.6	3.6	11.3	191.7	330.2	Clay
Rhodic Haplustox-RHT	0-10	195.5	205.1	599.4	3.9	3.7	12.2	103.6	224.5	122.8	Clay
	10-20	154.9	236.6	608.6	3.6	3.8	12.8	103.6	227.9	124.7	Clay
	20-40	169.2	223.5	607.4	3.2	3.7	13.0	105.2	227.5	124.5	Clay
	60-100	212.1	202.2	585.8	2.8	3.4	12.8	106.8	219.4	120.1	Clay
Typic Haplustox-THT	0-10	580.1	60.0	359.9	1.0	0.8	2.2	24.6	297.3	1.3	Sandy clay
	10-20	635.0	51.1	313.9	0.9	0.6	2.0	22.2	259.0	1.1	Sandy clay loam
	20-40	644.1	53.5	302.5	0.8	0.5	1.7	19.0	249.6	1.1	Sandy clay loam
	60-100	553.0	72.1	375.0	0.7	0.4	2.0	22.1	309.4	1.3	Sandy clay

†Element content within the clay fraction, expressed in g kg^{-1} soil. The conversion of Al into Al_2O_3 and Fe into Fe_2O_3 can be achieved by multiplying the element content by (102 ÷ 54) and (160 ÷ 112), respectively. ‡Estimated by means of thermogravimetry using the clay fraction after Fe removal by DC.

For the experimental units in which we proceeded the dilution of the fine fraction by adding fine sand, the water added to achieve 60-70% of water retention capacity was proportionally adjusted to avoid O_2 limitation. Moreover, although the clay+silt content in Oxisols should not be lower than 150 g kg^{-1}, some of the soils in our experiment would no longer meet this criterion after the dilution of the fine fraction. Nevertheless, we do not expect such difference to have influenced our results in any way, other than the correct classification of the soils after the dilution of the fine fraction.

Since we collected soil samples from different depths, we prepared a suspension by mixing 2 g of soil from the 0-10 cm depth into 200 mL of deionized water, which were agitated continuously overnight. Afterwards, the inoculation consisted on pipetting an aliquot of 1 mL from the suspension (after its dilution), which was thoroughly mixed to the samples. This procedure was done for each soil separately to make sure there was no substantial differences on the microbial community among samples collected at different depths. Because our incubation experiment was conducted over a 12-month period, we do not expect that differences on the size and/or activity of the microbial community throughout the soils profile to have impacted on the final results reported here. However, we have not assessed any microbial biomass-related parameter to support the previous statement.

After the 12-month incubation experiment, the samples were air-dried and physically fractionated into sand and POM, the fraction >53 µm (data not included here), and the mineral fraction <53 µm and their associated organic matter. For the physical fractionation, a 5-g soil sample was dispersed into a 50 mL centrifuge tube containing 15 mL of hexametaphosphate g L^{-1} and 100 mm diameter glass bed. These samples were thoroughly dispersed under continuous stirring during 16 hours at 120 rpm. After physical fractionation, the samples were wet-sieved through a 53 µm screen, and the fractions were dried at 45 °C for 7 days. Afterwards, the samples were weighted, finely ground using an agate mortar and pestle yielding a final particle-size smaller than 149 µm. The C content and its respective stable isotope abundance (^{13}C content) were

determined using an isotope ration mass spectrometer (IRMS) with continuous flow (20-20, ANCA-GLS, Sercon, Crewe, UK). The abundance of the ^{13}C was expressed as $\delta^{13}C$ in parts per mil (‰) with reference to the international standard (Pee Dee Belemnite).

3.5. C-saturation level and C-saturation deficit as a function of the clay+silt fraction

Following increasing organic matter inputs to soils, clay- and silt-sized particles would eventually reach their protective-capacity or C-saturation level, either as individual mineral particles or in the form of aggregates (Castellano et al., 2015). Therefore, we assumed the SOC content associated to the fraction <53 µm to account for the protective-capacity level, and therefore the CSL in Oxisols. Therefore, proceeded as follows:

$$CSL,\ g\ C\ kg^{-1}\ soil = 5.5 + 0.26*(C+S)$$

where C+S is the fraction <53 µm content, expressed as a percentage (%) of the fine earth fraction (<2 mm). This equation has been proposed to link the total amount of clay+silt particles to the mineral-associated SOC retained by adsorption or particles aggregation in soils dominated by 1:1 phyllosilicates, such as Oxisols (Six et al., 2002a). After estimating the CSL, we calculated the CSD, as follows:

$$CSD,\% = \left(\frac{(CSL-SOC)}{CSL}\right) x\ 100$$

where SOC is the observed C content within the clay+silt fraction expressed in g kg^{-1} soil (as explained earlier) before the incubation experiment had started. In this way, we would avoid any effect of the treatments on the original SOC content within the fine fraction throughout the incubation period. Both, the CSL and the CSD were estimated for all samples included in our experiment, irrespective of the depth at which the samples were collected or the dilution of the fine fraction. Furthermore, because Oxisols often present relatively uniform texture and mineralogy with respect to depth (Schaefer, 2001), the samples collected throughout the soil profile, would provide a gradient

of CSD. In this case, the CSD would increase from the topsoil towards the bottom layers sampled.

3.6. Litter-derived C

The proportion (*f*) of litter-derived C within the fraction smaller <53 µm was calculated as follows:

$$f = \left(\frac{\delta_t - \delta_s}{\delta_l - \delta_s}\right) x\ 100$$

where δt is $\delta^{13}C$ of the <53 µm for the treatments receiving plant-litter, δs is $\delta^{13}C$ of the <53 µm in the control treatments (no plant litter additions), and δl is $\delta^{13}C$ of the plant litter (405.50‰).

3.7. Statistics

We tested our hypothesis in several steps. The litter-derived C within the fraction <53 µm was modeled as function of the litter-C inputs and the CSD. As such, we would estimate the variation on the contribution of the litter-derived C for the mineral-associated SOC as affected by the CSD and litter-C inputs. Subsequently we run regression analyses to test for the relationship between the the total increment in the SOC content in response to litter-C additions. Accordingly, the mass of litter-derived C remaining in the fraction <53 µm was expressed relative to the mass of original SOC, i.e. the “unlabeled C” remaining in the sample at the end of the incubation period. In addition, we run regressions to establish a relationship between the litter-derived C remaining in the sample after the incubation with respect to the total C addition at the beginning of the experiment. In this case, we plotted the litter-derived C within the fraction <53 µm against the litter-C mass added, which was expressed relative to the mass of the unlabeled SOC in the samples at the beginning of the experiment. Such calculation would allow us to infer on the conversion of the litter-C into mineral-organic associations with increasing C inputs with respect to the initial SOC content within the protected pool.

For all correlations and regression analyses, the significance of the estimated parameters was set at $p<0.05$ level. The statistical analyses

were performed using R-software®, Statistica STATSOFT® and the artwork was prepared using Sigma Plot® 11.

4. Results

4.1. Litter-derived C fraction and increment in the mineral-associated SOC content

As expected, the litter-derived C within the fine fraction increased steeply with increasing CSD, when we include all data set (sampling depth and the fine fraction dilution) in a single analysis (Fig 1). As such, for a given C input, the proportion of the litter-derived C within the mineral-associated SOC was determined by the magnitude of the CSD. For instance, in samples presenting positive CSD, the contribution of the litter-derived C for the mineral-associated SOC could reach approximately 20% of the total mineral-associated SOC even with small C additions (e.g., 4.5 mg g^{-1} soil). On the other hand, the litter-derived C within the fine fraction accounted for no more than 20% of the SOC content in the samples exhibiting negative CSD estimates (Fig. 1), even after higher C inputs (e.g., 18 mg g^{-1} soil). Overall, contributions of the litter-derived C for the mineral-associated SOC higher than 20% only occurred for the samples showing positive CSD. Consequently, for soils exhibiting low or negative CSD, the probability of promoting significant increments in their protected SOC pool would have been much smaller than for samples presenting high CSD (Fig. 1). Based on this data, the collection of soil samples at different depths provided a suitable gradient of CSD, which increased with soil depth.

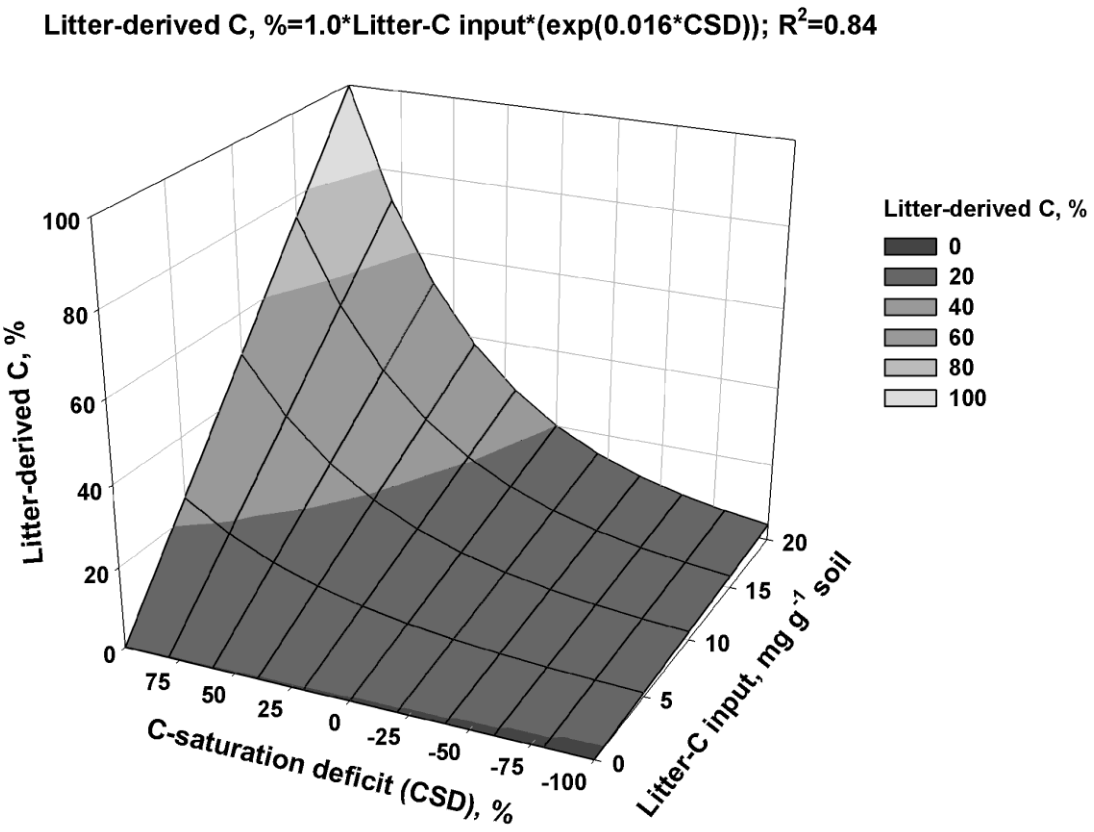

Figure 1. Litter-derived C fraction (%) as a function of litter inputs (0, 4.5, 9, and 18 mg g^{-1} soil) and the CSD estimated from the CSL based on the linear model (Six et al., 2002a). The estimated parameters are significant at $p<0.05$ (F-test). Number of observations=864.

Although the proportion of the litter-derived C within the fine fraction was mainly affected by the CSD (Fig. 1), the magnitude of the increment in the SOC content was strongly affected by the dilution of the fine fraction, further referred to as soil "texture" in this text (Fig. 2a-d). According to the C-saturation concept, the mineral-protected SOC would not increase in size due to C additions after this pool have reached its C-saturation level (Castellano et al., 2015). In our soils, the lack of increment in the mineral-associated SOC following the incorporation of the litter-C was more evident in the soils at their natural texture (Fig. 2a).

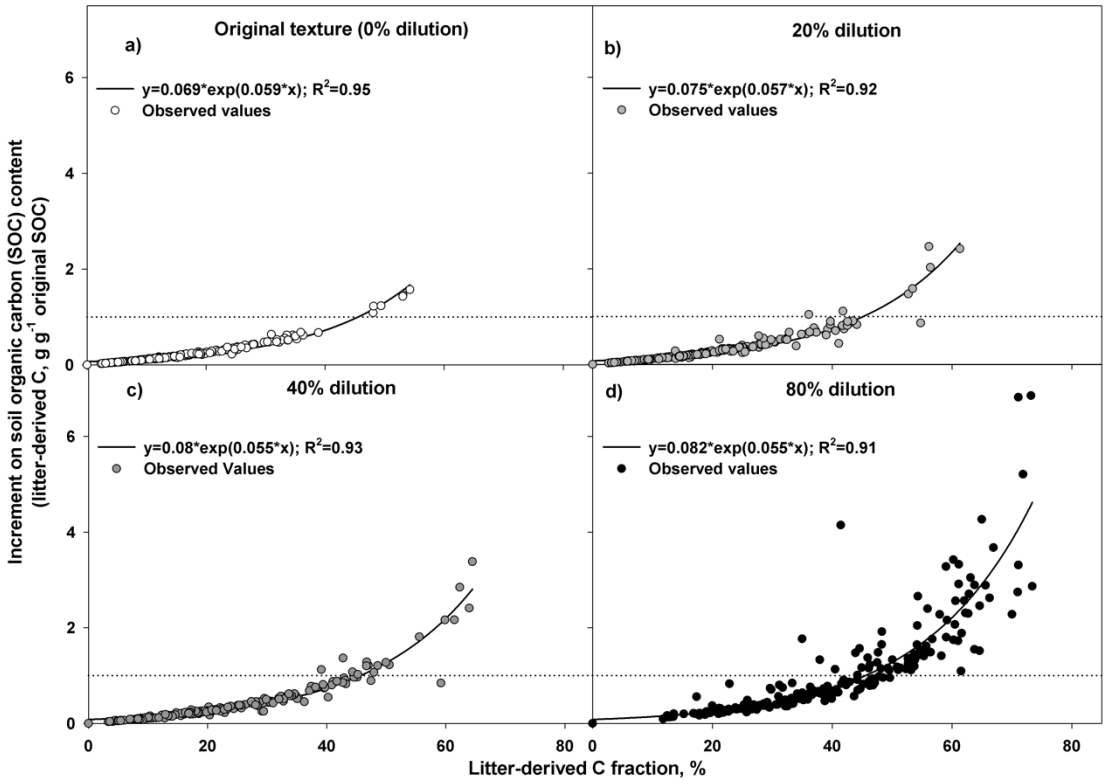

Figure 2. Increment on the soil organic carbon (SOC) content as a function of the litter-derived C fraction (%) following litter-C additions at 0.0, 4.5, 9.0 and 18.0 mg g^{-1} soil and the dilution of the fine fraction at a) 0%, b) 20%, c) 40% and d) 80%. The dotted line depicts the point at which the contribution of the litter-C equals the "unlabeled" SOC content (1:1 ratio). The estimated parameters are significant at $p<0.05$ (F test). Number of observations=288 for each texture (fine fraction dilution). The increment on the SOC content was expressed as g of litter-C g^{-1} "original" SOC (i.e. unlabeled SOC associated to the fraction <53 µm) prior to the incubation experiment had started.

Conversely, the samples in which the fine fraction was diluted (Fig. 2b-d), the increment achieved in the protected SOC content was comparatively higher than that observed in the same soils at their natural texture. However, the higher amount of clay+silt in the soils at their natural texture would indicate that the lack of increment in the protected SOC pool, would have been due to the C-saturation of micraggregates surfaces and their associated pore space area. This were the first indication that C-saturation in Oxisols should vary as a function of texture, according to our hypothesis being tested in this research.

According to the C-saturation concept, the efficiency by which the plant litter is converted into the protected SOC pool should be

progressively reduced with increasing C inputs, until reaching the CSL (Stewart et al., 2008). As the soil approaches its CSL, larger amounts of litter-C should be added to promote detectable changes on the protected C pool as compared to soils with high CSD (Fig 1). However, as the soil approach such threshold, increasing the C inputs would not cause a proportional increment within the protected C pool (Castellano et al., 2015). Indeed, as the C additions relative to the initial (unlabeled) SOC content increased in our study, the conversion of the plant litter into mineral-associated SOC reached a "plateau" as shown in Fig. 3, irrespective of texture. Interestingly, the asymptotic conversion of the litter-C into mineral-associated SOC also varied substantially with texture, as demonstrated in Fig. 3a-d.

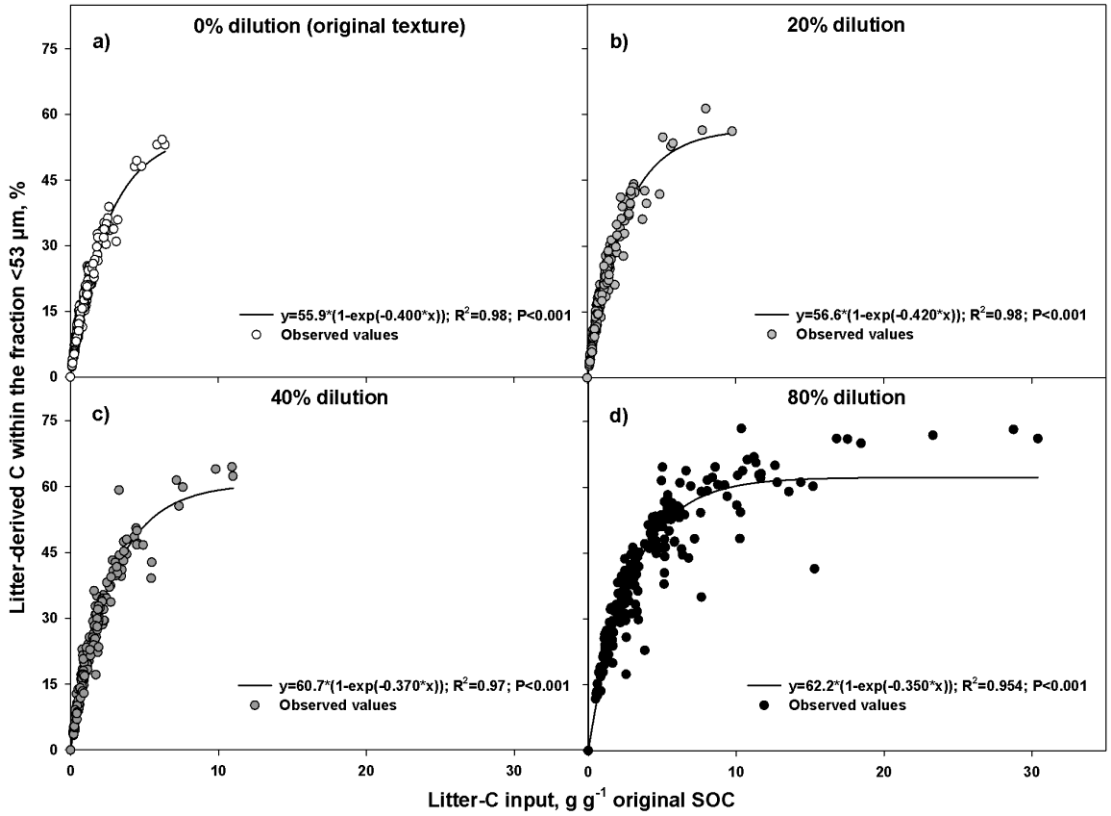

Figure 3. Litter-derived C fraction (%) as a function of C addition (g of litter-C g^{-1} initial SOC content within the fraction <53 µm) and the dilution of the fine fraction at a) 0% (original texture); b) 20%; c) 40%; d) 80%. For each texture, n=288 (6 Oxisols, 4 depths, 4 litter inputs and 3 replicates).

As we increased the dilution of the fine fraction, the litter-C addition was equivalent to a higher proportion of the initial SOC content within the fine fraction (Fig 3b-d) as compared to the samples at their natural texture (Fig. 3a). Nevertheless, despite the C added via plant litter being equivalent to almost 30 times the initial SOC for some of the Oxisols at the highest dilution, the litter-derived C fraction would not increase beyond 60-70% of the total protected SOC content (Fig. 3d). According to the regressions fitted, the soils would reach their CSL following C additions equivalent to 10 times the initial SOC content in the samples. At the CSL, the litter-derived C would vary from 56 up to 62% (Fig. 3a-d), with the higher values occurring in the coarse-textured soils. Therefore, despite the higher amount of clay+silt in the soils at their natural textures than in the samples in which the fraction was diluted, both type of samples reached "C-saturation". In this case, the samples that become "C-saturated" had a high initial CSD, in contrast to the samples in which the SOC did not increase following litter-C additions. Given the large difference in terms of clay+silt content among the samples as a function of the fine fraction dilution, we infer that C-saturation in fine-textured Oxisols of equivalent mineralogy and C inputs, the saturation of microaggregates surfaces and their associated pore space area seem to predominate. Conversely, in coarse textured Oxisols C-saturation should be mainly affected by the saturation of individual mineral particles (or less aggregated particles).

4.2 Linking SOC content within the clay+silt to the SOC in the whole soil

As we plotted the mineral-associated SOC content relative to the whole soil (g C kg^{-1} soil) as a function of the fine fraction content (g clay+silt kg^{-1} soil) and its C content (g C kg^{-1} clay+silt), some interesting patterns emerged (Fig. 4). As such, in some cases we observed SOC content as high as 100 g kg^{-1} clay+silt in soils for which the fine fraction was lower than 200 g kg^{-1} soil. Such data is in agreement with the relatively higher increment in the SOC content as the fine fraction mass was diluted in our experiment (Fig. 2 a-d). Otherwise,

as the mass of the fine fraction increased, there was a general trend of lower SOC content per unit of clay+silt (Fig. 4).

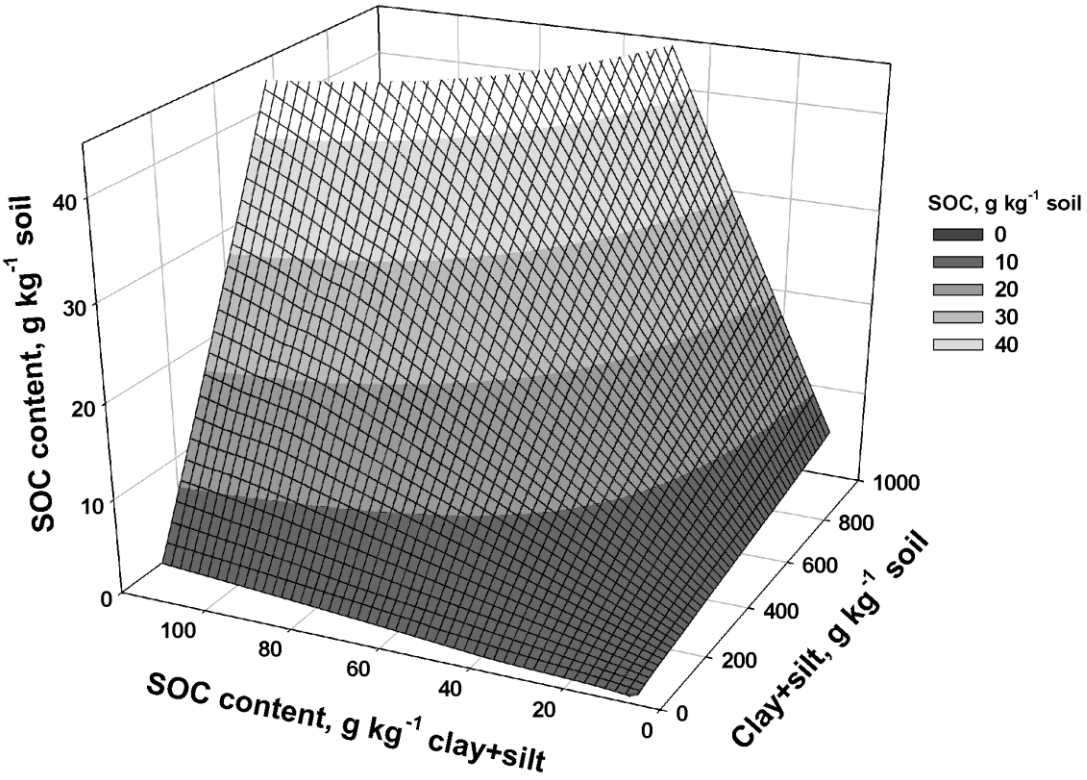

Figure 4. Mineral-associated soil organic carbon content (SOC, g kg^{-1} soil) as a function of the clay+silt content (g kg^{-1} soil) and the SOC content in this fraction (g C kg^{-1} clay+silt). Number of observations=1152.

Combined, these results corroborate the differential mechanisms accounting for the influence of texture on C-saturation in Oxisols. Therefore, the relatively low proportion of C mass per unit of clay+silt as the mass of this fraction increases is consistent with their saturation in the form of microaggregates. Otherwise, the high C content per unit of clay+silt as the mass of this fraction decreases, supports our hypothesis of C-saturation of isolated mineral particles or at least less affected by aggregation in coarse-textured Oxisols.

5. Discussion

5.1. Parameterization of CSL/CSD as function of depth of sampling and Oxisols texture

We expected the SOC content in samples collected at 0-10 cm depth would have been closer to CSL (i.e. at steady-state) as compared to the other soil layers included in our study (10-20, 20-40, and 60-100 cm depth). In combination, the sampling throughout the soil profile provided a gradient of CSD, which increased with soil depth. The main aspects supporting our assumption is that even when soil samples are collected at layers in the A down to the B horizon, which are often below one meter deep, there are no substantial changes in the mineralogy or in the texture of Oxisols (Schaefer, 2001). Theoretically, the inherent capacity for SOC storage in Oxisols should not vary with depth given their uniform chemical and physical properties throughout the profile.

Modeling the CSL as a linear function of the clay+silt content is based on the promise that these fractions account for both chemical (coprecipitation and adsorption of SOC by minerals) and physical processes such as the occlusion of SOC due to aggregation (Six et al., 2002a). Yet, quantitative assessment on the role of each mechanism remains elusive because their influence on SOC storage often overlap. As a result, appropriate parameterization of CSL and consequently the CSD is arguably the most critical step to predict the potential response of soils to further C inputs. Despite some significant progress made on this front over the last 20 years, defining such parameters remains an important issue, given the large numbers of factors affecting SOC storage (Feng et al., 2013; Beare et al., 2014). For instance, as we assumed a linear relationship between the mass of the fine fraction and the CSL, we observed some negative estimates for the CSD (Fig 1). This suggests that some of the Oxisols evaluated would have been able to protect a larger amount of C than would be expected based on a linear relationship between the mass of the fine fraction and SOC content. However, even if we had an underestimated CSD, this was probably less important because of the different depths at which we proceed the

sampling. Moreover, strong linear correlations between the amount of clay+silt and the SOC content in tropical soils also has been demonstrated in previous research (Feller and Beare, 1997). Although these authors have evaluated the SOC within the fraction <20 µm, the magnitude of the variation in the SOC content reported was quite similar to ours, ranging from values <10 up to 45 g kg^{-1} soil for samples collected in the topsoil (0-20 cm). Therefore, we do not expect that assuming a linear relationship between the clay+silt content and the SOC content would affect the inference we made on the mechanisms accounting for C storage and C-saturation as a function of texture in Oxisols (see sections below).

5.2. Soil C-saturation dynamics

Based on our results, we inferred two types of C-saturation patterns in the selected Oxisols. The first type, can be inferred from the lack of significant increment in the protected C pool following C inputs to soils, which probably dominated in samples with low initial CSD, i.e. samples collected in the topsoil. This pattern, seems the most recurring indication of C-saturation dynamics, in which there is no increment in the protected pool following C additions to soils (West and Six, 2007; Castellano et al., 2015). As we demonstrated in Fig. 1, the litter derived C within the fine fraction would account for a small proportion of the total mineral-associated SOC content in samples with low, or even negative CSD. As a result, the probability of promoting significant increments in the mineral-protected C pool would have been quite small in those soils. The lack of increment in the protected C pool following long-term litter-C inputs is often suggested to indicate C-saturation dynamics in field-based experiments (West and Six, 2007; Gulde et al., 2008; Chung et al., 2010; Brown et al., 2014). Probably, this type of C-saturation behavior in is more common in areas with high litter-C additions to the topsoil, as it is often reported soils under no-till, for instance (Corbeels et al., 2016). Over time, promoting increments to the protected SOC pool should become more difficult and the topsoil layers probably reach their CSL more quickly than deeper the layers (Castellano et al., 2012). Although our study was conducted under controlled conditions, the lack

of increment in the protected C pool following the incorporation of the litter-C seems to indicate a similar behavior of the Oxisols included in our study with earlier reports from field-based experiments.

We inferred a second type of C-saturation pattern, which occurred in soils that had high CSD at the beginning of the experiment. In this case, the litter-C added was equivalent to a large proportion of the initial mineral-associated SOC content (Fig. 3a-d). In contrast to the first type of C-saturation pattern, in this case the litter derived-C would account for more than 50% of the total mineral-associated C when the samples reached their CSL. Therefore, the litter-C additions would have been high enough to overcome the SOC storage capacity of the fine fraction under such circumstances. We only detected this second C-saturation pattern in such a short-term experiment because we could control the mass of the soil in which the litter-C was added, which is not easy to achieve in field-based experiments. Although such condition should be much less common in short-term field experiments, this data is useful for illustrating the limited capacity of soil for C storage (Hassink, 1997; Six et al., 2002a; Stewart et al., 2007; Heitkamp et al., 2012; Castellano et al., 2015). Our data also confirms predictions from previous research indicating the huge amount of litter-C additions that are needed to promote C-saturation (West and Six, 2007; Stewart et al., 2007). For this reason, promoting C-saturation itself is of less interest. However, with increasing C inputs, there is a decrease on the overall conversion of the plant litter into the protected C pool as the soils approach their CSL (Hassink, 1996; Stewart et al., 2008; Castellano et al., 2015). Therefore, although the mechanism leading to C-saturation are probably different in coarse or fine-textured Oxisols, the incorporation of the litter-derived C within the fine fraction increased asymptotically with respect to C additions (Fig. 3a-d).

5.3. The influence of texture on C-saturation - mechanisms

According to our results, the soils reached their CSL after the litter-derived C accounting for 56% up to 62% of the total mineral-associated SOC, with the lower values accounting for the soils at their

natural texture. The relatively lower amount of the litter-derived C needed for promoting C-saturation in the soils at their natural texture (Fig. 3a) suggests that such saturation was probably due to the preferential saturation of microaggregates surfaces and their associated pore space area (Anda et al., 2008). Our inference is in line with previous evidence provided by spectroscopic experiments indicating the occurrence of organic matter as discrete coatings on soil microaggregates surfaces (Hatton et al., 2012). This is mainly because with increasing amounts of clay- and silt-sized particles, there would be expected a high capacity for aggregation (Oades, 1988; Baldock and Skjemstad, 2000). Interestingly, the main feature of Oxisols is their strong microstructure/microaggregation, which makes these soils so distinctive relative to other soil orders (Beinroth, 1982; Schaefer, 2001; Schaefer et al., 2004; Buol, 2009). Therefore, we expect that with increasing clay+silt content, there is a simultaneous increment in Oxisols microaggregation (Barthès et al., 2008). With increasing C inputs, we suggest that these microaggregates and their pore space area are more likely to exhibit C-saturation, rather than individualized clay- or silt-sized particles.

In contrast to fine-textured Oxisols, we propose that with decreasing amounts of clay+silt, soils capacity for aggregation should be much smaller (Baldock and Skjemstad, 2000). Therefore, it can be expected the C-saturation of individual particles or less aggregated particles to predominate. Accordingly, the fine fraction of naturally coarse-textured soils should have a higher SOC content per unit of clay+silt than fine-textured soils (Amelung et al., 1998; Plante et al., 2006; Zinn et al., 2007; Stewart et al., 2007; Barthès et al., 2008; Curtin et al., 2016). As we used incubation experiments, the main factor leading to the dispersion of large aggregates probably was the mechanical dispersion of these structures when the fine earth fraction was mixed with sand to dilute the fine fraction. In addition, even discrete variations in the moisture content could have favored aggregate disruption upon drying/rewetting throughout the incubation period (Oades, 1988; Denef et al., 2001; Kaiser et al., 2015). As the aggregates break apart, this

could reduce particle-to-particle interactions, and possibly exposing reactive surfaces that were contributing to hold up their structure, particularly Al-/Fe-(hydr)oxides (Oades and Waters, 1991; Schaefer, 2001; Six et al., 2002b). These processes combined would result in higher C content per unit of clay+silt in coarse-textured Oxisols as compared to fine textured types (Zinn et al., 2007; Barthès et al., 2008). Also worth noting that with increasing SOC content per unit of clay+silt in corase-textured soils, probably there is a lower contribution of physical protection of organic matter against decomposition as compared to fine-textured Oxisols. This is mainly because the formation of mineral-organic associations occur irrespective of texture, but with increasing content of clay- and silt-sized particles, there is more potential for further protective effects due to particles aggregation (Lehmann et al., 2007). As stated before, the strong microaggregation of Oxisols has strong influence on the spatial distribution of SOC (Kinyangi et al., 2006; Lehmann et al., 2007) and its role on C storage and turnover should be considered in further studies. Additionally, given the inherent limitation of incubations experiments, the mechanisms we propose to underlie C-saturation in Oxisols should be further evaluated under field conditions experiments. These mechanisms probably have important implications for SOC storage, its turnover and C-saturation dynamics, and all these factors should be taken into account for evaluating the potential for increasing the protected C pool in Oxisols, especially in managed areas.

6. Conclusions

Based on our results, we can infer that different types of C-saturation patterns occurred in the Oxisols used in our incubation experiments. As such, we suggest that in samples with low initial CSD, the litter-derived C additions promoted low (if any) increment in the protected C pool. Otherwise, even for soils with high initial CSD, in some cases the litter-C additions were high enough to promote C-saturation. We propose that the mechanisms accounting for C-saturation in these soils were strongly affected by the texture. Therefore, it seems

that in fine-textured Oxisols, the C-saturation probably occurs due to the saturation of clay- and silt-sized particles forming aggregates. In this case, the organic matter would saturate microaggregates surfaces and/or their associated pore space area. Otherwise, in coarse-textured Oxisols, C-saturation is probably related to the saturation of individualized clay- and silt-sized particles (or less aggregated particles). Further evaluation of these mechanisms are important because Oxisols can occur at a range of textures and their strong microstructure probably plays an important role in both SOC storage and turnover in tropical ecosystems, where these soils predominate.

7. References

Amelung, W., W. Zech, X. Zhang, R.F. Follett, H. Tiessen, E. Knox, and K.-W. Flach. 1998. Carbon, nitrogen, and sulfur pools in particle-size fractions as influenced by climate. Soil Sci. Soc. Am. J. 62: 172.

Anda, M., J. Shamshuddin, I.C. Fauziah, and S.R. Syed Omar. 2008. Pore space and specific surface area of heavy clay oxisols as affected by their mineralogy and organic matter. Soil Sci. 173(8): 560–574.

Baldock, J.A., and J.O. Skjemstad. 2000. Role of the soil matrix and minerals in protecting natural organic materials against biological attack. Org. Geochem. 31(7-8): 697–710Available at http://linkinghub.elsevier.com/retrieve/pii/S0146638000000498.

Barthès, B.G., E. Kouakoua, M.-C. Larré-Larrouy, T.M. Razafimbelo, E.F. de Luca, A. Azontonde, C.S.V.J. Neves, P.L. de Freitas, and C.L. Feller. 2008. Texture and sesquioxide effects on water-stable aggregates and organic matter in some tropical soils. Geoderma 143(1-2): 14–25Available at http://linkinghub.elsevier.com/retrieve/pii/S0016706107002832.

Beare, M.H., S.J. McNeill, D. Curtin, R.L. Parfitt, H.S. Jones, M.B. Dodd, and J. Sharp. 2014. Estimating the organic carbon stabilisation capacity and saturation deficit of soils: a New Zealand case study. BiogeochemistryAvailable at http://link.springer.com/10.1007/s10533-014-9982-1 (verified 9 July

2014).

Beinroth, F.H. 1982. Some highly weathered soils of Puerto Rico, 1. Morphology, formation and classification. Geoderma 27(1-2): 1–73.

Brown, K.H., E.M. Bach, R. a. Drijber, K.S. Hofmockel, E.S. Jeske, J.E. Sawyer, and M.J. Castellano. 2014. A long-term nitrogen fertilizer gradient has little effect on soil organic matter in a high-intensity maize production system. Glob. Chang. Biol. 20(4): 1339–1350.

Buol, S.W. 2009. Soils and agriculture in central-west and north Brazil. Sci. Agric. 66(October): 697–707.

Castellano, M.J., J.P. Kaye, H. Lin, and J.P. Schmidt. 2012. Linking carbon saturation concepts to nitrogen saturation and retention. Ecosystems 15(2): 175–187.

Castellano, M.J., K.E. Mueller, D.C. Olk, J.E. Sawyer, and J. Six. 2015. Integrating plant litter quality, soil organic matter stabilization, and the carbon saturation concept. Glob. Chang. Biol. 21(9): 3200–3209Available at http://doi.wiley.com/10.1111/gcb.12982.

Chung, H., J.H. Grove, and J. Six. 2008. Indications for soil carbon saturation in a temperate agroecosystem. Soil Sci. Soc. Am. J. 72(4): 1132.

Chung, H., K.J. Ngo, A. Plante, and J. Six. 2010. Evidence for carbon saturation in a highly structured and organic-matter-rich soil. Soil Sci. Soc. Am. J. 74(1): 130Available at https://www.soils.org/publications/sssaj/abstracts/74/1/130 (verified 9 July 2014).

Corbeels, M., R.L. Marchão, M.S. Neto, E.G. Ferreira, B.E. Madari, E. Scopel, and O.R. Brito. 2016. Evidence of limited carbon sequestration in soils under no-tillage systems in the Cerrado of Brazil. Sci. Rep. 6(October 2015): 21450Available at http://www.nature.com/articles/srep21450.

Cotrufo, M.F., M.D. Wallenstein, C.M. Boot, K. Denef, and E. Paul. 2013. The microbial efficiency-matrix stabilization (MEMS) framework integrates plant litter decomposition with soil organic

matter stabilization: do labile plant inputs form stable soil organic matter? Glob. Chang. Biol. 19(4): 988–95Available at http://www.ncbi.nlm.nih.gov/pubmed/23504877 (verified 16 July 2014).

Curtin, D., M.H. Beare, and W. Qiu. 2016. Texture effects on carbon stabilisation and storage in New Zealand soils containing predominantly 2 : 1 clays. Soil Res. 54(1): 30–37Available at http://www.publish.csiro.au/?paper=SR14292.

Denef, K., J. Six, H. Bossuyt, S.D. Frey, E.T. Elliott, R. Merckx, and K. Paustian. 2001. Influence of dry-wet cycles on the interrelationship between aggregate, particulate organic matter, and microbial community dynamics. Soil Biol. Biochem. 33(12-13): 1599–1611.

Feller, C., and M.H. Beare. 1997. Physical control of soil organic matter dynamics in the tropics. Geoderma 79(1-4): 69–116.

Feng, W., A.F. Plante, and J. Six. 2013. Improving estimates of maximal organic carbon stabilization by fine soil particles. Biogeochemistry 112(1-3): 81–93Available at http://link.springer.com/10.1007/s10533-011-9679-7 (verified 9 July 2014).

Gulde, S., H. Chung, W. Amelung, C. Chang, and J. Six. 2008. Soil carbon saturation controls labile and stable carbon pool dynamics. Soil Sci. Soc. Am. J. 72(3): 605Available at https://www.soils.org/publications/sssaj/abstracts/72/3/605 (verified 22 August 2014).

Hassink, J. 1996. Preservation of plant residues in soils differing in unsaturated protective capacity. Soil Sci. Soc. Am. J. 60(2): 487–491Available at https://dl.sciencesocieties.org/publications/sssaj/abstracts/60/2/SS0600020487 (verified 9 July 2014).

Hassink, J. 1997. The capacity of soils to preserve organic C and N by their association with clay and silt particles. Plant Soil 191: 77–87Available at http://link.springer.com/article/10.1023/A:1004213929699 (verified

9 July 2014).

Hatton, P.-J., L. Remusat, B. Zeller, and D. Derrien. 2012. A multi-scale approach to determine accurate elemental and isotopic ratios by nano-scale secondary ion mass spectrometry imaging. Rapid Commun. Mass Spectrom. 26(11): 1363–71Available at http://onlinelibrary.wiley.com/doi/10.1002/rcm.6228/pdf (verified 28 July 2014).

Heitkamp, F., M. Wendland, K. Offenberger, and G. Gerold. 2012. Implications of input estimation, residue quality and carbon saturation on the predictive power of the Rothamsted Carbon Model. Geoderma 170: 168–175Available at http://dx.doi.org/10.1016/j.geoderma.2011.11.005.

Kaiser, M., M. Kleber, and A.A. Berhe. 2015. How air-drying and rewetting modify soil organic matter characteristics: An assessment to improve data interpretation and inference. Soil Biol. Biochem. 80: 324–340Available at http://dx.doi.org/10.1016/j.soilbio.2014.10.018.

Kinyangi, J., D. Solomon, B. Liang, M. Lerotic, S. Wirick, and J. Lehmann. 2006. Nanoscale biogeocomplexity of the organomineral assemblage in soil: Application of STXM microscopy and C 1s-NEXAFS spectroscopy. Soil Sci. Soc. Am. J. 70(5): 1708 – 1718Available at https://www.soils.org/publications/sssaj/abstracts/70/5/1708 (verified 9 August 2012).

Kleber, M., K. Eusterhues, M. Keiluweit, C. Mikutta, R. Mikutta, and P.S. Nico. 2015. Mineral–organic associations: Formation, properties, and relevance in soil environments. p. 1–140. *In* Advances in Agronomy. Elsevier Ltd.

Kögel-Knabner, I., G. Guggenberger, M. Kleber, E. Kandeler, K. Kalbitz, S. Scheu, K. Eusterhues, and P. Leinweber. 2008. Organo-mineral associations in temperate soils: Integrating biology, mineralogy, and organic matter chemistry. J. Plant Nutr. Soil Sci. 171(1): 61–82.

Kong, A.Y.Y., J. Six, D.C. Bryant, R.F. Denison, and C. van Kessel.

2005. The relationship between carbon input, aggregation, and soil organic carbon stabilization in sustainable cropping systems. Soil Sci. Soc. Am. J. 69(4): 1078.

Lal, R. 2004. Soil carbon sequestration to mitigate climate change. Geoderma 123(1-2): 1–22Available at http://linkinghub.elsevier.com/retrieve/pii/S0016706104000266 (verified 10 July 2014).

Lehmann, J., J. Kinyangi, and D. Solomon. 2007. Organic matter stabilization in soil microaggregates: implications from spatial heterogeneity of organic carbon contents and carbon forms. Biogeochemistry 85(1): 45–57Available at http://link.springer.com/10.1007/s10533-007-9105-3 (verified 9 July 2014).

Luo, Z., E. Wang, and O.J. Sun. 2010. Can no-tillage stimulate carbon sequestration in agricultural soils? A meta-analysis of paired experiments. Agric. Ecosyst. Environ. 139(1-2): 224–231Available at http://dx.doi.org/10.1016/j.agee.2010.08.006.

Mikutta, R., and K. Kaiser. 2011. Organic matter bound to mineral surfaces: Resistance to chemical and biological oxidation. Soil Biol. Biochem. 43(8): 1738–1741Available at http://dx.doi.org/10.1016/j.soilbio.2011.04.012.

Oades, J.M. 1988. The retention of organic matter in soils. Biogeochemistry 5(1): 35–70Available at http://link.springer.com/10.1007/BF02180317.

Oades, J., and A. Waters. 1991. Aggregate hierarchy in soils. Aust. J. Soil Res. 29(6): 815.

Plante, A.F., R.T. Conant, C.E. Stewart, K. Paustian, and J. Six. 2006. Impact of soil texture on the distribution of soil organic matter in physical and chemical fractions. Soil Sci. Soc. Am. J. 70(1): 287Available at https://www.soils.org/publications/sssaj/abstracts/70/1/287 (verified 27 August 2014).

Powlson, D.S., A.P. Whitmore, and K.W.T. Goulding. 2011. Soil carbon sequestration to mitigate climate change: A critical re-examination to identify the true and the false. Eur. J. Soil Sci. 62(1): 42–55.

Schaefer, C.E.G.R. 2001. Brazilian latosols and their B horizon microstructure as long-term biotic constructs. Aust. J. Soil Res. 39(5): 909–926.

Schaefer, C.E.G.R., J.D. Fabris, and J.C. Ker. 2008. Minerals in the clay fraction of Brazilian Latosols (Oxisols): a review. Clay Miner. 43(1): 137–154Available at http://openurl.ingenta.com/content/xref?genre=article&issn=0009-8558&volume=43&issue=1&spage=137 (verified 9 July 2014).

Schaefer, C.E.G.R., R.J. Gilkes, and R.B.A. Fernandes. 2004. EDS/SEM study on microaggregates of Brazilian Latosols, in relation to P adsorption and clay fraction attributes. Geoderma 123(1-2): 69–81Available at http://linkinghub.elsevier.com/retrieve/pii/S0016706104000333 (verified 30 August 2014).

Schmidt, M.W.I., M.S. Torn, S. Abiven, T. Dittmar, G. Guggenberger, I.A. Janssens, M. Kleber, I. Kögel-Knabner, J. Lehmann, D.A.C. Manning, P. Nannipieri, D.P. Rasse, S. Weiner, and S.E. Trumbore. 2011. Persistence of soil organic matter as an ecosystem property. Nature 478(7367): 49–56Available at http://www.ncbi.nlm.nih.gov/pubmed/21979045 (verified 16 July 2014).

Six, J., R. Conant, E. Paul, and K. Paustian. 2002a. Stabilization mechanisms of soil organic matter: implications for C-saturation of soils. Plant Soil 241: 155–176Available at http://download.springer.com/static/pdf/500/art%253A10.1023%252FA%253A1016125726789.pdf?auth66=1407681395_d4f9da458e92f5bbc5ac62e0807ae300&ext=.pdf (verified 8 August 2014).

Six, J., C. Feller, K. Denef, S.M. Ogle, J.C. de Moraes, and A. Albrecht. 2002b. Soil organic matter, biota and aggregation in temperate and tropical soils - Effects of no-tillage. Agronomie 22(7-8): 755–775.

Soil Survey Staff. 2014. Keys to Soil Taxonomy (U-NRC Service, Ed.). 12th ed. Washington, DC.

Stewart, C.E., K. Paustian, R.T. Conant, A.F. Plante, and J. Six. 2007. Soil carbon saturation: concept, evidence and evaluation. Biogeochemistry 86(1): 19–31Available at http://link.springer.com/10.1007/s10533-007-9140-0 (verified 9 July 2014).

Stewart, C.E., K. Paustian, R.T. Conant, A.F. Plante, and J. Six. 2008. Soil carbon saturation: Evaluation and corroboration by long-term incubations. Soil Biol. Biochem. 40(7): 1741–1750Available at http://linkinghub.elsevier.com/retrieve/pii/S0038071708000989 (verified 31 August 2014).

Stewart, C.E., K. Paustian, R.T. Conant, A.F. Plante, and J. Six. 2009. Soil carbon saturation: Implications for measurable carbon pool dynamics in long-term incubations. Soil Biol. Biochem. 41(2): 357–366Available at http://dx.doi.org/10.1016/j.soilbio.2008.11.011.

West, T.O., and J. Six. 2007. Considering the influence of sequestration duration and carbon saturation on estimates of soil carbon capacity. Clim. Change 80(1-2): 25–41.

Zinn, Y.L., R. Lal, J.M. Bigham, and D.V.S. Resck. 2007. Edaphic controls on soil organic carbon retention in the Brazilian Cerrado: Texture and mineralogy. Soil Sci. Soc. Am. J. 71(4): 1204–1214Available at https://www.soils.org/publications/sssaj/abstracts/71/4/1204 (verified 9 July 2014).

Litter decomposition and $^{13}C/^{15}N$ incorporation into mineral-organic associations in Oxisols (chapter two)

1.Abstract

Rationale: The persistence soil organic matter (SOM) is thought to be driven by physical processes and chemical reactions within the mineral matrix that lead to the formation of mineral-organic associations. However, the formation of such interactions is much less understood in soils dominated by low-activity clays such as in Oxisols. ***Objectives***: Therefore, we investigated the connection between plant litter decomposition and the formation of mineral-organic associations in some highly weathered Oxisols. ***Methods***: We incubated samples collected at 4 depths (0-10, 10-20, 20-40 and 60-100 cm) from 6 representative Oxisols using a double labeled plant litter (i.e. ^{13}C at 405‰ and ^{15}N at 74 atom%) and quantified the proportion of these tracers remaining in mineral-organic associations after 12 months. ***Results***: We observed strong evidence of microbial-derived compounds being retained within mineral-organic association. As such, while 37.3% of the initial input of litter-N was recovered in the fraction <53 µm, it was only 23.7% for the litter-C input. Both isotopic-unlabeled and labeled organic matter were strongly correlated to amorphous Al-/Fe-(hydr)oxides. ***Discussion***: The decoupling between the isotopic tracers was probably related to the preferential preservation of N-rich compounds in associations with amorphous Al-/Fe-(hydr)oxides. Apparently, these minerals are the main components involved in the formation and persistence of mineral-organic associations in Oxisols. ***Conclusions***: If such interactions are of widespread occurrence, the large C pool found in tropical ecosystems may be much more sensitive to environmental changes than currently expected, because amorphous Al-/Fe-(hydr)oxides account for only a small fraction of the total (hydr)oxides content in Oxisols.

2. Introduction

The global soil organic carbon (SOC) stock is an important asset that ultimately regulates the flux of energy and nutrients through ecosystems (Janzen, 2015). Despite the general consensus that part of the CO_2 fixed in photosynthesis in terrestrial ecosystems will eventually be incorporated into the SOC stock, connecting plant litter decomposition to SOM formation it is still challenging (Cotrufo et al., 2015). In the soil environment, the plant litter undergoes hydrolytic and oxidative decomposition, with continuous decrease in molecular size and solubility in water (Hedges and Keil, 1999; Kleber et al., 2015). According to this framework, once dissolved or solvated by the soil solution, part of the organic molecules may form direct associations with soil minerals. In another pathway, the litter-derived compounds can be further partitioned into microbial biomass or CO_2 (i.e. microbial growth or respiration). The C incorporated into the biomass, may become part of mineral-organic associations due to deliberate attachment of microbes onto mineral surfaces and/or the production of extracellular polymeric substances (EPS) (Miltner et al., 2012; Cotrufo et al., 2013; Kleber et al., 2015).

From the decaying plant litter towards mineral-associated SOM, there is a significant reduction on the overall C:N ratio, which is often attributed to the preferential accumulation of microbial products within the mineral matrix (Simpson et al., 2007; Fierer et al., 2009; Cotrufo et al., 2013). Chemically, the molecular composition of mineral-associated SOM is much more similar to microbial products than with the original plant material applied to the soils (Grandy and Neff, 2008; Mambelli et al., 2011; Plaza et al., 2013; Heckman et al., 2013). As a result, the plant litter N seems to be incorporated within mineral-organic associations at a higher efficiency relative to the litter-derived C (Bird et al., 2008; Hatton et al., 2012, 2015a). Additionally, the long-term persistence of N-rich compounds in soils may be facilitated by the presence functional groups (e.g., amide) and the mechanisms by which these components interact with mineral surfaces (Keiluweit et al., 2012).

It is widely accepted that the presence of reactive minerals is a prerequisite for the development of mineral-organic associations, which could render SOM temporarily inaccessible to decomposers (Baldock and Skjemstad, 2000; Kögel-Knabner et al., 2008; Dungait et al., 2012). Among the most reactive minerals in soils, Al- and Fe-(hydr)oxides play an important role on the formation of mineral-organic associations (Torn et al., 1997; Kleber et al., 2005; Lutzow et al., 2006; Kögel-Knabner et al., 2008). The formation of these associations seems to slow down SOM mineralization, thus favoring its persistence in soils (Rasmussen et al., 2006). Arguably, the presence of reactive minerals with high specific surface area (SSA) and high charge density will affect directly the overall capacity of soils to protect SOM against decomposition (Doetterl et al., 2015). These findings raise important questions concerning the formation of mineral-organic associations in highly weathered soils, particularly in Oxisols, which are dominated by low-activity clays (Feller and Beare, 1997).

In Oxisols, kaolinite is the predominant mineral, which is a non-expansive phyllosilicate, presenting low physic-chemical activity (i.e. low charge density, limited cation exchange capacity and also low SSA) (Melo et al., 2001). Otherwise, these soils also contain variable amounts of Al-(hydr)oxides (mostly gibbsite), and Fe-(hydr)oxides such as goethite and hematite, both of which presenting widespread occurrence (Schaefer et al., 2008). Although (hydr)oxides seem to play an important role on SOM persistence, some specific characteristics of Oxisols might affect their ability to form protective associations with organic compounds. First, these (hydr)oxides present high crystallinity degree, which reduces their SSA significantly relative to low crystalline phases (Kaiser and Guggenberger, 2003). Second, low crystalline (hydr)oxides usually account for a minimal fraction of the total (hydr)oxides content in Oxisols (Schaefer et al., 2008). And third, the strong microstructure of these soils might block part of the reactive mineral surfaces in which SOM could be protected, although microaggregation might favor C persistence due to physical protection in Oxisols (Anda et al., 2008; Barré et al., 2014). Combined, these aspects would define specific

features of Oxisols that could affect C cycling and its persistence in tropical ecosystems.

Our conceptual approach to investigate the role of minerals for the development of mineral-organic associations within the fine fraction (<53 µm) of Oxisols consisted on performing relatively long-term incubation experiments (12 months of duration) using natural soil samples. In order to assess the incorporation of C and N within mineral-organic associations in these soils, we used double labeled plant litter (^{13}C and ^{15}N isotope tracers) that would allow us testing the hypothesis of preferential retention of N-rich compounds by reactive minerals. Such inference would be based on the relative proportion of the labels recovered within mineral-organic associations. We also tested the hypothesis that amorphous Al-/Fe-(hydr)oxides would account for most of the reactive surfaces involved in mineral-organic associations in Oxisols. Therefore, the objectives of this research were to link the relationship between litter decomposition, assess the formation and infer the persistence of mineral-organic associations in Oxisols.

3. Material and methods

Soils characterization

Briefly, the soils were collected in a transect ranging from 40 to 51° W and 18 to 20° S, but despite being relatively close to each other, these are very representative Oxisols, particularly in terms of mineralogy and texture. The selected Oxisols were either under native vegetation on forests remnants of the Mata Atlântica (Atlantic Rainforest) or in the Cerrado (savanna-like). The Typic Hapludox (THD), the Humic Hapludox (HHD) and Xanthic Hapludox (XHD) were collected within the Atlantic Rainforest biome, while the Xanthic Haplustox (XHT), the Rhodic Haplustox (RHT) and the Typic Haplustox (THT) were collected within the Cerrado biome. Further details on the vegetation traits and overall distribution of both biomes on the Brazilian territory can be found elsewhere (Ratter et al. 1997; Morellato et al. 2000). According to the Koppen classification, the climate within the Atlantic Rainforest is predominantly Aw, tropical with dry winter and for the soils within the

Cerrado is predominantly Cwa, temperate moist with dry winter and warm summer (Alvares et al. 2013). The annual precipitation is practically the same for both climate types, ranging from 1300 to 1600 mm per year (Alvares et al., 2013), although the rain season for the area under the Cwa climate type is mostly concentrated in the period from October to March. The sampling consisted on collecting the soil material at different depths (0-10, 10-20, 20-40, and 60-100 cm) and after collection, the samples were kept on plastic bags and transported to the laboratory.

Physical and mineralogical analyses

The samples were air-dried and sieved on a 2-mm screen to yield the fine earth fraction. The water holding capacity (WHC) of the soils was estimated by means of saturating 20 g of the fine earth fraction with deionized water into a 25.4 mm diameter steel ring and submitted to a tension equivalent to -30 kPa. After reaching equilibrium, the samples were weighted and dried at 105 °C for 48 hours.

The texture analysis was preceded by chemical dispersion 5 g of the fine earth fraction using 5 mL of sodium hydroxide (NaOH) 0.1 mol L^{-1} and 25 mL of deionized water into a 50 mL centrifuge tube, under continuous stirring during 16 hours at 120 rpm. After complete dispersion, the samples were wet-sieved through a 53-µm mesh screen to separate the sand- from the silt- and clay-sized fractions. The fraction <53 µm was used for quantifying clay and silt content by using the pipette method, by applying the Stoke's law. The fractions obtained were dried at 105 °C during 48 hours and weighted. Chemical properties of the soils, nutrients availability (Ca, Mg, K and P) are given in supplementary Table 1.

For the mineralogical analysis, 5 g of the fine earth fraction was dispersed into 5 mL of sodium hydroxide (NaOH) 0.1 mol L^{-1} and 25 mL of deionized water into a 50 mL centrifuge tube during 16 hours under continuous stirring at 120 rpm. After dispersion, the samples were wet-sieved through a 53 µm mesh screen to separate the sand- from the silt- and clay-sized fractions. The fractions <53 µm were dried at 45 °C, after

which 1 gram of the fraction <53 µm was treated during 18 hours at 25 °C with 50 ml of 6% (v/v) NaOCl adjusted to pH 8 to remove SOM. The residue was centrifuged at 3000 rpm for 30 minutes, washed with deionized water and this procedure was repeated three times in total (Zimmermann et al., 2007).

Finished the oxidation of organic matter, the clay fraction was separated using siphoning after the sedimentation of the silt fraction according to the Stoke's Law. After the complete separation of the silt and clay fractions, the material was dried at 45 °C and the mineralogical composition was qualitatively assessed by X-ray diffraction (XRD) using fine powdered material (<149 µm). The XRD analyses for non-oriented samples were conducted using Co-Ka radiation (λ=0.178896 nm) at 30 mA and 40 kV from a Rigaku D-MAX vertical goniometer equipped with a graphite monochromator. XRD patterns were obtained between 4 and 60° 2θ in 0.02° steps at a scan rate of 10° 2θ/min for accurate measurements of the d-spacing.

Selective dissolution of Fe-(hydr)oxides

Samples of the clay samples were submitted to selective dissolution of both amorphous and crystalline Fe-(hydr)oxides by treating the samples with ammonium oxalate (AO) and dithionite-citrate-bicarbonate (DC), respectively. The procedure to extract the amorphous Fe-(hydr)oxides consisted on treating 0.25 g of clay with 10 mL of AO 0.2 mol L^{-1} pH 3.0 in the dark. The samples were kept in the dark by covering the centrifuge tubes using aluminum foils and were shaken for 2 hours at 120 rpm. After the extraction procedure, the samples were centrifuged at 3000 rpm, the supernatant was collected and stored into centrifuge tubes to quantify the amounts of Fe and Al released during the treatment. The extraction of crystalline Fe-(hydr)oxides consisted on treating 0.25 g of clay with 10 mL do DC 0.2 mol L^{-1} in centrifuge tubes, which were kept under water bath for 30 minutes at 50 °C. Afterwards, the samples were centrifuged at 2000 rpm during 20 minutes, the supernatant collected and stored. The extraction procedure using DC was repeated three times. The amounts of Fe and Al extracted by AO and DC

were determined by Atomic Absorption Spectrometry (Varian Spectra AA, 220FS).

The clay used for the extraction of Fe-DC was used to estimate the content of kaolinite and gibbsite by thermogravimetry (Karathanasis and Harris, 1994). For this procedure, 5 mg of the clay was deposited on an alumina crucible and submitted to heat flow from 25 up to 750 °C under N_2 atmosphere flowing at 50 mL min^{-1} using a Shimadzu (model DTG60H).

^{13}C and ^{15}N isotope labeling

Briefly, the plant material used as the source of C and N in our incubation experiment was produced by growing an eucalypt hybrid (*Eucalyptus urophylla* x *Eucalyptus grandis*) under controlled conditions. Therefore, three seedlings (120-days) were grown into a 10 L vase on a nutrient solution (pH 5.5) for 18 weeks with continuous oxygen supply. For the isotope labeling, the seedlings were kept on a 448 dm^3 chamber in which the ^{13}C added by acidifying $Na_2{}^{13}CO_3$ (^{13}C at 99 atom%, Isotec Inc. Miamisburg, Ohio) with H_2SO_4. The $^{13}CO_2$ was added by preparing a $Na_2{}^{13}CO_3$ solution at 0.18 mol L^{-1} and mixed with 50 mL of H_2SO_4 3.8 mol L^{-1}. The CO_2 concentration within the chamber was kept at 500 ppm throughout the labeling experiment. The ^{15}N label was added through a nutrient solution (N-NH_4^+ 0.9 mmol L^{-1}) applied once a week, by adding $(^{15}NH_4)_2SO_4$ (98 atom% excess, Sigma-Aldrich). At the end of the isotope labeling, the seedlings were collected and separated into leaves, twigs, stem and roots (predominantly fine roots, diameter <2 mm), and dried under forced air circulation at 45 °C until constant weight. After drying, the plant material was milled to achieve a particle-size <500 µm using a Wiley mill. For further homogenization, the plant material was subsequently finely ground using a ball-mill after which the final particle-size achieved was <149 µm. The samples were analyzed using an Isotopic Ratio Mass Spectrometer (IRMS) with continuous flux (20-20, ANCA-GLS, Sercon, Crewe, UK). The C and N content, and their respective stable isotope abundance (^{13}C and ^{15}N) for each of the components of the plants are shown in Table 1.

Table 1. Components of the plant litter, their C and N content, and their respective stable isotopes concentration

Component	Mass, g[†]	C, g kg^{-1}	δ^{13}C, ‰	N, g kg^{-1}	^{15}N, atom %	C:N
Bark	21.9	425.0	318.6	5.2	81.4	82
Leaves	135.9	455.0	508.5	18.3	76.2	25
Twiggs	40.5	427.0	423.1	7.6	72.3	56
Stem	52.3	452.0	210.4	2.2	70.7	205
Roots	58.5	457.0	358.4	10.4	66.7	44
Corrected mean[‡]	-	**449.0**	**405.5**	**11.8**	**74.3**	**38**

[†]The mass of each component produced (grams per plant). The plant litter was added to the soils as a mixture, for which the amount of each component was proportional to their content on the plant grown for ^{13}C and ^{15}N labeling. [‡]The mean value was corrected considering the C and N content and the proportion of each component for total dry matter of the labeled plant.

Incubation experiment

The experimental units consisted on air tight vials (150 mL) containing 20 grams of the fine earth fraction (<2mm). The moisture content of the samples was kept at approximately 60-70% of the WHC of each soil. In terms of C inputs, we used plant litter additions at 0, 10, 20, and 40 mg g^{-1} soil (equivalent to C additions at 0.0, 4.5, 9.0, and 18 mg g^{-1} soil, respectively). For each C input, the mass of the components of the litter added was equivalent to their proportion in the whole plant, as shown in Table 1.

The incubation was carried out during 12 months in a chamber with controlled temperature (25 °C ±1). During the first 4 weeks the vessels were opened 3 times a week during 1 hour to avoid O_2 limitation for the decomposers. After the first month, the vessels were opened only once a week and the weight of the experimental units were monitored to avoid water limitation. As such, each experimental unit was weighted after every 2 weeks and compared to the total weight measured at the first day of the incubation. When necessary, deionized water was added using a pipette to assure the moisture content was kept between 60 and 70% of the WHC. For each treatment, we had 3 replicates.

Because we collected soil samples from different depths, we prepared a suspension by mixing 1 g of soil from the 0-10 cm depth into 100 mL of deionized water to inoculate the samples from the other soil layers (10-20, 20-40 and 60-100 cm depth). This procedure was done for

each soil separately to make sure there was not any substantial difference on the microbial community throughout the soil profile. Since our incubation experiment was conducted over a whole year, we do not expect that differences on the size and/or activity of the microbial community would impact on the final results reported here. However, we have not assessed any microbial biomass-related parameters to support the previous statement.

After the 12-month incubation, the samples were air-dried and physically fractionated into sand (particle-size >53 µm) and its associated particulate organic matter (POM), and the clay+silt fraction (particle-size <53 µm) and their associated organic matter. For the physical fractionation, a 5-g subsample was dispersed into a 50 mL centrifuge tube containing 15 mL of hexametaphosphate g L^{-1} and 100 mm diameter glass bead, under continuous stirring throughout 16 hours at 120 rpm. After physical fractionation, the samples were wet-sieved through a 53 µm screen, and the fractions were dried at 45 °C for 7 days. Afterwards, the samples were weighted, finely ground using an agate mortar and pestle in order to achieve a final particle-size <149 µm. The C, N content and their respective stable isotope abundance (^{13}C and ^{15}N content) were determined using an IRMS with continuous flux (20-20, ANCA-GLS, Sercon, Crewe, UK). The ^{13}C results were expressed as $\delta^{13}C$ in parts per mil (‰) with reference to the internation stardard (Pee Dee Belemnite) and the ^{15}N abundance was expressed in atom%.

Litter-derived C and N

The proportion (*f*) of litter-derived C and N in the fraction <53 µm was calculated as follows

$$f = \frac{\delta_t - \delta_s}{\delta_l - \delta_s}$$

in which δ_t is $\delta^{13}C$ of the <53 µm for the treatments receiving plant-litter, δ_s is $\delta^{13}C$ of the <53 µm in the control treatments (no plant litter addition), and δ_l is $\delta^{13}C$ of the plant litter (405.50‰). The same formula was used to assess the litter-derived N, for which the δ_l was 74.30

atom%. The total amount of litter-derived C and N associated to the <53 µm was calculated as

$$Er,\% = \left(\frac{f\ x\ Ec}{total\ input}\right) x\ 100$$

where *Er%* is the fraction of the element (C or N) recovered, expressed in percent (%), *Ec* is the total element content (C or N) associated to the <53 µm fraction in the whole 20-gram of soil sample after the incubation experiment, and *total input* is the total C or N added via plant litter.

Statistics

The influence of specific properties of the 6 Oxisols, depth of sampling, and plant litter inputs on the litter-C and N recovered, their C and N content and C:N ratio (after the 12-month incubation experiment) were assessed by means of analysis of variance (ANOVA). The effects of mineralogy on SOM were assessed by means of simple correlation analyses. The statistical analyses were performed using the Statistica® 13 and the artwork was prepared on Sigma Plot® 11.

4. Results

Oxisols mineralogy

The texture and mineralogy of the clay fraction of the selected Oxisols are presented in Table 2. Most of the minerals occurring in the clay-sized fraction of the selected Oxisols were also present on the silt-sized fraction, as determined by XRD analyses (Supplementary Figures 1 and 2). Such overlapping cannot be attributed to problems during the siphoning of the clay fraction because the silt content was low for most of the soils. For some Oxisols, however, the high silt content is due to their strong microaggregation, because even after organic matter oxidation the silt content remained quite high (as observed for the HHD and RHT, Table 2). The XRD data confirms that the high silt content is mostly due to “pseudo-silt” in these soils (Supplementary Figure 2) because other than quartz, the same minerals occur both in the clay and silt fractions.

Table 2. Oxisols texture (sand, silt and clay content), extractable Al and Fe by ammonium oxalate (AO) and dithionite-citrate-bicarbonate (DC) and kaolinite and gibbsite content within the clay fraction

Oxisol	Depth	Sand	Silt	Clay	Al_{AO}†	Fe_{AO}†	Al_{DC}†	Fe_{DC}†	Kaolinite‡	Gibbsite‡	Texture Class
	cm	g kg^{-1} soil									
Typic Hapludox-THD	0-10	363.8	33.1	603.2	0.8	0.7	12.2	49.1	439.5	32.1	Clay
	10-20	289.8	33.7	676.7	0.9	0.9	15.1	54.3	493.1	36.1	Clay
	20-40	249.3	31.6	719.2	1.0	0.8	13.2	54.8	524.1	38.3	Clay
	60-100	234.4	31.1	734.6	1.1	0.5	14.0	56.9	535.2	39.1	Clay
Humic Hapludox-HHD	0-10	324.9	78.4	596.8	4.1	2.2	14.5	36.2	354.4	136.3	Clay
	10-20	355.3	55.4	589.4	3.9	2.2	13.6	37.9	350.0	134.6	Clay
	20-40	316.0	51.4	632.7	4.4	2.5	15.2	40.2	375.8	144.5	Clay
	60-100	307.9	34.7	657.5	3.3	1.7	15.2	47.7	390.5	150.2	Clay
Xanthic Hapludox-XHD	0-10	752.8	24.2	223.1	0.4	0.2	1.6	4.9	200.9	1.2	Sand clay loam
	10-20	629.0	38.2	332.9	0.6	0.3	2.7	7.6	299.8	1.8	Sandy clay
	20-40	622.8	38.0	339.3	0.5	0.3	2.5	7.9	305.5	1.8	Sandy clay
	60-100	606.8	35.7	357.6	0.7	0.2	2.8	9.2	322.0	1.9	Sandy clay
Xanthic Haplustox-XHT	0-10	395.9	86.6	517.6	2.5	0.6	4.2	11.7	176.3	303.8	Clay
	10-20	388.6	80.0	531.5	1.8	0.5	3.6	10.7	181.3	311.9	Clay
	20-40	378.6	59.4	562.1	2.4	0.7	3.9	11.8	191.5	329.9	Clay
	60-100	393.0	44.4	562.6	2.3	0.6	3.6	11.3	191.7	330.2	Clay
Rhodic Haplustox-RHT	0-10	195.5	205.1	599.4	3.9	3.7	12.2	103.6	224.5	122.8	Clay
	10-20	154.9	236.6	608.6	3.6	3.8	12.8	103.6	227.9	124.7	Clay
	20-40	169.2	223.5	607.4	3.2	3.7	13.0	105.2	227.5	124.5	Clay
	60-100	212.1	202.2	585.8	2.8	3.4	12.8	106.8	219.4	120.1	Clay
Typic Haplustox-THT	0-10	580.1	60.0	359.9	1.0	0.8	2.2	24.6	297.3	1.3	Sandy clay
	10-20	635.0	51.1	313.9	0.9	0.6	2.0	22.2	259.0	1.1	Sandy clay loam
	20-40	644.1	53.5	302.5	0.8	0.5	1.7	19.0	249.6	1.1	Sandy clay loam
	60-100	553.0	72.1	375.0	0.7	0.4	2.0	22.1	309.4	1.3	Sandy clay

†Element content within the clay fraction, expressed in g kg^{-1} soil. The conversion of Al into Al_2O_3 and Fe into Fe_2O_3 can be achieved by multiplying the element content by (102 ÷ 54) and (160 ÷ 112), respectively. ‡Estimated by means of thermogravimetry using the clay fraction after Fe removal by DC.

Within the silt- and sand-sized fractions, quartz was the predominant mineral, and it does not occur in the clay fraction of Oxisols (Schaefer et al., 2008). In the clay fraction, kaolinite was the only phyllosilicate present and it was of ubiquitous occurrence in the 6 selected Oxisols, although its amounts varied considerably among these soils (Table 2). Other than kaolinite, the clay fraction also presented variable amounts of Al- and Fe-(hydr)oxides. Based on X-ray diffraction, the only Al-(hydr)oxide present in the samples was gibbsite (γ-$Al(OH)_3$). Among the Fe-(hydr)oxides, goethite (α-FeOOH) and hematite (α-Fe_2O_3) were the main minerals identified. Anatase (TiO_2), ilmenite ($FeTiO_3$) and maghemite (γ-Fe_2O_3) also were detected in both clay- and silt-sized fractions (Supplementary Figures 1 and 2).

Litter-derived C and N in the fraction <53 µm

Relative to the initial input, the proportion of C and N recovered within the fraction <53 µm was 23.7 and 37.3%, respectively (Fig 1).

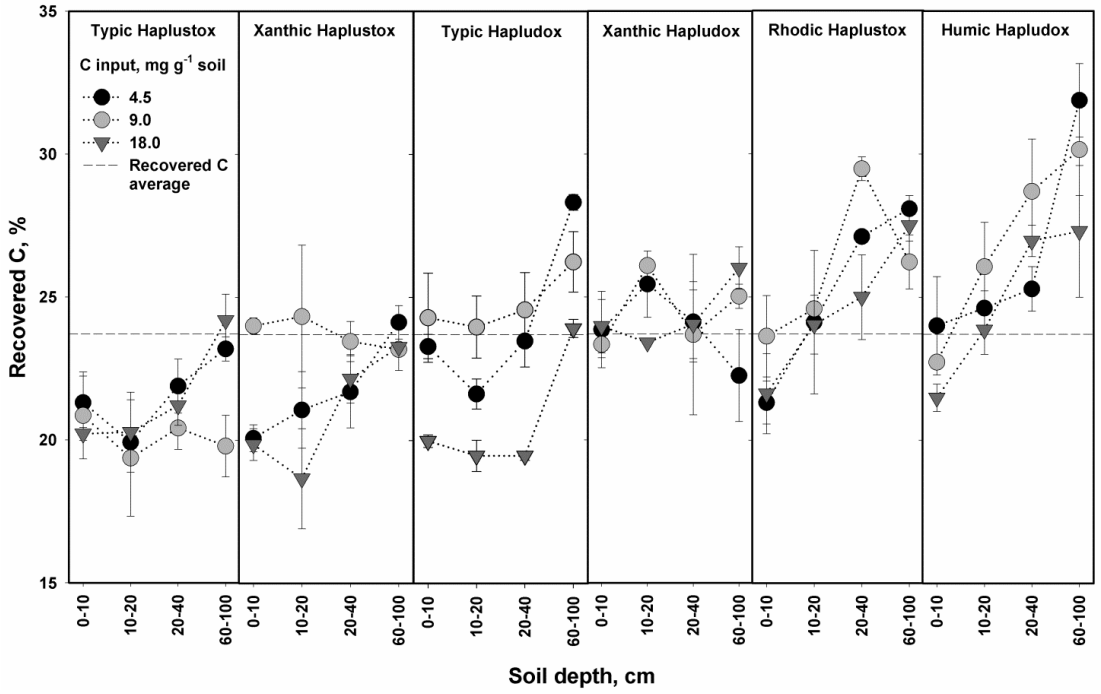

Figure 1. Litter-C recovered within the mineral fraction (<53 µm), expressed as a percentage of the initial input (via plant litter) ranging from 4.5 up to 18 mg g^{-1} soil applied in samples collected at 0-10, 10-20, 20-40 and 60-100 cm depth in 6 Oxisols. The vertical bars denote the standard error of the means, n=3. The average amount of C recovered across the soils was 23.7% of the initial input.

Among the Oxisols, the recovered C fraction was significantly higher ($P<0.01$) in the RHT and in the HHD. In these soils, the recovered C fraction was 25.2 and 26.1% in the RHT and in the HHD, respectively (Fig 1). In contrast, the proportion of the added C recovered within the fine fraction was significantly lower ($P<0.01$) in the THT and in the XHT. The mean values for the recovered C fraction in these soils were 21.0 and 22.1%, respectively (Fig 1). For the THD and the XHD, the averaged amounts of the C added recovered within the mineral fraction were 23.2 and 24.3%.

We also observed significant differences among the Oxisols for the N recovered within the fraction <53 µm (Fig 2).

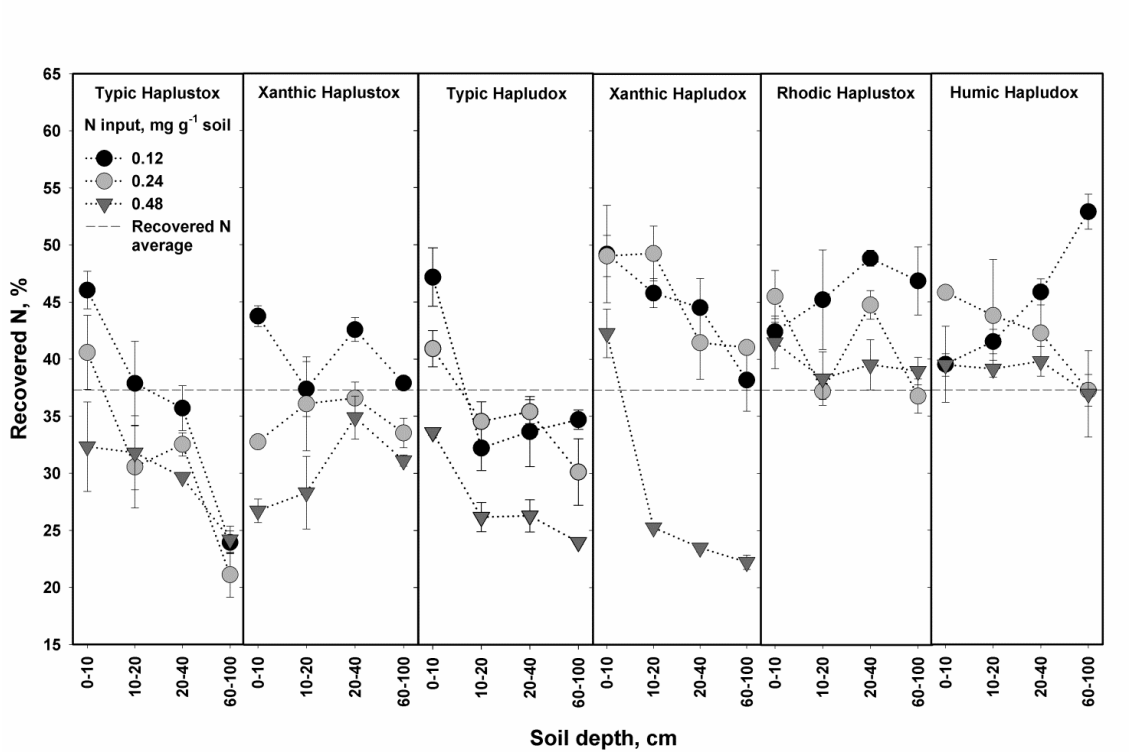

Figure 2. Litter-N recovered within the mineral fraction (<53 µm), expressed as a percentage of the initial input (via plant litter) ranging from 0.12 up to 0.48 mg g^{-1} soil applied in samples collected at 0-10, 10-20, 20-40 and 60-100 cm depth in 6 Oxisols. The vertical bars denote the standard error of the means, n=3. The average amount of C recovered across the soils was 37.3% of the initial input.

As such, the HHD and RHT were the soils with higher N recovery ($P<0.01$), which were about 42.0 and 42.2% relative to the initial input. In the XHD, the recovered N was approximately 39.3% while lower mean values were observed for the THT, XHT and for the THD. In the latter

soils, the recovered N within the fine fraction was 32.2, 33.2 and 35.1% of the initial input, respectively. Therefore, the variability among the Oxisols was proportionally higher for the recovered N as compared to the recovered C fraction. The main aspect related to the variability on the recovered N among the soils was due to the addition of the plant litter to samples collected at different depths (Fig 2).

In terms of absolute values, the C recovered varied from about 18 up to 32% of the initial input (Fig 2). As such, in the soils with higher incorporation of C in the fine fraction (in the HHD and in the RHT), the recovered C fraction increased significantly with depth (Fig 2). Although, similar trend occurred for the soils with lower C recovery (the THT and the XHT), the amount of C incorporated into the fine fraction was somewhat less affected by soil depth (Fig 1). Additionally, the variability on the recovered C was much more significant for the THT, the XHT, the THD and for the XHD. The differences among the Oxisols were even higher with respect to the incorporation of N with increasing soil depth. In contrast to the recovered C in the HHD and in the RHT, the incorporation of N has not increased systematically with depth, except at the lower addition of plant litter (N input equivalent to 0.12 mg g^{-1} soil). In the other 4 Oxisols (THT, XHT, THD and XHD) the recovered N decreased significantly with both increasing plant litter inputs and soil depth (Fig 2). The abundance of the ^{13}C and ^{15}N isotopes within the fraction <53 µm after the incubation experiment are given in Supplementary Fig 3 and 4.

Those differences observed for the total amounts of C and N recovered within the fine fraction were reflected on the C:N ratio of the labeled SOM. Among the studied Oxisols, lower C:N ratios were observed for the RHT and for the HHD, with lower variability as a function of soil depth or litter input levels (Fig 3).

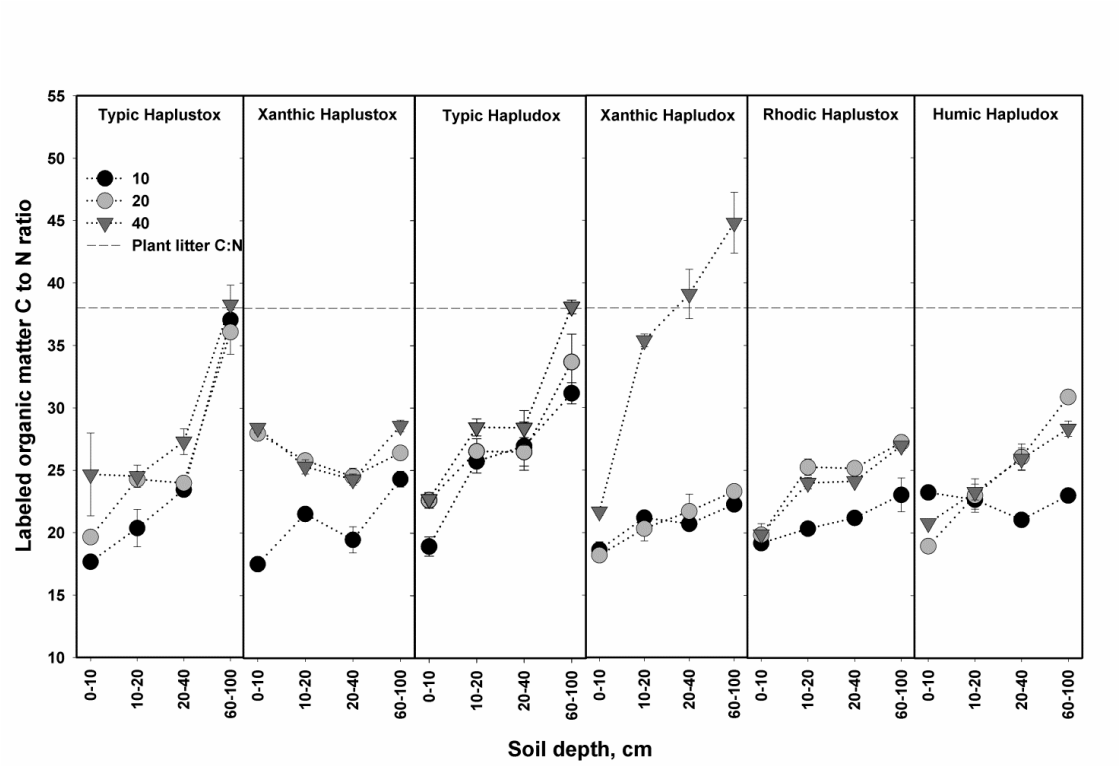

Figure 3. Labeled organic matter (^{13}C and ^{15}N) C to N ratio within the mineral fraction (<53 µm) as affected by plant litter input ranging from 10 up to 40 mg g^{-1} soil applied in samples collected at 0-10, 10-20, 20-40 and 60-100 cm depth in 6 Oxisols. For simplicity, the plant litter input is expressed in dry matter to illustrate its C:N ratio. The vertical bars denote the standard error of the means, n=3. The averaged C to N ratio of the plant litter used for the incubation experiment (C:N=38).

The average C:N ratio for the labeled SOM in these soils varied between 20 and 30:1, with higher values observed for the deeper soil layers. Similarly, in the XHT the labeled SOM also presented a C:N ratio ranging from about 20 to 30:1, which was corroborated by the lower percentage of recovered C in this soil (Fig 1). In the XHD, the C:N ratio was remarkably low, ranging from about 20 to 25:1 irrespective of depth for plant litter inputs ranging from 10 and 20 mg g^{-1} soil. However, for the highest litter input (40 mg g^{-1} soil), the C:N varied substantially from 22 in the 0-10 cm depth up to 45:1 in 60-100 cm depth layer. Also in the THT and in the THD, the C:N increased substantially with soil depth, ranging from 20 to 25:1 in the 0-10 cm depth up to 38:1 at the 60-100 cm depth layer (Fig 3).

Combined, the incorporation of C and N and the respective C:N ratio of the labeled SOM, suggest a significant N-enrichment within the mineral fraction (Fig 1, 2, and 3). The averaged efficiency of N incorporation was about 60% higher than for C throughout the incubation experiment. Although we observed some significant variability among the Oxisols, such tendency indicates that most of the organic matter left in associations with minerals was first incorporated by the microbial biomass. It was also interesting that with increasing soil depth, the litter-C recovered increased substantially, while the opposite occurred for litter-N, except for the RHT and for the HHD.

As a result of C and N incorporation from the decomposing plant litter, some significant increments occurred for both elements within the fraction <53 µm in all Oxisols (Supplementary Table 2). Irrespective of soil depth, higher increments occurred in the treatments receiving the highest C inputs (18 mg g^{-1} soil). Overall, the same trend occurred for N, despite its higher variability as compared to C particularly with respect to different litter inputs and soil depth. However, given the higher addition of C compared to N the magnitude of the increment of the former element was slightly higher as previously demonstrated.

The influence of Oxisols' mineralogy on SOM

The correlations among minerals and SOM parameters in the Oxisols are shown in Table 3. According to these analyses, soil organic carbon (SOC) presented better correlations with amorphous Al-/Fe-(hydr)oxides than with clay, kaolinite, gibbsite or even with crystalline Fe-(hydr)oxides content. While the correlation coefficients among SOC content, Al_{AO} and Fe_{AO} were 0.80 and 0.67, respectively, for clay, Al_{DC}, Fe_{DC}, kaolinite and gibbsite, these coefficients were 0.42, 0.56, 0.41, -0.04, and 0.30, respectively. All of these coefficients were highly significant ($P<0.01$), except for kaolinite ($P<0.47$). Despite representing only a small amount of the whole fine fraction mass (Table 2), amorphous Al-/Fe-(hydr)oxides seem to be highly effective in protecting SOM in Oxisols (Table 3).

Table 3. Person's correlation coefficients between mineral parameters and organic matter within the fine fraction (<53 µm) in 6 Oxisols

n[a]		Clay	Al_{DC}	Fe_{DC}	Al_{AO}	Fe_{AO}	$Al+Fe_{AO}$	Kaolinite	Gibbsite	^{15}N	$N^{\#}$	$N^{\S}$	C:N	^{13}C	$C^{\#}$	$C^{\S}$
24	Clay[b]	1														
24	Al_{DC}[b]¶	0.87^{***}	1													
24	Fe_{DC}[b]¶	0.59^{***}	0.73^{***}	1												
24	Al_{AO}[b]†	0.57^{***}	0.62^{***}	0.52^{***}	1											
24	Fe_{AO}[b]†	0.49^{***}	0.66^{***}	0.87^{***}	0.81^{***}	1										
24	$Al+Fe_{AO}$[b]	0.56^{***}	0.67^{***}	0.72^{***}	0.96^{***}	0.95^{***}	1									
24	Kaolinite[b]‡	0.47^{***}	0.56^{***}	0.11^{*}	-0.18^{***}	-0.15^{***}	-0.18^{***}	1								
24	Gibbsite[b]‡	0.41^{***}	$0.07^{}$	-0.03^{ns}	0.56^{***}	0.19^{***}	0.40^{***}	-0.46^{***}	1							
288	^{15}N[c]	-0.24^{***}	-0.27^{***}	-0.02^{ns}	-0.26^{***}	-0.24^{***}	-0.26^{***}	-0.04^{ns}	-0.12^{**}	1						
288	$N^{\#}$	-0.15^{***}	0.10^{*}	0.04^{ns}	0.29^{***}	0.25^{***}	0.28^{***}	-0.15^{***}	-0.08^{ns}	-0.20^{***}	1					
288	$N^{\S}$	0.39^{***}	0.54^{***}	0.51^{***}	0.69^{***}	0.68^{***}	0.72^{***}	-0.03^{ns}	0.17^{***}	-0.32^{***}	0.74^{***}	1				
288	C:N	-0.01^{ns}	-0.14^{**}	-0.31^{***}	0.15^{***}	-0.16^{***}	0.00^{ns}	-0.15^{***}	0.37^{***}	0.44^{***}	-0.41^{***}	-0.41^{***}	1			
288	^{13}C[d]	-0.21^{***}	-0.26^{***}	-0.18^{***}	-0.32^{***}	-0.27^{***}	-0.31^{***}	0.02^{ns}	-0.16^{***}	0.97^{***}	-0.27^{***}	-0.36^{***}	0.42^{***}	1		
288	$C^{\#}$	-0.14^{**}	0.10^{ns}	-0.09^{ns}	0.38^{***}	0.22^{***}	0.32^{***}	-0.16^{***}	0.04^{ns}	-0.10^{ns}	0.94^{***}	0.67^{***}	-0.13^{**}	-0.19^{***}	1	
288	$C^{\S}$	0.42^{***}	0.57^{***}	0.41^{***}	0.80^{***}	0.67^{***}	0.77^{***}	-0.04^{ns}	0.30^{***}	-0.25^{***}	0.71^{***}	0.95^{***}	-0.16^{***}	-0.31^{***}	0.74^{***}	1

[a]The number of observations (n) for mineral parameters were 24 (6 Oxisols at 4 depths) and for organic matter variables, the number of observations were 288 (6 Oxisols, 4 depths, 4 litter inputs and 3 replicates). [b]Minerals content within the clay fraction expressed in gkg^{-1} soil; [c]Atom%; [d]Delta PDB (‰); [#]C and [#]N concentration in the fraction (<53 µm), expressed in g kg^{-1} of fraction; [§]C and [§]N content in the fraction (<53 µm), expressed in g kg^{-1} soil; ¶DC, dithionite-citrate-bicarbonate; †AO, Ammonium oxalate; ‡Content estimated from thermogravimetry. Coefficients followed by ***, **, * are significant at P<0.01, P<0.05 and P<0.10 level respectively; ^{ns}, non-significant (P>0.10).

Color code	Correlation coefficient range (+)	Color code	Correlation coefficient range (-)
	>0.75		>0.75
	0.45-0.74		0.45-0.74
	0.30-0.44		0.30-0.44
	0.29-0.15		0.29-0.15
	<0.15		<0.15

The correlation coefficient ranges were defined arbitrarily.

Even more intriguing is that the total amount of Al-/Fe-(hydr)oxides is considerably lower than the SOC content itself. For example, the SOC content increased exponentially with Al_{AO} content (Fig 4; R^2=0.76, P<0.01).

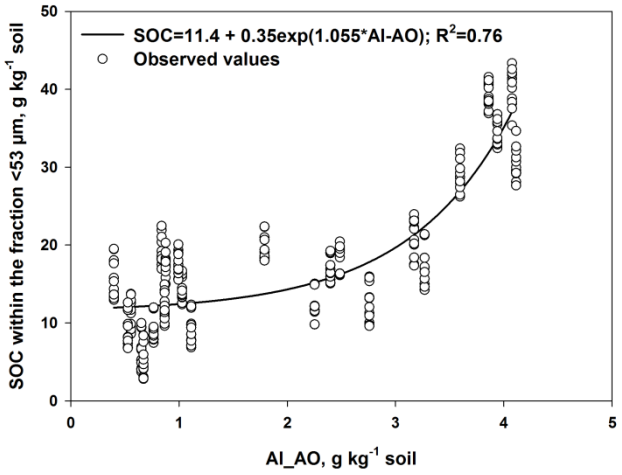

Figure 4. Correlation between Al extractable by ammonium oxalate (Al-AO) in the clay fraction (fraction <2 µm) and the SOC content in the fraction <53 µm. All parameter shown in the fitted regression are significant at P<0.02 according to the t test.

Despite the litter-N being retained at higher efficiency than C, the correlations among N content and the mineralogical parameters followed the same trend as observed for the SOC content (Table 3). Fe_{DC} was the only mineralogical parameter that seemed to present better relationship with N content as compared to SOC (r=0.51 and r=0.41, respectively).

Some characteristics of the samples and the correlations among mineral parameters and C and N content, suggest that in fact these (hydr)oxides are very important for the development of mineral-organic associations in Oxisols. As such, isomorphic substitution of Fe by Al on the structure of amorphous and crystalline Fe-(hydr)oxides may contribute to increase their SSA (Norrish and Taylor, 1961), which may increase the availability of reactive surfaces to interact with SOM. For instance, Al-DC and Al-AO presented slightly better correlations with SOM than Fe-AO or Fe-DC (Table 2). Since the Al is released in the procedures used to dissolve Fe-(hydr)oxides, the most simple

explanation would be that Al occurs as a Fe substituent within these minerals structures (Schulze, 1984). Amorphous Al- and Fe-(hydr)oxides also presented higher correlation with their crystalline counterparts than with clay, kaolinite or gibbsite content. It is possible that the amorphous fractions occur as an external layer enclosing the crystalline core of these (hydr)oxides. Thus, while AO would dissolve only the outer region of crystalline (hydr)oxides, DC would dissolve both the outer (amorphous material) and the crystalline core at once.

From a quantitative point of view, the newly developed mineral-organic associations were much smaller than the preexisting SOM. For this reason, it would not be advisable to conclude that these (hydr)oxides are also part of the newly developed mineral-organic associations. In order to verify the influence of Al-/Fe-(hydr)oxides on the development of mineral-organic associations, we performed correlations among these variables and the recovered C and N (Table 4). By proceeding this way, we would exclude the influence of the unlabeled SOM on the correlations. As such, it seems that these minerals are in fact actively involved in the formation of mineral-organic associations, since the correlations among these components and the recovered C and N remained strong even with decreasing content of unlabeled SOM at deeper soil layers (Table 4).

Actually, the correlations among the minerals (amorphous and even crystalline Al-/Fe-(hydr)oxides) and the recovered C and N, only were significant for the soil samples collected at 20-40 and 60-100 cm depth (Table 4). Therefore, the strong correlations observed for Al-/Fe-AO when we included all data in a single analysis was not due to the influence of the unlabeled SOM only. Interestingly, for the recovered C and N in the 0-10 and 10-20 cm depth, the correlations were considerably weaker as compared to the samples collected at 20-40 and 60-100 cm depth (Table 4).

Table 4. Person's correlation coefficients among mineral parameters and the percentage of litter C and N recovered within the fine fraction (<53 µm) in the Oxisols grouped by soil depth (0-10, 10-20, 20-40 and 60-100 cm)

	0-10 cm		10-20 cm		20-40 cm		60-100 cm	
Variable[a]	**C**	**N**	**C**	**N**	**C**	**N**	**C**	**N**
Clay	-0.10^{ns}	-0.24^{*}	0.12^{ns}	-0.03^{ns}	0.30^{**}	0.20^{ns}	0.51^{***}	0.30^{**}
Al_{DC}	0.10^{ns}	0.04^{ns}	0.22^{ns}	0.06^{ns}	0.51^{***}	0.31^{**}	0.70^{***}	0.44^{***}
Fe_{DC}	-0.01^{ns}	0.10^{ns}	0.16^{ns}	0.11^{ns}	0.46^{***}	0.33^{**}	0.47^{***}	0.36^{***}
Al_{AO}	-0.04^{ns}	-0.09^{ns}	0.33^{**}	0.33^{**}	0.57^{***}	0.56^{***}	0.57^{***}	0.63^{***}
Fe_{AO}	-0.01^{ns}	0.09^{ns}	0.30^{**}	0.28^{**}	0.64^{***}	0.56^{***}	0.48^{***}	0.53^{***}
$Al+Fe_{AO}$	-0.03^{ns}	-0.01^{ns}	0.33^{**}	0.32^{**}	0.64^{***}	0.58^{***}	0.56^{***}	0.62^{***}
Kaolinite	0.03^{ns}	0.01^{ns}	0.04^{ns}	-0.14^{ns}	-0.01^{ns}	$-.25^{*}$	0.25^{*}	-0.16^{ns}
Gibbsite	-0.15^{ns}	-0.39^{***}	-0.02^{ns}	0.00^{ns}	0.10^{ns}	0.29^{**}	0.07^{ns}	0.32^{**}

[a]The number of observations for mineral parameters were 6 (6 Oxisols) and for SOM parameters, the number of observations were 54 (6 Oxisols, 3 litter inputs and 3 replicates). The units of all parameters are the same as presented in Table 3. Coefficients followed by ***, **, * are significant at P<0.01, P<0.05 and P<0.10 respectively; ^{ns}, non-significant (P>0.10).

C olor code	Correlation coefficient (+)	C olor code	Correlation coefficient (-)
	>0.75		>0.75
	0.45-0.74		0.45-0.74
	0.30-0.44		0.30-0.44
	0.29-0.15		0.29-0.15
	<0.15		<0.15

The correlation coefficient ranges were defined arbitrarily.

In two of the Oxisols (HHD and RHT) we observed a significantly higher accumulation of the C and N added. In comparison to the other Oxisols evaluated, the incorporation of C and N in these soils was relatively uniform, either as a function of litter inputs or soil depth (Fig 2 and 3). Despite the relative uniform incorporation of C and N into mineral-organic associations in the HHD and in the RHT, their chemical properties were highly different (Table 2; Supplementary Table 1). As such, the natural fertility (including pH and exchangeable Ca and Mg content) of the RHT was much higher than for HHD. Furthermore, the Fe extracted by DC and AO is much higher in the RHT (Table 2). In terms of mineralogy, the higher Fe content in the RHT favors the formation of hematite, which seems absent in the HHD (Supplementary Figures 1 and 2). Other than hematite, their content of kaolinite and gibbsite are reasonably similar, although the phyllosilicate is more abundant in the HHD. Despite these soils presenting much more differences than similarities, they have in common very similar amounts of Al-/Fe-AO and Al-/Fe-DC (Table 2). Thus, it is reasonable that the occurrence of these minerals might favor, directly or indirectly, the accumulation of C and N in mineral organic associations in Oxisols.

5. Discussion

Linking plant-litter decomposition to SOM formation

In our study, we observed that approximately 23.7% of the litter-C and 37.3% of the litter-N added was recovered in associations within the mineral matrix after the 12-month incubation experiment. In a similar incubation experiment conducted over 8 months, Diochon *et al.* (2016) observed that approximately about 12% of the C added via plant litter (barley, *Hordeum vulgare* L.) was retained within the silt- and clay-sized fractions in a Canadian Eutric Cambissol. In this study, while the C:N ratio of the plant litter was approximately 40:1, the C:N ratio of mineral-organic associations developed was 20 units lower. Such, reduction in the C:N from the plant litter towards the mineral-associated C, also suggests a higher accumulation of N as we observed in our Oxisols.

Although our study was limited to plant litter decomposition within 12 months under laboratory conditions, similar trend indicating higher accumulation of litter-N relative to C also has been reported for field-based experiments. As such, Cotrufo *et al.* (2015) conducted a 3-year decomposition experiment in a temperate Grassland in Kansas, USA. In this study, approximately 20% of the C and 58% of the N added via plant litter (big bluestem, *Andropogon gerardii*) was transferred into the fraction <2mm in the soil. Furthermore, Hatton *et al.* (2015a) also reported higher accumulation of litter-N relative to litter-C within SOM light fraction (density <1.75 g cm^3), and the operationally defined "humic" and "humin" fractions, in a 5-year field experiment conducted in an Ultic Haploxeralf under a mixed conifer temperate forest in California, USA. Relative to our study, some of the results reported here, were generated under conditions significantly different with regard to the experimental setup (soils, climate conditions, plant litter types) and fractionation procedures to isolate SOM fractions. Yet, all these reports have in common the concentration of N relative to C during the decomposition of the plant litter. Such common trend is in line with the hypothesis of a strong influence of soil microbial community processing plant litter decomposition (Bird et al., 2008; Hatton et al., 2012, 2015a; Cotrufo et al., 2015; Diochon et al., 2016).

Throughout our incubation experiment, a series of events probably contributed for the different incorporation rates for C and N in mineral organic associations (Fig 1 and 2). Initially, the plant litter added probably was depolymerized into smaller biopolymers down to monomers due to enzymatic activity (Hedges and Keil, 1999). Therefore, as the enzymatic breakdown progressed, the components of the plant litter became smaller and with higher ability to dissolve in water. This is important because as the solubility in water increases, the diffusion of these compounds also increases, which may facilitate their assimilation by soil microbes (Kleber et al., 2015). Once the organic compounds are small enough to be absorbed by soil microbes (<500 Da), these compounds can be either respired or converted into biomass (Hedges and Keil, 1999). However, after the addition of C via plant litter containing a

relatively complex mixture of compounds, it is difficult to predict the exact proportion of C that is converted into biomass or CO_2. This is mainly because the partitioning between microbial anabolism and respiration can be affected by a range of factors, including substrate chemistry and temperature (Frey et al., 2013). Throughout our incubation experiment, the litter-C fraction effectively assimilated into microbial biomass may have become associated to minerals by deliberate attachment of microbes and/or due the production of EPS (Fig 5). The production of EPS specifically, is often related to the attachment of microbial colonies onto mineral surfaces.

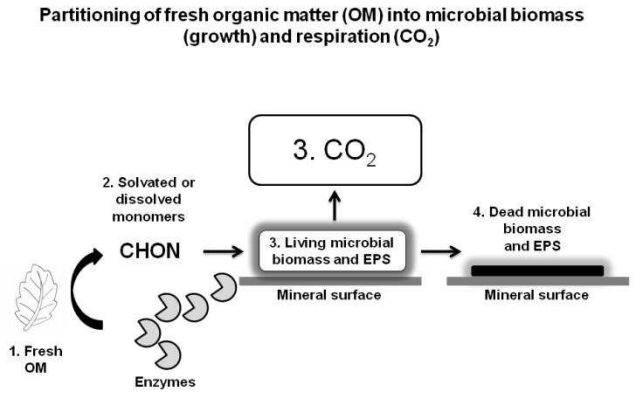

Figure 5. The fresh organic matter (OM) added to the soil (1) is depolymerized by microbial enzymes; become dissolved or solvated (2), and is subsequently partitioned into microbial biomass (growth) and respiration (CO_2) (3); and the mineral-organic associations would be formed after deliberate attachment of microbes onto mineral surfaces and/or EPS production, used for cell adherence onto the mineral surface. In Oxisols, Al-/Fe-(hydr)oxides seem to play a critical role on the formation and persistence of these mineral-organic associations. EPS=Extracellular polymeric substances. Adapted from Kleber et al. (2015).

Conversely, direct preservation of the plant material within the soil mineral matrix is also possible (Cotrufo et al., 2015) and its occurrence cannot be ruled out in our incubation experiment. However, there is strong evidence that in aerobic soils, biotic processing is the major driver leading to the formation of mineral-organic associations (Mambelli et al., 2011; Hatton et al., 2015b). For instance, had the

abiotic preservation being the predominant process leading to the development of mineral-organic associations in our study, there would be no such a big difference in terms of the amount of C and N recovered within the fine fraction. In such scenario, the newly developed mineral-organic associations should have a C:N similar to that in the original plant litter.

The relative concentration of N with respect to C during plant litter decomposition is a common feature among many terrestrial ecosystems and it seems that such pattern is a result from interactions between reactive minerals and N-rich compounds (Keiluweit et al., 2012). This suggests that after the plant material being incorporated by the microbial biomass, further interactions between the resynthesized organic compounds and minerals may render the N-rich compounds (temporarily) inaccessible. The mechanisms underlying such inaccessibility of N may be attributed to chemical interactions between N-containing functional groups (e.g., amide) and reactive mineral surfaces (Keiluweit et al., 2012; Liu et al., 2013; Kleber et al., 2015). Additionally, structural conformation of microbial proteins that are not prone to dissolve in the soil water also may persist in soils due to its hydrophobicity (Masoom et al., 2016). With regard to the reactive minerals in Oxisols, it seems that Al-/Fe-(hydr)oxides with low crystallinity degree may be among the main drivers of the development of mineral-organic associations, particularly those enriched in N (Keiluweit et al., 2012; Kleber et al., 2015).

6. Conclusions and implications for C cycling in the tropics

Our data points out to some specific interactions that contribute for the formation of SOM in Oxisols. It seems that most of the C and N within the plant litter is incorporated by soil microbes, before being retained in mineral-organic associations, specifically with amorphous Al-/Fe-(hydr)oxides. These components presented good correlation with both, the total SOM in the Oxisols, i.e. unlabeled SOM and the labeled mineral-organic associations developed throughout the incubation experiment. The main aspect regarding the amorphous Al-/Fe-

(hydr)oxides is that they contribute to very small amount of the fraction <53 µm in Oxisols. For this reason, the total C stored in the tropics, which is about 30% of the global soil C stock (Jobbágy and Jackson, 2000) may be highly sensitive to environmental changes in the long-term. However, since our dataset was restricted to 6 Oxisols only, further research is still needed to improve the current understanding on the drivers of mineral-organic associations in these soils and their influence on C cycling in tropical environments.

7. References

Alvares, C.A., J.L. Stape, P.C. Sentelhas, J.L. De Moraes Gonçalves, and G. Sparovek. 2013. Köppen's climate classification map for Brazil. Meteorol. Zeitschrift 22(6): 711–728.

Anda, M., J. Shamshuddin, I.C. Fauziah, and S.R. Syed Omar. 2008. Pore space and specific surface area of heavy clay oxisols as affected by their mineralogy and organic matter. Soil Sci. 173(8): 560–574.

Baldock, J.., and J.. Skjemstad. 2000. Role of the soil matrix and minerals in protecting natural organic materials against biological attack. Org. Geochem. 31(7-8): 697–710.

Barré, P., O. Fernandez-Ugalde, I. Virto, B. Velde, and C. Chenu. 2014. Impact of phyllosilicate mineralogy on organic carbon stabilization in soils: incomplete knowledge and exciting prospects. Geoderma 235-236: 382–395.

Bird, J.A., M. Kleber, and M.S. Torn. 2008. 13C and 15N stabilization dynamics in soil organic matter fractions during needle and fine root decomposition. Org. Geochem. 39(4): 465–477.

Cotrufo, M.F., J.L. Soong, A.J. Horton, E.E. Campbell, M.L. Haddix, D.H. Wall, and W.J. Parton. 2015. Formation of soil organic matter via biochemical and physical pathways of litter mass loss. Nat. Geosci. 8(10): 776–779.

Cotrufo, M.F., M.D. Wallenstein, C.M. Boot, K. Denef, and E. Paul. 2013. The microbial efficiency-matrix stabilization (MEMS) framework integrates plant litter decomposition with soil organic

matter stabilization: do labile plant inputs form stable soil organic matter? Glob. Chang. Biol. 19(4): 988–95.

Diochon, A., A.W. Gillespie, B.H. Ellert, H.H. Janzen, and E.G. Gregorich. 2016. Recovery and dynamics of decomposing plant residue in soil: an evaluation of three fractionation methods. Eur. J. Soil Sci. 67(2): 196-205.

Doetterl, S., A. Stevens, J. Six, R. Merckx, K. Van Oost, M. Casanova Pinto, A. Casanova-Katny, C. Muñoz, M. Boudin, E. Zagal Venegas, and P. Boeckx. 2015. Soil carbon storage controlled by interactions between geochemistry and climate. Nat. Geosci. 8(10):780-783.

Dungait, J.A.J., D.W. Hopkins, A.S. Gregory, and A.P. Whitmore. 2012. Soil organic matter turnover is governed by accessibility not recalcitrance. Glob. Chang. Biol. 18(6): 1781–1796.

Feller, C., and M.H. Beare. 1997. Physical control of soil organic matter dynamics in the tropics. Geoderma 79(1-4): 69–116.

Fierer, N., M.S. Strickland, D. Liptzin, M.A. Bradford, and C.C. Cleveland. 2009. Global patterns in belowground communities. Ecol. Lett. 12(11): 1238–1249.

Frey, S.D., J. Lee, J.M. Melillo, and J. Six. 2013. The temperature response of soil microbial efficiency and its feedback to climate. Nat. Clim. Chang. 3(4): 395–398.

Grandy, A.S., and J.C. Neff. 2008. Molecular C dynamics downstream: The biochemical decomposition sequence and its impact on soil organic matter structure and function. Sci. Total Environ. 404(2-3): 297–307.

Hatton, P.J., C. Castanha, M.S. Torn, and J.A. Bird. 2015a. Litter type control on soil C and N stabilization dynamics in a temperate forest. Glob. Chang. Biol. 21(3): 1358–1367.

Hatton, P., M. Kleber, B. Zeller, C. Moni, A.F. Plante, K. Townsend, L. Gelhaye, K. Lajtha, and D. Derrien. 2012. Transfer of litter-derived N to soil mineral–organic associations: Evidence from decadal 15N tracer experiments. Org. Geochem. 42(12): 1489–1501.

Hatton, P.-J., L. Remusat, B. Zeller, E. a. Brewer, and D. Derrien. 2015b. NanoSIMS investigation of glycine-derived C and N retention with soil organo-mineral associations. Biogeochemistry 125(3): 303–313.

Heckman, K., a. S. Grandy, X. Gao, M. Keiluweit, K. Wickings, K. Carpenter, J. Chorover, and C. Rasmussen. 2013. Sorptive fractionation of organic matter and formation of organo-hydroxy-aluminum complexes during litter biodegradation in the presence of gibbsite. Geochim. Cosmochim. Acta 121: 667–683.

Hedges, J.I., and R.G. Keil. 1999. Organic geochemical perspectives on estuarine processes: Sorption reactions and consequences. Mar. Chem. 65(1-2): 55–65.

Janzen, H.H. 2015. Beyond carbon sequestration: soil as conduit of solar energy. Eur. J. Soil Sci. 66(1): 19–32.

Jobbágy, E., and R. Jackson. 2000. The vertical distribution of soil organic carbon and its relation to climate and vegetation. Ecol. Appl. 10(2): 423–436.

Kaiser, K., and G. Guggenberger. 2003. Mineral surfaces and soil organic matter. Eur. J. Soil Sci. 54(2): 219–236.

Karathanasis, A.D., and W.G. Harris. 1994. Quantitative thermal analysis of soil materials. p. pp–360–411. *In* Amonette, J.E., Zelazny, L.W. (eds.), Quantitative methods in soil mineralogy. Soil Science Society of America, Madison, WI.

Keiluweit, M., J.J. Bougoure, L.H. Zeglin, D.D. Myrold, P.K. Weber, J. Pett-Ridge, M. Kleber, and P.S. Nico. 2012. Nano-scale investigation of the association of microbial nitrogen residues with iron (hydr)oxides in a forest soil O-horizon. Geochim. Cosmochim. Acta 95: 213–226.

Kleber, M., K. Eusterhues, M. Keiluweit, C. Mikutta, R. Mikutta, and P.S. Nico. 2015. Mineral–organic associations: Formation, properties, and relevance in soil environments. p. 1–140. *In* Advances in Agronomy. Elsevier Ltd.

Kleber, M., R. Mikutta, M.S. Torn, and R. Jahn. 2005. Poorly crystalline mineral phases protect organic matter in acid subsoil horizons. Eur. J. Soil Sci. 56(December): 717–725.

Kögel-Knabner, I., G. Guggenberger, M. Kleber, E. Kandeler, K. Kalbitz, S. Scheu, K. Eusterhues, and P. Leinweber. 2008. Organo-mineral associations in temperate soils: Integrating biology, mineralogy, and organic matter chemistry. J. Plant Nutr. Soil Sci. 171(1): 61–82.

Liu, X., K. Eusterhues, J. Thieme, V. Ciobota, C. Höschen, C.W. Mueller, K. Küsel, I. Kögel-Knabner, P. Rösch, J. Popp, and K.U. Totsche. 2013. STXM and NanoSIMS investigations on EPS fractions before and after adsorption to goethite. Environ. Sci. Technol. 47(7): 3158–66.

Lutzow, M. V., I. Kogel-Knabner, K. Ekschmitt, E. Matzner, G. Guggenberger, B. Marschner, and H. Flessa. 2006. Stabilization of organic matter in temperate soils: mechanisms and their relevance under different soil conditions - a review. Eur. J. Soil Sci. 57(4): 426–445.

Mambelli, S., J.A. Bird, G. Gleixner, T.E. Dawson, and M.S. Torn. 2011. Relative contribution of foliar and fine root pine litter to the molecular composition of soil organic matter after in situ degradation. Org. Geochem. 42(9): 1099–1108.

Masoom, H., D. Courtier-Murias, H. Farooq, R. Soong, B.P. Kelleher, C. Zhang, W.E. Maas, M. Fey, R. Kumar, M. Monette, H.J. Stronks, M.J. Simpson, and A.J. Simpson. 2016. Soil organic matter in its native state: unravelling the most complex biomaterial on Earth. Environ. Sci. Technol. 50(4): 1670-1680.

Melo, V., B. Singh, C.E.G.R. Schaefer, R.F. Novais, and M.P.F. Fontes. 2001. Chemical and mineralogical properties of kaolinite-rich Brazilian soils. Soil Sci. Soc. Am. J. 65(4): 1324.

Miltner, A., P. Bombach, B. Schmidt-Brücken, and M. Kästner. 2012. SOM genesis: Microbial biomass as a significant source. Biogeochemistry 111(1-3): 41–55.

Norrish, K., and R.M. Taylor. 1961. The isomorphous replacement of iron by aluminium in soil goethites. J. Soil Sci. 12(2): 294–306.

Plaza, C., D. Courtier-Murias, J.M. Fernández, A. Polo, and A.J. Simpson. 2013. Physical, chemical, and biochemical mechanisms of soil organic matter stabilization under conservation tillage systems: A central role for microbes and microbial by-products in C sequestration. Soil Biol. Biochem. 57: 124–134.

Rasmussen, C., R.J. Southard, and W.R. Horwath. 2006. Mineral control of organic carbon mineralization in a range of temperate conifer forest soils. Glob. Chang. Biol. 12(5): 834–847.

Schaefer, C.E.G.R., J.D. Fabris, and J.C. Ker. 2008. Minerals in the clay fraction of Brazilian Latosols (Oxisols): a review. Clay Miner. 43(1): 137–154.

Schulze, D.G. 1984. The influence of aluminum on iron oxides. VIII. Unit-cell dimensions of Al-substituted goethites and estimation of Al from them. Clays Clay Miner. 32(1): 36–44.

Simpson, A.J., M.J. Simpson, E. Smith, and B.P. Kelleher. 2007. Microbially derived inputs to soil organic matter: Are current estimates too low? Environ. Sci. Technol. 41(23): 8070–8076.

Torn, M., S. Trumbore, and O. Chadwick. 1997. Mineral control of soil organic carbon storage and turnover. Nature 389: 170–173.

Zimmermann, M., J. Leifeld, S. Abiven, M.W.I. Schmidt, and J. Fuhrer. 2007. Sodium hypochlorite separates an older soil organic matter fraction than acid hydrolysis. Geoderma 139(1-2): 171–179.

APENDIX (Chapter two)

Supplementary Table 1. Chemical properties of the selectecd Oxisols

Soil[a]	Horizon	Depth	pH_{H2O}	P[*]	K[*]	Ca^{2+}[†]	Mg^{2+}[†]	Al^{3+}[†]	H+Al[‡]	[#]SB	ECEC[§]	CEC[¶]	BS[ǂ]	$ECEC_{corr.}$[γ]	$CEC_{corr.}$[γ]
	-	cm	-	mg dm^{-3}		$cmol_c$ dm^{-3}							%	$cmol_c$ kg^{-1} clay	
THD	A	0-10	4.4	2.0	38.0	0.2	0.2	1.7	6.6	0.5	2.2	7.1	6.6	3.6	12
THD	A	10-20	4.4	2.0	24.0	0.1	0.1	1.3	5.8	0.3	1.6	6.1	4.2	2.3	9
THD	AB	20-40	4.4	1.0	13.0	0.1	0.1	1.4	5.6	0.2	1.6	5.8	4.0	2.3	8
THD	B	60-100	4.9	0.5	2.0	0.1	0.1	0.7	4.0	0.2	0.9	4.2	4.2	1.2	6
HHD	A	0-10	4.8	1.6	24.0	0.1	0.1	1.1	10.9	0.3	1.4	11.2	2.4	2.3	19
HHD	A	10-20	5.2	1.5	15.0	0.1	0.1	1.0	9.6	0.2	1.2	9.8	2.0	2.0	17
HHD	AB	20-40	5.4	0.6	20.0	0.1	0.1	0.6	7.9	0.2	0.8	8.1	2.1	1.2	13
HHD	B	60-100	5.5	0.0	6.0	0.1	0.0	0.2	4.1	0.1	0.3	4.2	2.3	0.4	6
XHD	A	0-10	5.4	3.4	57.0	2.6	0.8	0.1	2.1	3.5	3.6	5.6	62.4	16.1	25
XHD	A	10-20	4.9	1.1	21.0	1.0	0.3	0.4	4.0	1.4	1.8	5.4	26.1	5.4	16
XHD	AB	20-40	5.0	0.7	9.0	0.9	0.4	0.6	3.6	1.3	1.9	4.9	26.1	5.5	14
XHD	B	60-100	4.9	0.0	1.0	0.6	0.2	0.3	2.5	0.8	1.1	3.3	24.3	3.1	9
XHT	A	0-10	4.9	0.9	31.0	0.3	0.1	0.4	2.3	0.5	0.9	2.8	18.4	1.8	5
XHT	A	10-20	5.0	0.8	35.0	0.3	0.1	0.4	5.6	0.4	0.8	6.0	7.1	1.6	11
XHT	AB	20-40	5.3	0.4	29.0	0.2	0.1	0.4	5.0	0.4	0.8	5.4	6.6	1.3	10
XHT	B	60-100	5.7	0.0	10.0	0.1	0.0	0.0	2.8	0.2	0.2	3.0	5.3	0.3	5
RHT	A	0-10	6.5	14.0	187.0	6.4	4.8	0.0	3.3	11.6	11.6	14.9	77.9	19.4	25
RHT	A	10-20	6.7	7.3	150.0	5.6	4.1	0.0	3.3	10.0	10.0	13.3	75.2	16.4	22
RHT	AB	20-40	6.6	6.7	111.0	3.0	3.2	0.0	3.5	6.5	6.5	10.0	65.1	10.8	17
RHT	B	60-100	6.1	11.0	97.0	0.8	0.8	0.0	4.0	1.9	1.9	5.9	32.2	3.2	10
THT	A	0-10	4.5	6.3	51.0	0.5	0.3	1.3	7.8	0.9	2.2	8.7	10.5	6.1	24
THT	A	10-20	4.5	4.2	23.0	0.1	0.1	1.4	5.3	0.2	1.6	5.5	4.1	5.2	18
THT	AB	20-40	4.4	1.8	11.0	0.1	0.0	0.4	4.5	0.2	0.6	4.7	3.4	1.8	15
THT	B	60-100	4.9	0.0	29.0	0.1	0.0	1.1	2.3	0.2	1.3	2.5	6.3	3.3	7

[a]Oxisols acronyms, the full classification is given in the main text (Table 2).[*]Extracted by Mehlich-1; [†]Extracted by KCl 1 mol L^{-1}; [‡]Extracted by Calcium Acetate 0.5 mol L^{-1} pH 7.0; [#]SB=(Ca^{2+}+Mg^{2+}+K^{+}): Sum of bases; [§]ECEC=SB+Al^{3+}: Effective cation exchange capacity; [¶]CEC=SB+(H+Al): Cation exchange capacity at pH 7.0. [ǂ]BS: base saturation ((SB/CEC)x100); [γ]ECEC and CEC Corrected by kg of clay.

Supplementary Table 2. Soil C and N content as affected by depth of sampling and litter-C and N inputs in the selected Oxisols

Soil	Depth	Litter-C input, mg g^{-1} soil				Litter-N input, mg g^{-1} soil			
	cm	0.0	4.5	9.0	18.0	0.0	0.12	0.24	0.48
		Carbon content, g kg^{-1} soil				Nitrogen content, g kg^{-1} soil			
THD	0-10	17.50c	18.60bc	19.60ab	21.30a	1.54b	1.86a	1.88a	1.75a
THD	10-20	15.80c	16.90ab	18.30a	18.30a	1.35b	1.50b	1.68a	1.50b
THD	20-40	12.70c	13.50bc	14.80ab	16.40a	1.04c	1.13bc	1.31a	1.28ab
THD	60-100	7.30c	8.30bc	9.70b	12.10a	0.57b	0.67ab	0.74ab	0.75a
HHD	0-10	38.20b	39.00b	42.00a	42.30a	2.70b	2.80b	3.02a	3.00a
HHD	10-20	32.80b	34.05ab	35.10a	35.90a	2.24a	2.38a	2.30a	2.33a
HHD	20-40	28.40b	29.60ab	30.40a	33.10a	1.87b	2.17a	1.82b	2.09a
HHD	60-100	14.60c	16.50bc	18.00ab	19.70a	0.83b	1.04a	0.85ab	1.03a
XHD	0-10	13.40c	13.70c	16.40b	18.90a	1.18c	1.30b	1.47a	1.51a
XHD	10-20	8.80b	9.55b	11.80a	13.40a	0.60c	0.87b	1.06a	0.84b
XHD	20-40	7.00bc	8.00b	8.70b	12.10a	0.50b	0.73a	0.70a	0.72a
XHD	60-100	4.00c	5.10bc	6.70b	9.60a	0.27b	0.44a	0.51a	0.47a
XHT	0-10	16.20b	16.30b	18.90a	19.90a	0.91c	1.20b	1.28ab	1.12a
XHT	10-20	18.30b	19.00b	20.80a	20.90a	1.21b	1.28ab	1.38a	1.30ab
XHT	20-40	15.30c	16.40bc	17.10b	19.10a	1.08b	1.14ab	1.18ab	1.23a
XHT	60-100	9.80c	11.60b	12.15b	15.00a	0.60b	0.69ab	0.71ab	0.79a
RHT	0-10	37.70b	38.40b	40.00a	41.00a	3.56b	3.83a	3.86a	3.74a
RHT	10-20	26.90c	28.30bc	29.10b	31.80a	2.42b	2.60b	2.53ab	2.73a
RHT	20-40	17.80c	20.30b	22.50a	23.40a	1.45b	1.72a	1.78a	1.83a
RHT	60-100	9.80d	11.40c	13.20b	15.70a	0.66b	0.77b	0.80ab	0.96a
THT	0-10	15.90c	17.15bc	18.40ab	19.00a	1.21b	1.30a	1.36a	1.38a
THT	10-20	10.50b	10.60b	12.20b	14.35a	0.75c	0.81bc	0.85b	0.98a
THT	20-40	7.70c	8.60bc	9.40b	11.90a	0.55c	0.64bc	0.65b	0.77a
THT	60-100	2.90c	4.20bc	5.30b	8.10a	0.23b	0.28b	0.31b	0.44a

For a given depth within each of the 6 Oxisols, means followed by the same lowercase letter do not differ accoding to the Tukey's test at $P<0.05$.

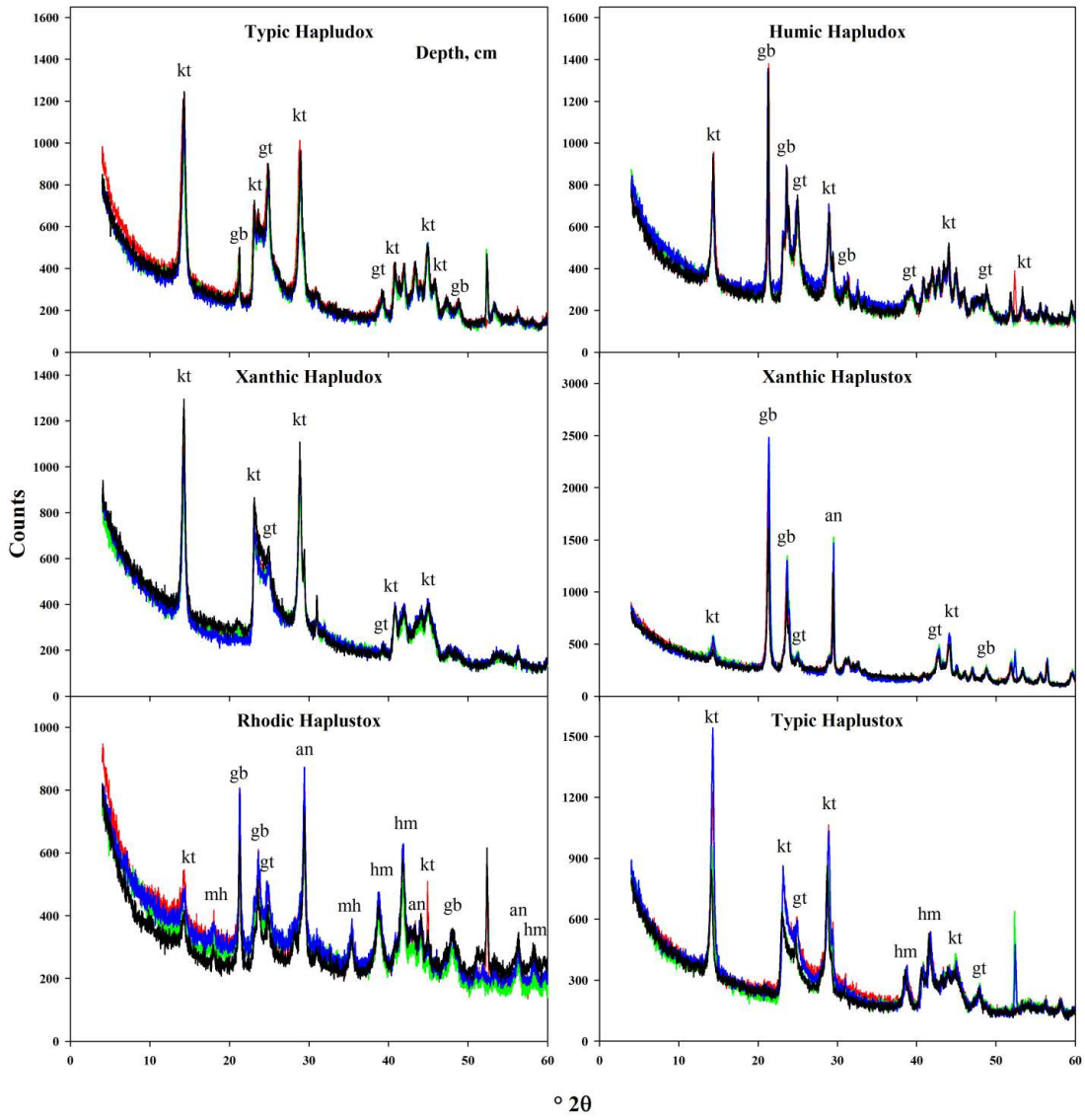

Supplementary Figure 1. Mineralogy of the clay fraction of the selected Oxisols as defined by X-Ray diffraction patterns, using powdered non-oriented samples, Co Kα radiation λ = 1.789 nm; kt = kaolinite, gb = gibbsite, gt = goethite, hm = hematite, an = anatase and mh = maghemite.

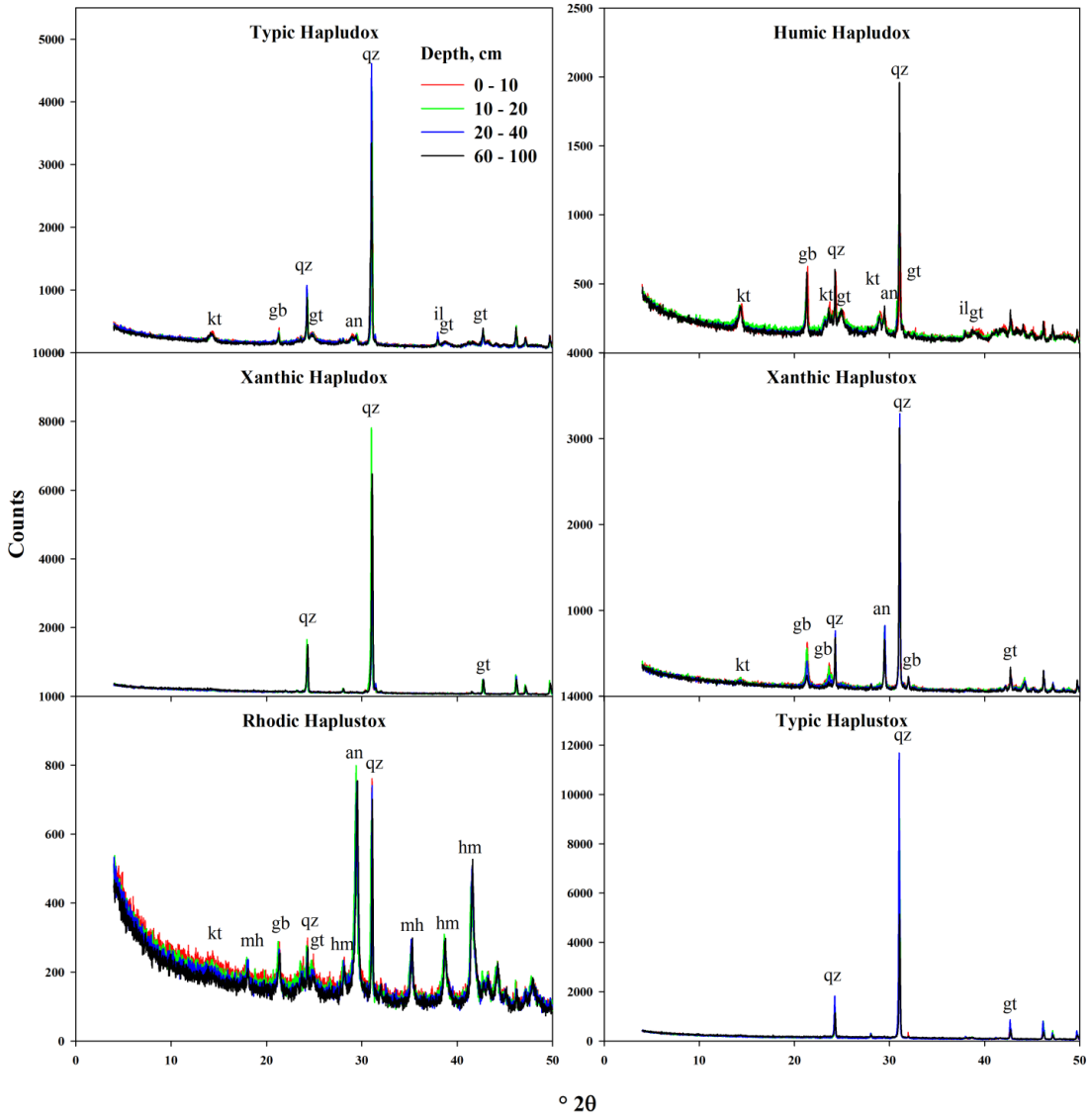

Supplementary Figure 2. Mineralogy of the silt fraction of the selected Oxisols as defined by X-Ray diffraction patterns, using powdered non-oriented samples, Co Kα radiation λ = 1.789 nm; kt: kaolinite, gb: gibbsite, gt: goethite, hm: hematite, an: anatase and mh: maghemite, and qz: quartz. The occurrence of "pseudo-silt" is more evident in the Humic Hapludox and in the Rhodic Haplustox.

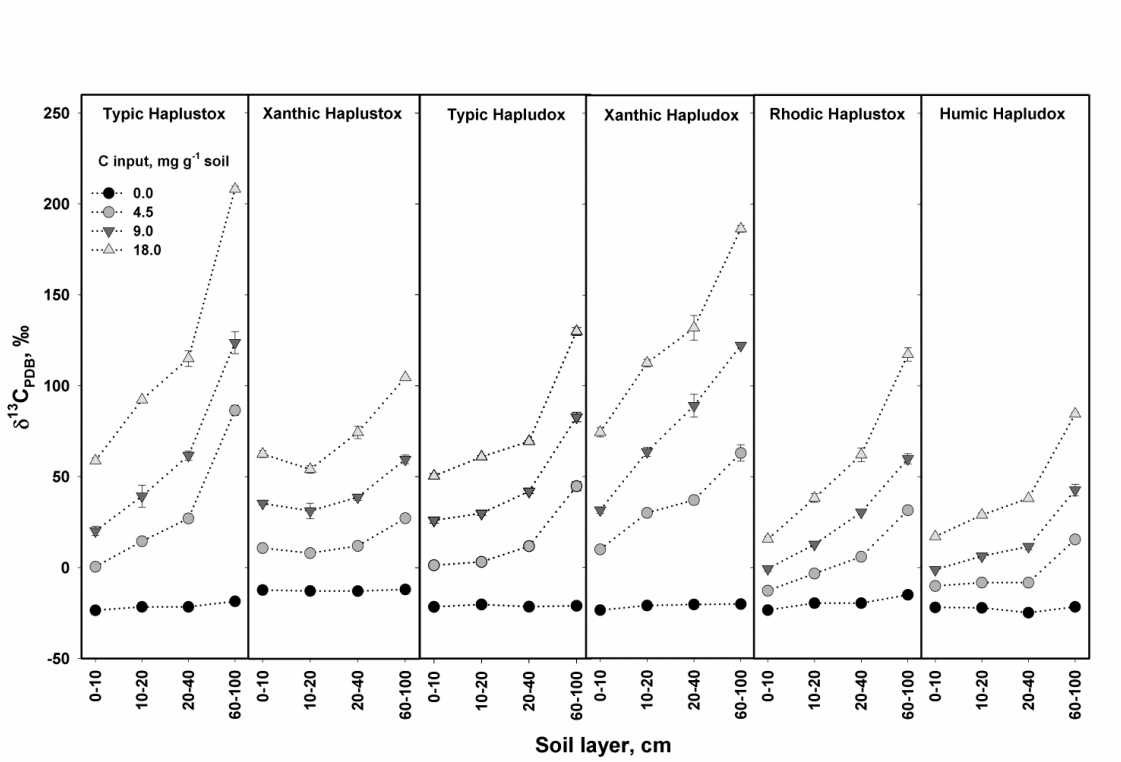

Supplementary Figure 3. ^{13}C abundance (‰) as a function of plant litter-C inputs and soils depth in the selected Oxisols. The vertical bars denote the standard error of the mean, n=3.

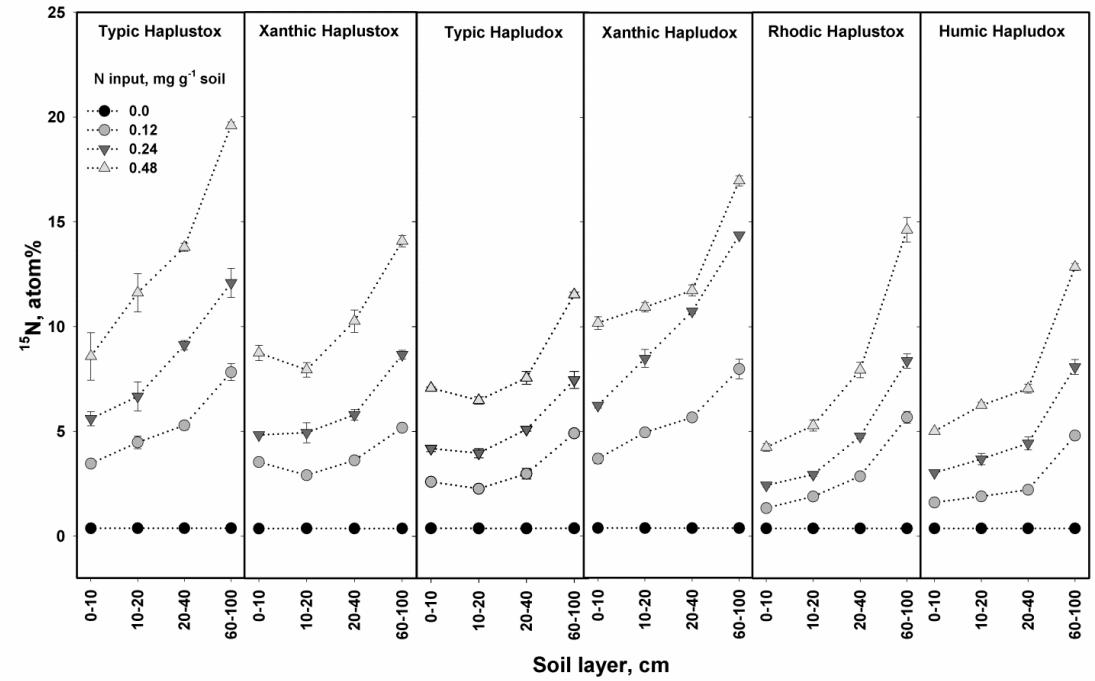

Supplementary Figure 4. ^{15}N abundance (atom%) as a function of plant litter-C inputs and soils depth in the selected Oxisols. The vertical bars denote the standard error of the mean, n=3.

Al-/Fe-(hydr)oxides–organic matter associations in a Brazilian humic Oxisol as revealed by elemental mapping and thermal analysis (chapter three)

1. Abstract

Tropical ecosystems store substantial amounts of C as soil organic matter (SOM), despite the climate conditions usually favoring its decomposition. However, the specific mechanisms driving the persistence of SOM in tropical soils are not well-known. Inferring such mechanisms in natural systems is often difficult because soil C stocks are a result of many interactions among organisms, physical processes and chemical reactions. All these factors combine to drive the formation of mineral-organic associations and the persistence of SOM in terrestrial ecosystems. In this study, we applied scanning electron microscopy (STEM) to probe the chemical heterogeneity of mineral-organic associations within the fraction <53 µm in a humic Oxisol. Additionally, synchrotron-based X-ray diffraction coupled to thermal analysis were used to follow mineral dehydroxylation and SOM oxidation under a He-O_2 (80%-20%) atmosphere. Based on the STEM elemental mapping, we observed preferential associations between SOM and Al-/Fe-(hydr)oxides. Moreover, the oxidation of SOM led to three strong CO_2 peaks at 234, 353 and another above 600 °C. We suggest that SOM forms associations with Al-/Fe-(hydr)oxides through polar functional groups that interact with hydroxyls groups on these minerals. Hence, with increasing temperatures up to 400 °C, the dehydroxylation of the Al-/Fe-(hydr)oxides overlapped with the oxidation of its associated SOM. Otherwise, we propose that nonpolar organic compounds should be oxidized at temperatures above 600 °C and decoupled from mineral dehydroxylation, either Al-/Fe-(hydr)oxides or kaolinite. Our study contributes to improve the current understanding on the elemental composition and the mechanisms leading to the formation of mineral-organic associations in highly weathered Oxisols

2. Introduction

Worldwide, terrestrial ecosystems store about 1500 Pg of C in the form of soil organic matter (SOM) only within the first meter depth (Jobbágy and Jackson, 2000). Such huge amount of C is a result from many interactions among organisms, physical and chemical processes within the mineral matrix of soils (Schmidt et al., 2011). However, the ability of soils to protect SOM against decomposition is closely related to the reactivity of the mineral matrix (Lutzow et al., 2006). As such, the formation of protective associations is restricted to minerals presenting large specific surface area (SSA) and high charge density (Kögel-Knabner et al., 2008; Lutzow et al., 2006). Because the formation of mineral-organic associations ultimately depend on the presence of reactive minerals (Baldock and Skjemstad, 2000), the accumulation of low-activity clays as soil pedogenesis advance (Schaefer et al., 2008), raises questions on the mechanisms accounting for the persistence of SOM in highly weathered soils in tropical regions (Barré et al., 2014).

Highly weathered soils such as Oxisols, predominate on stable and old geomorphic surfaces in ecosystems characterized by intense biological activity, under warm and humid climate (Schaefer, 2001). Under such conditions, with intensive leaching of silica and bases, the vast majority of the primary minerals have been extensively weathered by dissolution and hydrolysis (Wilson, 1999). These processes favor the accumulation of kaolinite, the predominant phyllosilicate in Oxisols (Schaefer et al., 2008). With greater removal of silica, even kaolinite can be weathered to gibbsite (Wilson, 1999), which also can precipitate in the soil solution as a result of the release of Al^{3+} from the weathering minerals (Chadwick and Chorover, 2001). Additionally, throughout the weathering sequence, the dissolution of Fe-bearing primary minerals releases Fe^{2+} that is oxidized to Fe^{3+}, which hydrolysis leads to the formation of Fe-(hydr)oxides (Wilson, 2004). In Oxisols, the most stable and widespread forms of Fe-(hydr)oxides are goethite and hematite (Fontes and Weed, 1991; Schaefer et al., 2008). Although it is well-known that Oxisols account for substantial amounts of C, especially in humic Oxisols (Andrade et al., 2004), the underlying mechanisms

leading to the formation of mineral-organic associations in these soils are relatively poorly understood (Barré et al., 2014).

The specific mechanisms by which mineral-organic associations occur in Oxisols should be a function of the properties of the minerals that predominate within the silt- and clay-sized fractions (Zinn et al., 2007). Despite its high abundance in Oxisols, the reactivity of kaolinite towards SOM is low due to the absence of permanent charges and low SSA (Keil and Mayer, 2014; Kleber et al., 2015). Although kaolinite still has hydroxyl groups (Si-OH and Al-OH) that can generate pH-dependent charges, these sites are mostly restricted to broken edges or other structural defects (Barré et al., 2014). Consequently, kaolinite exhibits predominantly noncharged surfaces that are more likely to form associations with nonpolar organic compounds by hydrophobic interactions, e.g., associations with molecules containing predominantly alkyl and/or aromatic C (Kleber et al., 2015). Otherwise, the noncharged surfaces of kaolinite also could interact with SOM through van der Waals forces and/or by H-bonding (Keil and Mayer, 2014; Lutzow et al., 2006).

In sharp contrast to kaolinite, Al-/Fe-(hydr)oxides can exhibit variable crystallinity degree, often high SSA and therefore, these minerals are much more active on the formation of mineral-organic associations (Heckman et al., 2013; Keiluweit et al., 2012; Mikutta et al., 2011, 2007). The main mechanism by which Al-/Fe-(hydr)oxides interact with organic compounds is predominantly due to ligand exchange between hydroxyl groups at the surface of these minerals and carboxylic, alcoholic and phenolic groups of organic compounds (Kleber et al., 2015; Mikutta et al., 2009, 2007). Other than ligand exchange reactions, Al-/Fe-(hydr)oxides can form associations with SOM by H-bonding or even by van der Waals forces (Cagnasso et al., 2010; Chernyshova et al., 2011). Furthermore, in acidic soils such as the vast majority of Oxisols, the cation bridges should be intermediated by Fe^{3+} and Al^{3+} that are able to form complexes with soluble components of SOM (Mikutta et al., 2007; Oades, 1988). However, given the overall complexity of natural soils, much of the inference on the mechanisms

leading to the formation of mineral-organic are based on artificial systems, including pure minerals and/or simpler proxies of SOM (Chen and Sparks, 2015; Mikutta et al., 2011, 2007; Saidy et al., 2013). For this reason, inferring these mechanisms in natural soils is a critical step for the understanding on the formation and persistence of SOM in terrestrial ecosystems.

Here we address the chemical composition of mineral-organic associations in a humic Oxisol by (i) assessing the spatial distribution of SOM as related to the mineral phase using scanning transmission electron microscopy (STEM); (ii) linking mineral dehydroxylation to SOM thermal oxidation, by analyzing the gases evolved from the sample heated stepwise from 25 up to 700 °C, and simultaneously recording synchrotron-based X-ray diffraction (XRD) patterns to detect changes on the mineral phases under heat flow. Therefore, we tested the hypothesis that Al-/Fe-(hydr)oxides are the main drivers of mineral-organic associations in humic Oxisols. Hence, as the (hydr)oxides undergo dehydroxylation (loss of functional groups), this reaction also should release adsorbed SOM, followed by its thermal oxidation to CO_2. The objectives of this research were to assess the spatial heterogeneity of SOM and infer the mechanisms underlying the formation of mineral-organic associations in humic Oxisols.3.

3. Material and methods

3.1. Soil sampling, physical and chemical characterization

The samples were collected in a Humic Hapludox located in Araponga county, Minas Gerais state at southeastern Brazil, within the Atlantic Rainforest biome. The selected soil was under native vegetation in a highland area (ca. 1200 m above the sea level), where the climate is classified as Cwb according to the Köeppen classification (Kottek et al., 2006). The parent material for the soils in this area is predominantly migmatite (Benites et al., 2005). At this site, we dug a pit to collect soil

samples at the 0-20 cm depth, upper section of the ±1 m deep A horizon. After collection, the soil samples were placed in plastic bags and immediately transported to the laboratory for further processing. The soil material was air-dried and sieved through a 2-mm mesh sieve to obtain the fine earth fraction. Part of the fine earth fraction was used for physical and chemical characterization, including texture, nutrient content and mineralogical analysis.

The physical separation of the sand, silt and clay-sized fractions began with chemical dispersion of 10 g of the fine earth fraction into 40 mL of sodium hydroxide 0.05 mol L^{-1}. After 16 hours under continuous stirring, the sample was centrifuged at 2000 rpm and washed with deionized water. Afterwards, the sample was treated with 25 mL of NaOCl 6% (v/v) and heated up to 75-80 °C for 15 minutes in a water bath to oxidize organic matter as recommended by Mikutta et al. (2005). After organic matter removal, the sand was separated through wet-sieving using a 53-µm mesh sieve. The remaining silt and clay-sized fractions were separated through sedimentation by applying the Stoke's Law. These fractions were dried at 72 °C during a week, weighted and used for subsequent mineralogical characterization. Physical properties of the soil are given in Table 1.

Table 1. Site location and some physical and chemical properties of the selected Oxisol.

Site location and altitude	Araponga, Minas Gerais, Brazil. Coordinates: 20°39' S; 42°29' W, and altitude 1265 m asl
Sand content and mineralogy	246.4 g kg^{-1} soil, mineralogy: quartz
Silt content and mineralogy	205.8 g kg^{-1} soil, mineralogy: kaolinite, gibbsite, goethite, anatase, quartz, ilmenite
Clay content and mineralogy	547.4 g kg^{-1} soil, mineralogy: kaolinite, gibbsite, goethite, anatase
Fe_{AO}	12 g kg^{-1} clay
Fe_{DC}	74 g kg^{-1} clay; Fe_{AO}/Fe_{DC}=0.16 g g^{-1}
Al_{AO}	25 g kg^{-1} clay
Al_{DC}	28 g kg^{-1} clay; Al_{AO}/Al_{DC}=0.89 g g^{-1}
Gibbsite[¶]	201 g kg^{-1} clay
Kaolinite[¶]	449 g kg^{-1} clay
Gibbsite dehydroxylation[†]	250-300 °C
Goethite dehydroxylation[†#]	300-400 °C
Kaolinite dehydroxylation[†]	400-600 °C
Organic carbon content	111 g kg^{-1} of silt+clay (fraction <53 µm)
Organic nitrogen content	7 g kg^{-1} of silt+clay (fraction <53 µm)
C:N ratio	15:1
pH(H_2O)	4.5
Ca^{2+}, $cmol_c$ dm^{-3} soil	0.1
Mg^{2+}, $cmol_c$ dm^{-3} soil	0.05
Al^{3+}, $cmol_c$ dm^{-3} soil	1.0
P, mg dm^{-3}	3.1
K, mg dm^{-3}	14.0

[¶]Estimated based on thermogravimetry; [†]Karathanasis and Harris (1994). According to these authors, gibbsite and short-range order Al-(hydr)oxides should undergo dehydroxylation at the same temperature range; [#]According to Schwertmann (1984), low-crystalline goethites might suffer dehydroxylation at temperatures below 300 °C.

Soil chemical characterization consisted on determining pH in water (10 cm^3 soil into 25 mL of deionized water) using a pH meter (Prolab-PHB 500). Exchangeable Ca and Mg were extracted using KCl 1 mol L^{-1} (10 cm^3 soil into 100 mL solution), and their concentrations were determined by atomic absorption spectrometry in a Varian Spectra AA (model 220F). The same KCl extract also was used to quantify exchangeable Al, which concentration was determined by the titration method, using NaOH 0.025 mol L^{-1}. P and K availability was assessed by using the double acid extractant Mehlich-1 ($HCl + H_2SO_4$), by mixing 10 cm^3 of soil with 50 mL of the extractant.

3.2. XRD analysis

XRD analyses (non-oriented samples) were conducted using Co-Ka radiation (λ = 0.178896 nm) at 30 mA and 40 kV from a Rigaku D-MAX vertical goniometer equipped with a graphite monochromator. XRD patterns were obtained between 4 and 60° 2θ in 0.02° steps at a scan rate of 10° 2θ/min for accurate measurements of *d*-spacing and line broadening determinations.

3.3. Selective dissolution of Fe-(hydr)oxides

Clay samples were submitted to selective dissolution of both short-range order (poorly crystalline) and well crystalline Fe-(hydr)oxides by respectively treating the samples with ammonium oxalate (AO) and dithionite-citrate-bicarbonate (DCB) (Mehra, 1958). In both extractions, the amount of Fe and Al released was determined. After the dissolution step, the amounts of Fe and Al extracted by AO and DCB were quantified using an atomic absorption spectrometer (Varian Spectra AA,

220FS). The total content of Al and Fe extracted by both AO and DCB is given in Table 1.

3.4. Soil organic matter fractionation

We weighted 10 grams of the fine earth fraction in centrifuge tubes and suspended the material into 30 mL of sodium hexametaphosphate 5 g L^{-1}, according to (Cambardella and Elliott, 1992). After dispersion, the samples were wet-sieved through a 53 µm mesh screen to separate particulate organic matter and sand (fraction >53 µm) from the clay and silt with its associated organic matter as well (fraction <53 µm). The C and N content within the fraction <53 µm was determined by dry combustion using an Element Analyzer CHNS/O, Perkin Elmer, 2400. The fraction <53 µm was used in subsequent steps to evaluate the composition of mineral-organic associations by applying elemental imaging and thermal analyses.

3.5. Elemental imaging: Scanning Transmission Electron Microscopy (STEM) and Energy Dispersive X-ray Spectroscopy (EDS)

For the elemental imaging, we prepared a suspension by weighting 1 mg of the fraction <53 µm into a microcentrifuge tube (2 mL total capacity) and adding 1 mL of ultrapure water. Aliquots of 1 µL were taken from the suspension and deposited onto a clean Au-coated Si-wafer (Sigma Aldrich, St. Louis, MI- USA) and air dried.

The first stage of the elemental imaging was performed in a scanning electron microscope (SEM) FEI Quanta 200 at environmental

mode (30 Torr). In order to avoid sample charging, an accelerating voltage of 10 kV was applied. This procedure was used to locate C-rich areas (C-hotspots) within the probed mineral-organic associations. See Fig. S1 on support information for further details for sample preparation steps. After locating the C-hotspots, these areas were further protected with an additional (ca. 50-nm) Au-sputtering using a metal sputter (EMS150). The additional sputtering was required to reduce charging and to preserve the physical and chemical composition of the regions of interest (ROI's). This procedure was necessary because we used a Focused Ion Beam (FIB) to obtain a thin section (ca. 100 nm thick) across the ROI using a FEI Nova Nanolab 600. This sectioned area was used in the transmission electron microscopy analyses. The same procedure has been described elsewhere (Archanjo et al., 2015; Jorio et al., 2012). For further details on sample preparation steps, the reader is redirected to the Fig. S2 and S3 on support information.

Scanning transmission electron microscopy (STEM) and energy dispersive X-ray spectroscopy (EDS) microscopy were performed on a Cs-corrected FEI Titan 80/300 transmission electron microscope, equipped with an EDAX analyzer. The elemental mappings were obtained by integrating characteristic X-ray signals during a drift-corrected STEM spectrum imaging experiment, and STEM images were acquired using a high-angle annular dark-field (HAADF) detector. These analyses allowed the characterization of the morphology of the mineral-organic associations and SOM spatial distribution at the nanoscale level (i.e. mapping C, O, Fe, Al, and Si spatial distribution). Imaging analyses and processing were performed using the TIA software.

3.6. Thermal analyses

We used the finely powdered mineral-organic fraction (<53 µm) to evaluate mineral dehydroxylation, organic matter oxidation and XRD patterns. These measurements were conducted at the XPD beamline of the Brazilian Synchrotron Light Laboratory, in Campinas, SP. The experiment consisted on heating the sample (100 mg of the <53 µm fraction) from room temperature (25 °C) up to 700 °C. The reactions occurred under a controlled oxidizing atmosphere (80% He/20% O_2) with total gas flux fixed at 150 mL min^{-1}. The data collection for the gases evolved from the sample as it was heated was continuous, even during the period in which the temperature was kept fixed for XRD patter measurements. The gases evolved from the sample under heating were detected by mass spectrometry using a Pfeiffer Vacuum ThermoStar GSD T series 1-300 atomic mass units (Wetzlar, Hesse, Germany). We collected data for H_2O-derived ions (m/z 17 and 18) and SOM-derived ions (m/z 12, 28, 44), although the complete oxidation of organic phase also should also release H_2O-derived ions. We selected these ions because they should allow us making inference about the temperature range at which SOM undergo oxidation and relate it to minerals dehydroxylation.

We performed XRD measurements at 17, 105, 300, 400, 600 and 700 °C and an additional spectrum was collected after the sample had been cooled down (from 700 to 25 °C). The time required for collecting each of the XRD spectrum varied between 18 and 20 minutes. For this reason, during the XRD measurements, the temperature was held constant. The XRD patterns were collected at 7000 eV (λ=0.17714 nm) for the interval

between 10 and 60 °2θ and steps of 0.005° using a Dectris Mythen 1K detector (Baden, Switzerland).

4. Results

4.1. Elemental imaging of the mineral-organic associations

The morphology and elemental composition of the mineral-organic associations were very heterogeneous. As depicted in Fig. 1, the spatial distribution of C was more related to O, Fe, and Al than with Si in the selected ROI probed by the STEM imaging. SOM in this selected ROI is apparently located around an Al-/Fe-(hydr)oxides individual particle or coating a microaggregate approximately <200 µm-size. As such, the concentration of C seems higher on the outside region than in the central area, where the concentration of Fe and Al is higher (Fig. 1). Furthermore, there is no overlapping between areas with high Al and Si concentration, indicating the absence of kaolinite in this selected ROI. In a second ROI probed, we observed some overlapping of Al, Si and Fe, indicating the presence of kaolinite and Fe-(hydr)oxides, probably occurring as a coating on the phyllosilicate (see Fig. S4 on support information).

In both probed ROI's (Fig. 1 and Fig. S4), there was no overlapping between the distribution of Pt, Ga or with C. This is important because Pt and Ga were introduced during the sputtering used to protect the ROI's prior to the elemental mapping (see support information Fig. S2 and S3). Since the distribution of these elements was not overlapping with C, Si, Al and Fe (Fig. S4), we are confident that the probed ROI's were preserved by the sputtering and the images in Fig. 1 and Fig. S4, in

fact represent the heterogeneity of mineral-organic associations in the sample.

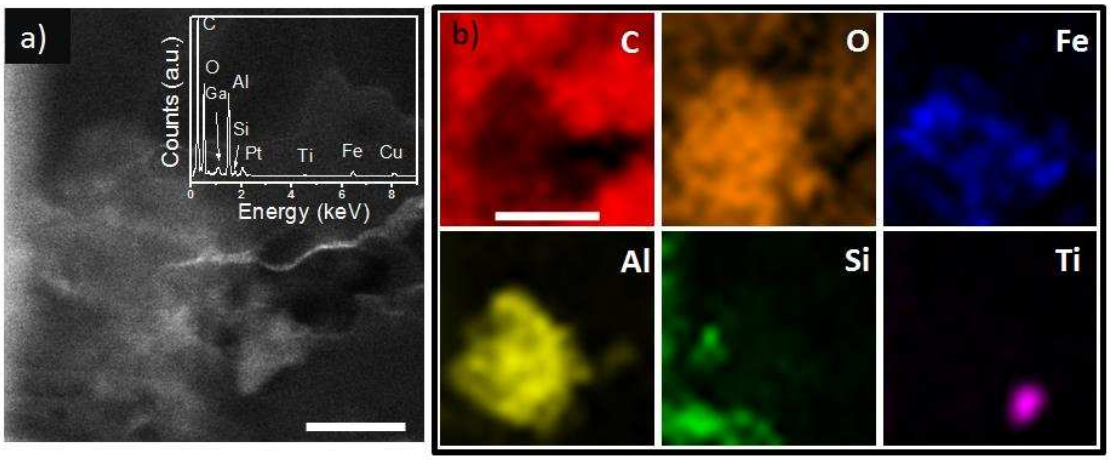

Figure 1. Chemical heterogeneity of mineral-organic associations (silt+clay and its associated SOM) in the selected Oxisols, a) STEM-HAADF image and the inset shows the EDS spectrum of the analyzed area (scale bar 100 nm), b) EDS elemental maps for C, O, Fe, Al, Si and Ti (scale bar 200 nm). The presence of Ga, Pt (from sample preparation protection layer) and Cu (from TEM grid) in the spectrum is due to secondary effects and had no influence in the elemental maps.

In both probed ROI's (Fig. 1 and Fig. S4), there was no overlapping between the distribution of Pt, Ga or with C. This is important because Pt and Ga were introduced during the sputtering used to protect the ROI's prior to the elemental mapping (see support information Fig. S2 and S3). Since the distribution of these elements was not overlapping with C, Si, Al and Fe (Fig. S4), we are confident that the probed ROI's were preserved by the sputtering and the images in Fig. 1 and Fig. S4, in fact represent the heterogeneity of mineral-organic associations in the sample.

4.2. Mineral dehydroxylation and SOM oxidation

Throughout the thermal experiment, we observed good correlation

between the temperature range at which dehydration and mineral dehydroxylation led to the release of H_2O-derived ions from the sample (m/z 17 and 18) (Fig. 2). Thus, the readings for these ions presented a first peak at 70-80 °C, which was probably due to dehydration of the sample (i.e. loss of hygroscopic H_2O). With increasing temperatures, the readings for the ion m/z 18 led to strong peaks at 239, 383 and 584 °C that were well within the temperature range at which gibbsite, goethite and kaolinite would undergo dehydroxylation, respectively. At temperatures above 600 °C also occurred peaks for the ions m/z 17 and 18, which could not be attributed to any of the minerals present in the sample. Therefore, it is likely that these peaks might have been due to H_2O released by complete oxidation of SOM at temperatures above 600 °C (Fig. 2).

The oxidation of SOM under our experimental conditions led to the release of ions such as C, CO and CO_2 (m/z 12, 28 and 44, respectively). We could not detect the ion with m/z 30 (NO) and for this reason, we assigned the ion with m/z 44 as CO_2 only. However, based on the m/z only is not possible to totally exclude the occurrence of N_2O (m/z 44) in the evolved gas detected. Overall, the oxidation pattern of SOM at temperatures between 200 and 400 °C led to two intense peaks of CO_2 at 234 and 353 °C. Therefore, the first peak occurred well within the temperature range in which gibbsite and/or short-range order Al-(hydroxides) minerals suffered dehydroxylation (200-300 °C) (Karathanasis and Harris, 1994). Similarly, the second peak of CO_2 overlapped with the temperature range (300 and 400 °C), where goethite suffers dehydroxylation (Karathanasis and Harris, 1994). Interestingly,

while the first CO_2 peak at 234 °C presented very good overlapping with H_2O release, the increase in readings for the ion m/z 18 was considerably smaller for the second peak of CO_2 at 353 °C (Fig. 2). Both peaks of CO_2 (at 234 and 353 °C) presented very similar shape, although the second one reached a slightly lower maximum intensity. The shape of the CO_2 peaks at temperatures below 400 °C suggests that SOM oxidation proceeded at high rates, and both peaks presented relatively small width. As such, these peaks reached their maximum intensities approximately 15 minutes after the CO_2 readings started to increase for the first, and 10 minutes for the second peak (Fig. 2).

The H_2O peak observed at 383 °C was significantly different with respect to the shape and intensity of the first H_2O peak at 239 °C, which presented higher maximum intensity. Thus, as goethite underwent dehydroxylation, a lower amount of H_2O was released from the sample as compared to gibbsite. Indeed, the total mass loss of goethite due to dehydroxylation should be approximately 10-11% of its total mass, while for gibbsite it would be at least three times higher (Karathanasis and Harris, 1994). After reaching its highest intensity at 383 °C, the H_2O ion intensity remained quite stable as the temperature was kept constant at 400 °C. This was in sharp contrast with the first H_2O peak observed at 239 °C, for which the ion intensity was significantly reduced even with constant increment in temperature from 239 up to 300 °C (Fig. 2).

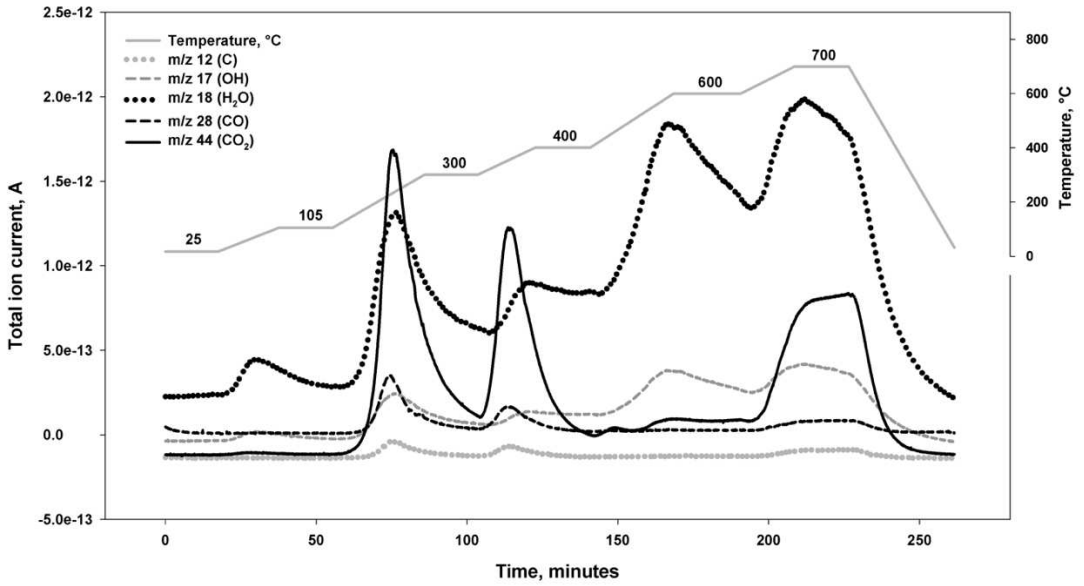

Figure 2. Evolved gases from mineral-organic associations (silt+clay and its associated SOM) as function of temperature and duration of the thermal treatment. The gases released from the sample detected by means of mass spectrometry. Minerals dehydroxylation released water, which main ions presented m/z 17 and 18 (OH, and H_2O, respectively), and SOM-derived ions presented m/z 12, 28 and 44 (attributed to C, CO and CO_2, respectively). The temperature increment was interrupted at 105, 300, 400, 600, and 700 °C in order to collect the X-ray diffraction pattern of the mineral within the sample. The heating flow rates applied were: 4.4, 6.5, 5.3, 7.4, 5.5 °C min^{-1} as the temperature varied from 17-105, 105-300, 300-400, 400-600 and 600-700 °C, respectively.

At temperatures between 400 and 600 °C, there was a significant dip on the intensity of the CO_2 ions (m/z 12, 28 and 44, Fig. 2). Thus, at this temperature range, there was little (if any) oxidation of SOM components in the sample. On the other hand, the intensity of the ions with m/z 17 and 18 increased steadily and reached a third peak at 584 °C. This H_2O peak is consistent with the temperature range at which kaolinite should undergo dehydroxylation (400-600 °C). Although kaolinite would lose only 14% of its mass due to dehydroxylation, this

mineral was the most abundant component in the sample, accounting for at least 45% of the the clay fraction. In addition, since SOM was not oxidized between 400-600 °C (the CO_2 readings remained quite low), the most likely source of the H_2O ions was indeed kaolinite. As the temperature was kept constant at 600 °C, the intensity of the ions with m/z 17 and 18 decreased steadily. At both temperature ranges, 400-600 °C and 600-700 °C, the maximum intensities of the H_2O ions for both intervals were very similar.

When the sample was heated from 600 up to 700 °C, the CO_2 ion intensity increased significantly as compared to the interval between 400 to 600 °C. Importantly, the shape of the CO_2 peaks at 234 and 353 °C were very different from the peak observed between 600 and 700 °C. As compared to the first two, the third peak of CO_2 presented a lower absolute intensity and was significantly wider. In addition, the intensity of this peak remained stable despite the temperature being fixed at 700 °C (Fig. 2). Based on the shape of the CO_2 peaks it seems that the reactions leading to SOM oxidation at this later stage of the thermal treatment occurred at slower rates as compared to those below 400 °C.

4.3. Synchrotron-based XRD patterns

Simultaneously to the thermal decomposition experiment, we also monitored the changes in the mineralogy of the sample using synchrotron-based XRD patterns (Fig. 3). The H_2O released from the sample with a strong peak at 239 °C was probably derived from gibbsite dehydroxylation. According to the XRD data, at 25 and 105 °C the main reflections of gibbsite, the planes *002* and *110* (d=0.484 and 0.437 nm,

respectively) were detected. Indeed, these major peaks of gibbsite were no longer present in the spectra as the temperature reached 300 °C (Fig. 3).

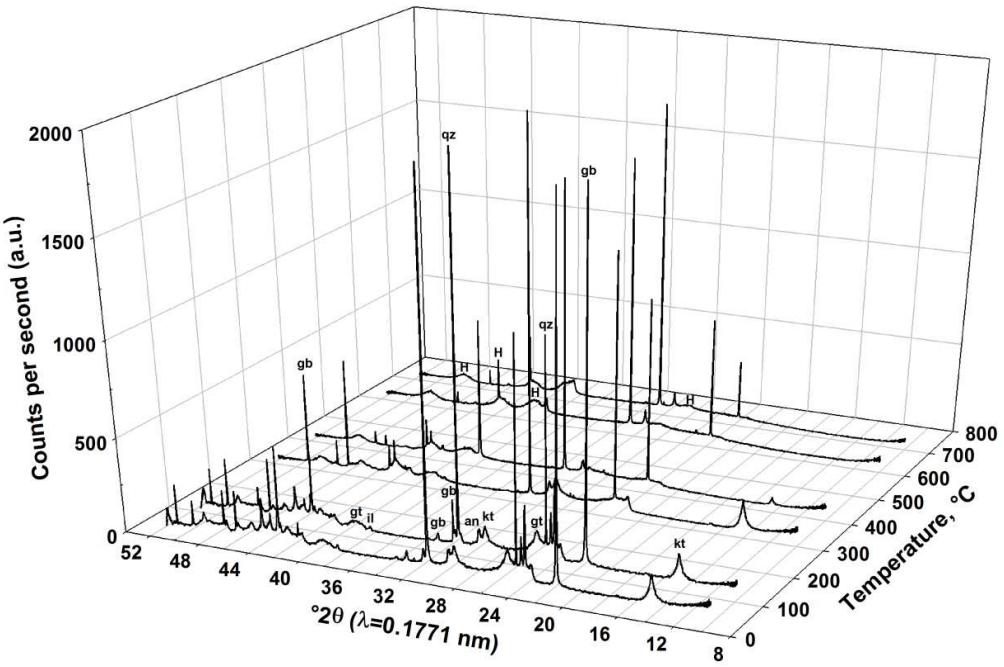

Figure 3. Synchrotron-based XRD patterns for the mineral-organic associations at 25, 105, 300, 400, 600 and 700 °C (non-oriented sample). The spectra were collected at 7000 eV and the minerals identified within the mineral-organic associations at 105 °C were: kaolinite (kt), gibbsite (gb), quartz (qz), goethite (gt), anatase (an), and ilmenite (il). Hematite (H) peaks are indicated at 600 and 700 °C.

For goethite, the most intense peaks were due its *101* and *111* planes (d=0.416 and 0.245 nm, respectively), which were present at 25 and 105 °C, but no longer appeared at 300 °C. Additionally, the peak derived from its *301* plane (d=0.267 nm), had a low resolution even at 25 or 105 °C, and for this reason the presence of goethite at 300-400 °C cannot be ruled out. Based on the low resolution of this peak, the presence of hematite also cannot be ruled out within the original sample.

However, as goethite underwent dehydroxylation, it was probably converted into hematite or proto-hematite (Gualtieri and Venturelli, 1999). Despite the low resolution, hematite is present at 700 °C as inferred from the peak of its plane *012* (d=371 nm). In addition, the planes *104* and *113*, (d=0.272 and 0.220 nm, respectively), also were detected at 600 °C (Fig. 3).

The XRD patterns also demonstrates that kaolinite is the only phyllosilicate present in our sample, with characteristic peaks from its *001* and *002* planes (d=0.721 and 0.359 nm, respectively). These peaks were present within the sample until the temperature reached 400 °C. As kaolinite underwent dehydroxylation between 400 and 600 °C, the aforementioned peaks no longer appeared in the spectrum collected at 600 °C (Fig. 3).

5. Discussion

5.1. Spatial heterogeneity of mineral-organic associations

Based on the elemental STEM mapping, the spatial distribution of SOM was closely related to Al-/Fe-(hydr)oxides, as inferred from Si and C distribution, Fig. 1. Such elemental distribution, suggests the presence of an organic layer coating the mineral particle, consistent with micromorphological observations of humic Oxisols from Brazil (Schaefer, 2001). Additionally, the spatial correlation between Al and Fe suggests these elements are combined to form a single mineral (such as an Al-substituted goethite) or that Al-/Fe-(hydr)oxides are predominantly combined into microagregates (Schaefer et al., 2008). Because our sample was dispersed prior to the imaging, the remaining

microaggregate was <200 µm (Fig. 1), but could have been part of a large structures as commonly observed in Oxisols (Muggler et al., 1999). In addition, the spatial correlation between SOM and Al-/Fe-hydroxides is also in line with previous research on the mechanisms by which these minerals should interact with SOM, i.e ligand exchange, coprecipitation and H-bonds (Keil and Mayer, 2014; Kleber et al., 2015; Lutzow et al., 2006).

Despite SOM being clearly part of an association with Al-/Fe-(hydr)oxides, the organic film enveloping the mineral particle is apparently thick (Fig. 1, Fig. S4). The first mechanism that would account for such pattern would be the occurrence of SOM as coatings or occluded in the pore-space area of microaggregates (Chenu and Plante, 2006; Remusat et al., 2012; Wan et al., 2007). Both mechanisms, either the coatings or the occlusion of SOM could be important for the persistence of C in Oxisols, given their strong microaggregation (Muggler et al., 1999; Schaefer et al., 2004). Another mechanism leading to the formation of thick films of SOM would be due to the capacity of organic molecules to self-assemble to form micelle-like structures and/or forming a zonal structure, with successive layers of organic compounds (Kleber et al., 2007). According to the self-assembly concept, the mineral matrix would directly retain organic molecules by forming ligand exchange complexes at the mineral-organic matter interface (Kleber et al., 2007). Subsequently, the adsorbed organic layer itself would be able interact with further organic materials through H-bonds and/or hydrophobic interactions (Lutzow et al., 2006). As extensively reviewed by these authors, some hydrophobic domains might favor the

persistence of SOM by preventing its hydration and the access of degrading enzymes. Therefore, the combination of direct attachment to the mineral matrix and hydrophobic interactions among organic moieties would allow the occurrence of such thick films of organic materials as shown in Fig. 1 and in supporting information Fig S4.

5.2. Reactions within the mineral-organic associations under heat flow

The most important aspect of our data is that we observed very good overlapping between the temperature range at which Al-/Fe-(hydr)oxides suffered dehydroxylation and intense oxidation of SOM (Fig. 2). Such overlapping between these reactions probably occurs because of interactions among these components as previously demonstrated in Fig. 1. Such inference is consistent with the fact that hydroxyl groups on Al-/Fe-(hydr)oxides surfaces are key components for the adsorption of organic compounds in soils (Kleber et al., 2015). Thus, the dehydroxylation of Al-/Fe-(hydr)oxides would release hydroxyl groups at which polar organic compounds had been attached to. This is based on the fact that the polarity and the ability of organic compounds to interact with reactive mineral surfaces increases with their molecular oxygen content (Keil and Mayer, 2014). For example, oxygen-rich groups such as –COOH would preferentially interact with mineral surfaces by ligand exchange and/or H-bonds (Heckman et al., 2013). Therefore, the thermal analysis indicates that associations between SOM and Al-/Fe-(hydr)oxides seem to account for a significant fraction of mineral-organic associations in humic Oxisols.

Based on the thermal reactions within the sample at 234 ºC, there was a proportional release of water and CO_2, as the Al-species underwent dehydroxylation (Fig. 2). Therefore, as the gibbsite and/or short range order Al species suffered dehydroxylation, the sample probably released a proportional amount of CO_2 and H_2O. Conversely, during goethite dehydroxylation there was a higher amount of CO_2 (with a strong peak at 353 ºC) as compared to H_2O. Thus, despite being present at lower concentrations than gibbsite, goethite was probably able to interact with a significant amount of SOM. Otherwise, it is possible that the dehydroxylation of goethite also occurred at temperatures below 300 °C. This is because low crystalline goethites should suffer dehydroxylation at temperatures below 300 °C (260-290), while high crystalline types would have been dehydroxylated at temperatures above 300 °C (Schwertmann, 1985, 1984). Irrespective of some overlapping in terms of the temperature range at which gibbsite and goethite underwent dehydroxylation, our data demonstrates clearly that the thermal treatment leading to alterations on the mineral surfaces were almost simultaneous to strong oxidation of SOM at temperatures between 200 and 400 °C (Fig. 2).

As SOM interacts with minerals, it should presumably become more resistant against thermal decomposition (Schulten and Leinweber, 1999). Experiments testing this hypothesis, however, have indicated a much more complicated figure due to the influence of specific properties of SOM components on its thermal oxidation (Feng et al., 2015, 2014; Heckman et al., 2011; Johnson et al., 2015). As such, while the “thermally labile” fraction would be oxidized at temperatures below 500

°C, mineral-associated molecules would be included into a “thermally refractory” pool of SOM, which would only suffer oxidation at temperatures above 600 °C (Johnson et al., 2015). Indeed, Heckman et al. (2011) reported higher amount of heat needed to oxidize organic matter bound to goethite as compared to the isolated organic fraction submitted to the same thermal treatment. Conversely, Feng et al. (2015) observed that isolated organic matter undergoing thermal treatment was oxidized at higher temperatures than when it was was adsorbed to goethite. Similar result were obtained in a previous study in which the increasing C loading, that is, the mass of organic matter per unit of mineral surface area, was not followed by higher sensitivity to thermal treatments (Feng et al., 2014). According to Feng et al. (2015), intrinsic properties of SOM components and/or their capacity to self-assemble, seem to be an important regulator of its thermal resistance, irrespective of its association with minerals. Therefore, despite the inherent difficulties for comparing the results of thermal oxidation of SOM performed under different conditions (Plante et al., 2009), the application of such treatments can be important to evaluate the behavior and the composition of mineral-organic associations (Feng et al., 2015; Fernández et al., 2012; Lopez-Capel et al., 2006). However, extrapolating such data to infer the resistance of SOM against decomposition in natural soils should be of less interest.

5.3. Inferring the formation of mineral-organic associations in humic Oxisols

Based on our results, we infer that the presence of hydroxyl groups on mineral surfaces play an important role on the formation of mineral-

organic associations in humic Oxisols. However, the physicochemical properties of the mineral phase at which these groups are attached to, seem more important than the presence of hydroxyl groups itself (Kleber et al., 2015). As such, despite the predominance of kaolinite, which also has structural hydroxyls groups, the reactivity of these components towards SOM is probably much smaller than those on Al-/Fe-(hydr)oxides surfaces. According to our elemental mapping and the thermal analysis, we suggest that oxygen-rich (polar functional groups) form preferential associations with hydroxyl groups on Al-/Fe-(hydr)oxides surfaces through mechanisms such as ligand exchange and/or H-bonding. Additionally, short-range order Al-/ Fe-(hydr)oxides could coprecipitate SOM, particularly in acidic soils (Kleber et al., 2015). Given their intimate associations, we infer that a significant fraction of SOM is oxidized at the same temperature range at which the (hydr)oxides underwent dehydroxylation in our thermal experiment (Fig. 2).

In contrast, we propose that predominantly nonpolar organic molecules should have been oxidized at higher temperatures and/or decoupled from mineral dehydroxylation. Therefore, we suggest that most of the CO_2 released above 600 °C in our study may have been derived predominantly from organic compounds with lower content of oxygen (i.e. nonpolar organic materials). Possible components of SOM to be included in this category would be lipids, lignin and aromatic proteins (Masoom et al., 2016). Since organic compounds with low polarity would be preferentially self-assembled through hydrophobic interactions (Keil and Mayer, 2014; Kleber et al., 2007; Lutzow et al., 2006), these

components would be less sensitive to mineral dehydroxylation. In addition, hydrophobic interactions seem to contribute to increase the resistance of SOM against thermal oxidation (Feng et al., 2015, 2014). Possibly, long-chain molecules (e.g., lipids) would lose their functional groups containing oxygen atoms at lower temperatures (below 400 °C). Otherwise, the remaining long C chains, polycondensed materials and/or aromatic rings structures (Kiersch et al., 2012a, 2012b) would require higher temperatures to be fragmented and thus, react with oxygen to form CO_2.

Despite our study being restricted to a single soil, the mineralogy of Oxisols is relatively uniform even in large areas such as the Brazilian territory (Schaefer et al., 2008). Therefore, the mechanisms described here could be common to many tropical soils, rather than a specific feature of humic Oxisols. Although humic Oxisols not presenting widespread occurrence in tropical regions, these soils retains large amounts of SOM (Andrade et al., 2004). However, further studies are warranted to include Oxisols with contrasting mineralogy and SOM content, across different biomes from tropical regions. A comprehensive evaluation of mineral-organic associations, including their formation and persistence, is very important given the predominance of Oxisols in tropical regions and the contributions of these areas for the global SOC stock.

6. Conclusions

Based on our results, we conclude that:

1. In humic Oxisols, SOM is preferentially associated with Al-/Fe-(hydr)oxides, despite the overall predominance of kaolinite in the fraction <53 µm.

2. We infer that polar organic compounds are preferentially associated to hydroxyls groups on Al-/Fe-(hydr)oxides surfaces, and therefore, their dehydroxylation overlap with SOM oxidation.

3. The fraction of SOM oxidized at higher temperatures was decoupled from mineral dehydroxylation, either from (hydr)oxides or kaolinite.

4. The advanced degree of microaggregate formation in deeply developed Oxisols, and increasing content of gibbsite and Fe-(hydr)oxides probably help to protect SOM both chemically and physically against mineralization.

7. References

Archanjo, B.S., D.L. Baptista, L.A. Sena, L.G. Cançado, N.P.S. Falcão, A. Jorio, and C.A. Achete. 2015. Nanoscale mapping of carbon oxidation in pyrogenic black carbon from ancient Amazonian anthrosols. Environ. Sci. Process. Impacts 17(4): 775–779.

Baldock, J.A., and J.O. Skjemstad. 2000. Role of the soil matrix and minerals in protecting natural organic materials against biological attack. Org. Geochem. 31(7-8): 697–710.

Barré, P., O. Fernandez-Ugalde, I. Virto, B. Velde, and C. Chenu. 2014. Impact of phyllosilicate mineralogy on organic carbon stabilization in soils: incomplete knowledge and exciting prospects. Geoderma 235-236: 382–395.

Benites, V.M., E.S. Mendonça, C.E.G.R. Schaefer, E.H. Novotny, E.L. Reis, and J.C. Ker. 2005. Properties of black soil humic acids from high altitude rocky complexes in Brazil. Geoderma 127(1-2): 104–113.

Cagnasso, M., V. Boero, M.A. Franchini, and J. Chorover. 2010. ATR-FTIR studies of phospholipid vesicle interactions with α-FeOOH and α-Fe2O3 surfaces. Colloids Surfaces B Biointerfaces 76(2):

456–467.

Cambardella, C.A., and E.T. Elliott. 1992. Particulate soil organic-matter changes across a grassland cultivation sequence. Soil Sci. Soc. Am. J. 56(3): 777.

Chadwick, O.A., and J. Chorover. 2001. The chemistry of pedogenic thresholds. Geoderma 100(3-4): 321–353.

Chenu, C., and A.F. Plante. 2006. Clay-sized organo-mineral complexes in a cultivation chronosequence: revisiting the concept of the "primary organo-mineral complex." Eur. J. Soil Sci. 57(4): 596–607.

Chernyshova, I. V., S. Ponnurangam, and P. Somasundaran. 2011. Adsorption of fatty acids on iron (hydr)oxides from aqueous solutions. Langmuir 27(16): 10007–10018.

Feng, W., J. Klaminder, and J.-F. Boily. 2015. Thermal stability of goethite-bound natural organic matter is impacted by carbon loading. J. Phys. Chem. A 119(51): 12790–12796.

Feng, W., A.F. Plante, A.K. Aufdenkampe, and J. Six. 2014. Soil organic matter stability in organo-mineral complexes as a function of increasing C loading. Soil Biol. Biochem. 69: 398–405.

Fontes, M.P.F., and S.B. Weed. 1991. Iron oxides in selected Brazilian Oxisols: I. Mineralogy. Soil Sci. Soc. Am. J. 55(4): 1143.

Giardina, C.P., C.M. Litton, S.E. Crow, and G.P. Asner. 2014. Warming-related increases in soil CO2 efflux are explained by increased below-ground carbon flux. Nat. Clim. Chang. 4(9): 822–827.

Gualtieri, A.F., and P. Venturelli. 1999. In situ study of the goethite-hematite phase transformation by real time synchotron powder diffraction. Am. Mineral. 84(c): 895–904.

Heckman, K., A.. Grandy, X. Gao, M. Keiluweit, K. Wickings, K. Carpenter, J. Chorover, and C. Rasmussen. 2013. Sorptive fractionation of organic matter and formation of organo-hydroxy-aluminum complexes during litter biodegradation in the presence of gibbsite. Geochim. Cosmochim. Acta 121: 667–683.

Heckman, K., A. Vazquez-Ortega, X. Gao, J. Chorover, and C. Rasmussen. 2011. Changes in water extractable organic matter during incubation of forest floor material in the presence of quartz, goethite and gibbsite surfaces. Geochim. Cosmochim. Acta 75(15): 4295–4309.

Janzen, H.H. 2015. Beyond carbon sequestration: soil as conduit of solar energy. Eur. J. Soil Sci. 66(1): 19–32.

Jobbágy, E., and R. Jackson. 2000. The vertical distribution of soil organic carbon and its relation to climate and vegetation. Ecol. Appl. 10(2): 423–436.

Johnson, K., G. Purvis, E. Lopez-Capel, C. Peacock, N. Gray, T. Wagner, C. März, L. Bowen, J. Ojeda, N. Finlay, S. Robertson, F. Worrall, and C. Greenwell. 2015. Towards a mechanistic understanding of carbon stabilization in manganese oxides. Nat. Commun. 6(May): 7628.

Jorio, A., J. Ribeiro-Soares, L.G. Cançado, N.P.S. Falcão, H.F. Dos Santos, D.L. Baptista, E.H. Martins Ferreira, B.S. Archanjo, and C.A. Achete. 2012. Microscopy and spectroscopy analysis of carbon nanostructures in highly fertile Amazonian anthrosoils. Soil Tillage Res. 122: 61–66.

Kaiser, K., and G. Guggenberger. 2003. Mineral surfaces and soil organic matter. Eur. J. Soil Sci. 54(2): 219–236.

Karathanasis, A.D., and W.G. Harris. 1994. Quantitative thermal analysis of soil materials. p. pp–360–411. *In* Amonette, J.E., Zelazny, L.W. (eds.), Quantitative methods in soil mineralogy. Soil Science Society of America, Madison, WI.

Keil, R.G., and L.M. Mayer. 2014. Mineral matrices and organic matter. p. 337–359. *In* Treatise on Geochemistry. 2nd ed. Elsevier.

Keiluweit, M., J.J. Bougoure, L.H. Zeglin, D.D. Myrold, P.K. Weber, J. Pett-Ridge, M. Kleber, and P.S. Nico. 2012. Nano-scale investigation of the association of microbial nitrogen residues with iron (hydr)oxides in a forest soil O-horizon. Geochim. Cosmochim. Acta 95: 213–226.

Kiersch, K., J. Kruse, K.-U. Eckhardt, A. Fendt, T. Streibel, R. Zimmermann, G. Broll, and P. Leinweber. 2012a. Impact of grassland burning on soil organic matter as revealed by a synchrotron- and pyrolysis–mass spectrometry-based multi-methodological approach. Org. Geochem. 44: 8–20.

Kiersch, K., J. Kruse, T.Z. Regier, and P. Leinweber. 2012b. Temperature resolved alteration of soil organic matter composition during laboratory heating as revealed by C and N XANES spectroscopy and Py-FIMS. Thermochim. Acta 537: 36–43.

Kinyangi, J., D. Solomon, B. Liang, M. Lerotic, S. Wirick, and J. Lehmann. 2006. Nanoscale biogeocomplexity of the organomineral assemblage in soil: Application of STXM microscopy and C 1s-NEXAFS spectroscopy. Soil Sci. Soc. Am. J. 70(5): 1708 – 1718.

Kleber, M., K. Eusterhues, M. Keiluweit, C. Mikutta, R. Mikutta, and P.S. Nico. 2015. Mineral–organic associations: Formation, properties, and relevance in soil environments. p. 1–140. *In* Advances in Agronomy. Elsevier Ltd.

Kleber, M., P. Sollins, and R. Sutton. 2007. A conceptual model of organo-mineral interactions in soils: self-assembly of organic molecular fragments into zonal structures on mineral surfaces. Biogeochemistry 85(1): 9–24.

Kottek, M., J. Grieser, C. Beck, B. Rudolf, and F. Rubel. 2006. World map of the Köppen-Geiger climate classification updated. Meteorol. Zeitschrift 15(3): 259–263.

Lehmann, J., D. Solomon, J. Kinyangi, L. Dathe, S. Wirick, and C. Jacobsen. 2008. Spatial complexity of soil organic matter forms at nanometre scales. Nat. Geosci. 1(4): 238–242.

Lutzow, M. V., I. Kogel-Knabner, K. Ekschmitt, E. Matzner, G. Guggenberger, B. Marschner, and H. Flessa. 2006. Stabilization of organic matter in temperate soils: mechanisms and their relevance under different soil conditions - a review. Eur. J. Soil Sci. 57(4): 426–445.

Masoom, H., D. Courtier-Murias, H. Farooq, R. Soong, B.P. Kelleher, C.

Zhang, W.E. Maas, M. Fey, R. Kumar, M. Monette, H.J. Stronks, M.J. Simpson, and A.J. Simpson. 2016. Soil organic matter in its native state: unravelling the most complex biomaterial on Earth. Environ. Sci. Technol.: acs.est.5b03410.

Mehra, O.P. 1958. Iron oxide removal from soils and clays by a dithionite-citrate system buffered with sodium bicarbonate. Clays Clay Miner. 7(1): 317–327.

Mikutta, R., M. Kleber, K. Kaiser, and R. Jahn. 2005. Review: Organic matter removal from soils using hydrogen peroxide, sodium hypochlorite, and disodium peroxodisulfate. Soil Sci. Soc. Am. J. 69(1): 120.

Mikutta, R., C. Mikutta, K. Kalbitz, T. Scheel, K. Kaiser, and R. Jahn. 2007. Biodegradation of forest floor organic matter bound to minerals via different binding mechanisms. Geochim. Cosmochim. Acta 71(10): 2569–2590.

Mikutta, R., U. Zang, J. Chorover, L. Haumaier, and K. Kalbitz. 2011. Stabilization of extracellular polymeric substances (Bacillus subtilis) by adsorption to and coprecipitation with Al forms. Geochim. Cosmochim. Acta 75(11): 3135–3154.

Oades, J.M. 1988. The retention of organic matter in soils. Biogeochemistry 5(1): 35–70.

Plante, A.F., J.M. Fernández, and J. Leifeld. 2009. Application of thermal analysis techniques in soil science. Geoderma 153(1-2): 1–10.

Schaefer, C.E.G.R. 2001. Brazilian latosols and their B horizon microstructure as long-term biotic constructs. Aust. J. Soil Res. 39(5): 909–926.

Schaefer, C.E.G.R., J.D. Fabris, and J.C. Ker. 2008. Minerals in the clay fraction of Brazilian Latosols (Oxisols): a review. Clay Miner. 43(1): 137–154.

Schmidt, M.W.I., M.S. Torn, S. Abiven, T. Dittmar, G. Guggenberger, I.A. Janssens, M. Kleber, I. Kögel-Knabner, J. Lehmann, D.A.C.

Manning, P. Nannipieri, D.P. Rasse, S. Weiner, and S.E. Trumbore. 2011. Persistence of soil organic matter as an ecosystem property. Nature 478(7367): 49–56.

Schulten, H.R., and P. Leinweber. 1999. Thermal stability and composition of mineral-bound organic matter in density fractions of soil. Eur. J. Soil Sci. 50(2): 237–248.

Schwertmann, U. 1984. The double dehydroxylation peak of goethite. Thermochim. Acta 78(1-3): 39–46.

Schwertmann, U. 1985. Properties of goethites of varying crystallinity. Clays Clay Miner. 33(5): 369–378.

Vogel, C., C.W. Mueller, C. Höschen, F. Buegger, K. Heister, S. Schulz, M. Schloter, and I. Kögel-Knabner. 2014. Submicron structures provide preferential spots for carbon and nitrogen sequestration in soils. Nat. Commun. 5: 2947.

Wilson, M.J. 1999. The origin and formation of clay minerals in soils: past, present and future perspectives. Clay Miner. 34(1): 7–25. 4.

APENDIX (Chapter three)

Support Information

Al-/Fe-(hydr)oxides–organic matter associations in a Brazilian Oxisol as revealed by elemental mapping and thermal analysis

1 - C-hotspot localization

The soil suspension, as previously described in the main text was dispersed onto the substrate, an Au-coated Si-wafer(Sigma-Aldrich). The hotspot localization was done following the EDS mapping of C, Al and O-rich phases, as shown in Fig. S1 a-c. The co-localized SEM and optical images (in bright and dark field) are shown in Fig S1d-f, respectively.

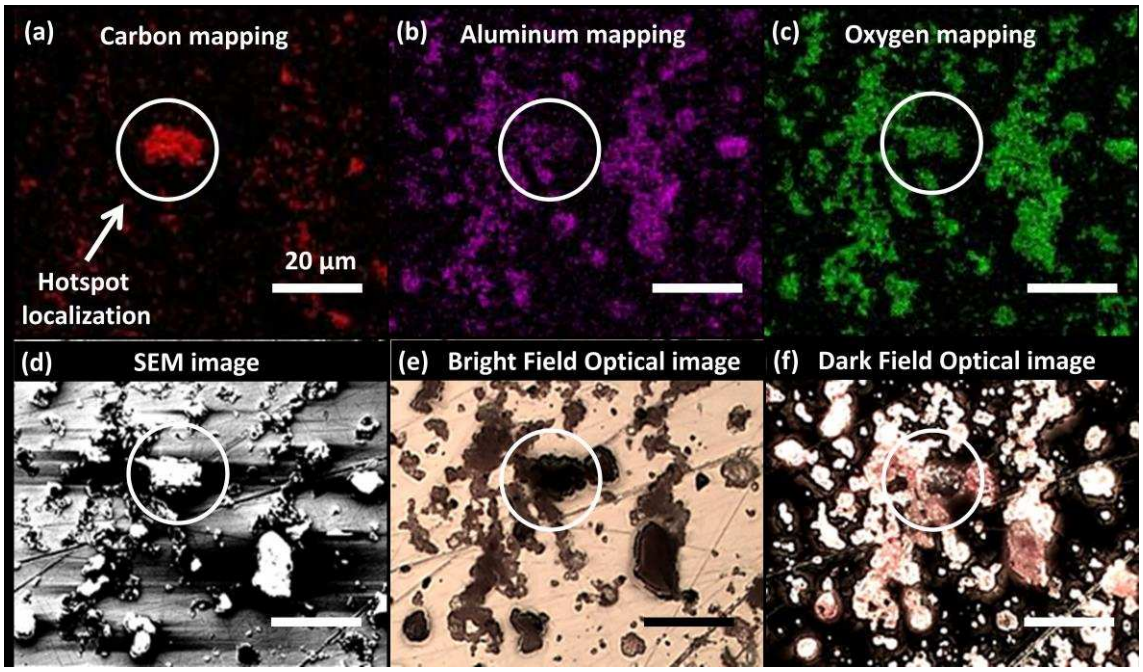

Figure S1: Hotspot localization based on EDs mapping (a-c). Correlative images of hotspot using SEM (d) and optical microscopy (e and f).

2 - Sample preparation for transmission electron microscopy (TEM)

The samples evaluated in this work were prepared following the lift-out method using a dual-beam microscope FEI Nova NanoLab 600. Firstly, a hotspot was localized (Fig. S2a and b) and an in-situ platinum deposition was performed in order to protect the sample from ion damage in the following steps. The initial protection layer (~ 100 nm) deposition was performed using the electron beam at 2 keV and 0.84 nA. Afterwards, the gallium ion beam was used at 30 keV and 0.3 nA to deposit a Pt layer having 2 µm thickness (Fig. S2c).

In order to mill the trenches, on both sides of the lamella (Fig. S2d and e), the gallium ion beam was used at 30 keV and 7 nA. The lamella was in-situ lifted-out and transferred to a TEM copper grid and attached via platinum deposition induced by ion beam (Fig. S2f and g). The ion beam was used at 30 keV and the ion current was reduced from 1 nA down to 0.1 nA as the lamella thickness was reduced from 2 µm down to 100 nm, respectively.

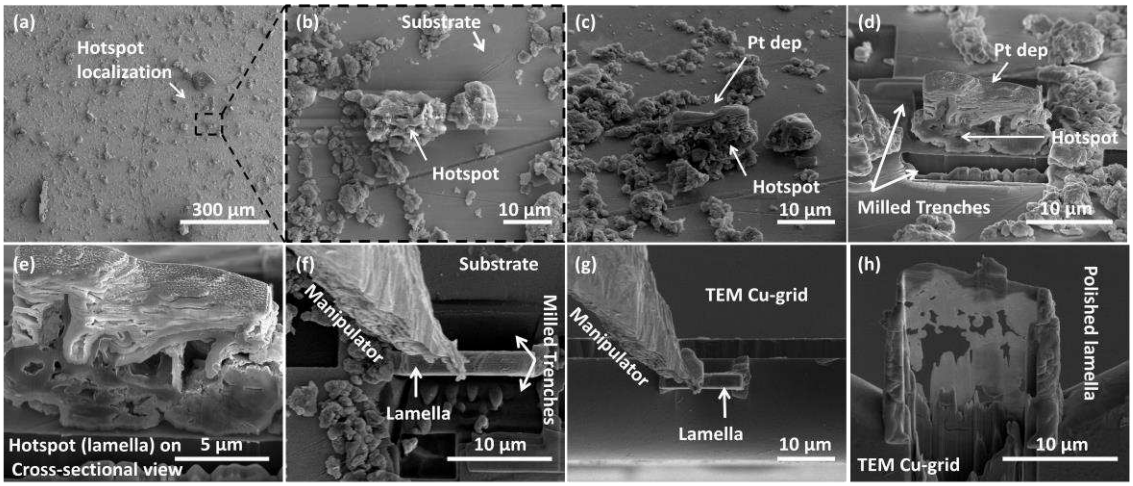

Figure S2. Images showing the sequence of the TEM hotspot sample preparation.

To conclude the hotspot sample preparation, the lamella was cleaned and polished using a low ion energy beam at 5 keV and 29 pA, with the advantage of minimizing ion beam damage.

In an intermediate TEM lamella preparation step, we have analyzed the sample cross section taking a EDS mapping, as can be observed in Fig. S3a and S3b. The EDS spectrum (Fig. 3c) shows the chemical elements presents in the investigated area.

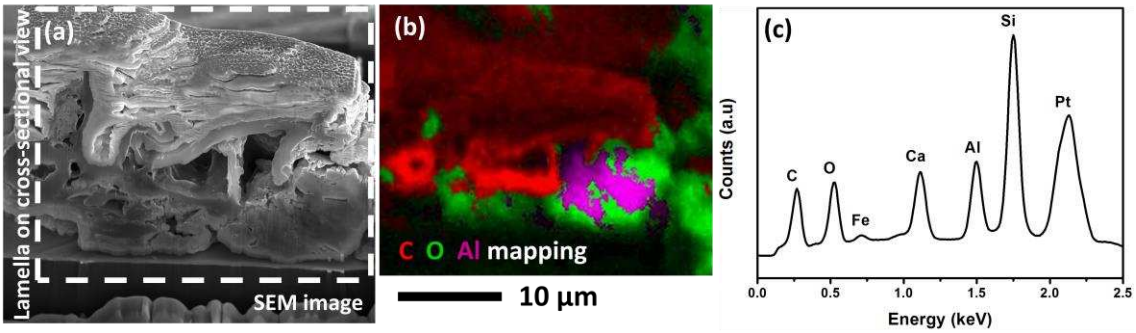

Figure S3. a) SEM image of lamella cross-section using SE detector, b) EDX mapping and c) EDX spectrum.

3- STEM-EDS analyses of a second region of interest (ROI) illustrating mineral-organic associations in the humic Oxisol

Complementary to Fig. 1 in the main text. In the second ROI analyzed, the mineral organic-associations depicted in the Fig. S4, the organic matter also seems localized around an Al-/Fe-(hydr)oxide particle. Based on the distribution of C, Al, Fe and Si, the organic matter occurs as a coating on the Al-/Fe-(hydr)oxides, which are likely adsorbed onto a kaolinite particle.

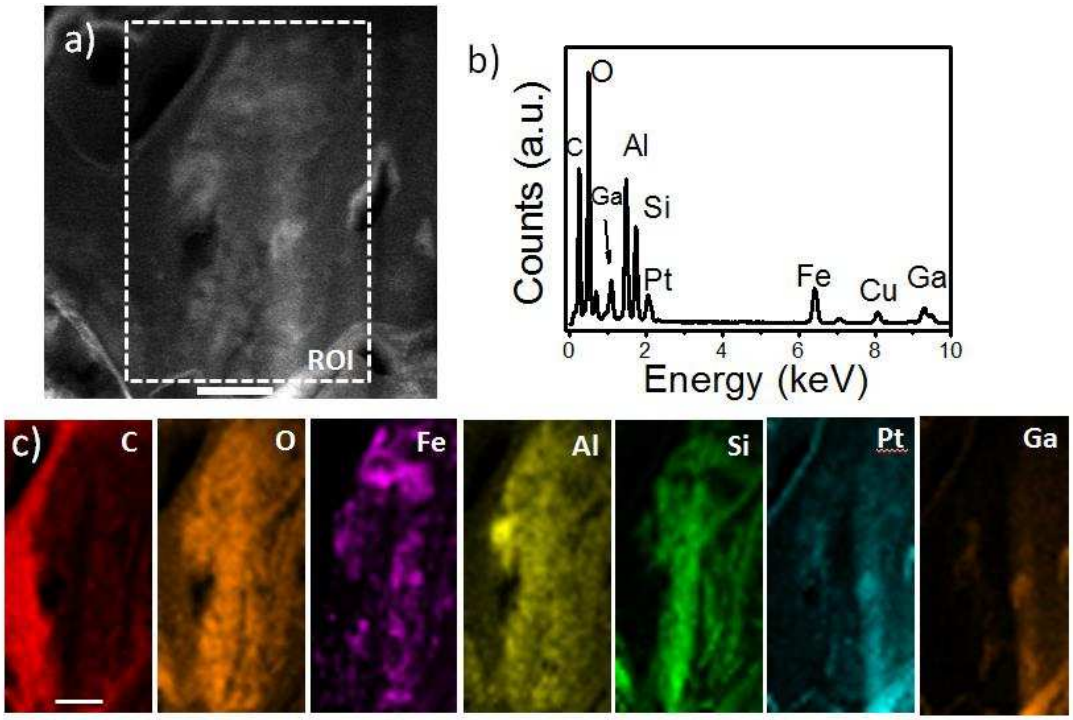

Figure S4. Chemical heterogeneity of mineral-organic association (silt+ clay and its associated SOM) within the region of interest (ROI) inside the dashed white square in (a) STEM-HAADF image. (b) EDS spectrum of ROI. Elemental mapping (c) shows the presented of C, O, Fe, Si, Ti and Al. Pt and Ga presence are due to the FIB sample preparation and Cu due to TEM grid. The scale bar shown in (a) and (b) represent 200 nm.

We infer the zonal distribution of organic matter with respect to the minerals because the distribution of C is relatively far away from the C-rich area. In contrast to Si, Fe and Al are relatively closer to the C rich region. The relative good overlap between Al and Si concentration within the selected ROI corroborates the hypothesis that a kaolinite particle is present in this selected ROI, which was not observed in the Fig. 1 in the main text.

General conclusions

1. Soil texture (i.e. the amount of the fraction <53 µm) limits the capacity for SOC sequestration.

2. The amount of the <53 µm is directly associated with C-saturation behavior.
3. With increasing content of the fraction <53 µm there is an increment in the physical protection of SOC.
4. Al-/Fe-(hydr)oxides are the main components within the mineral matrix involved on the formation and the persistence of mineral-organic associations in Oxisols.
5. The dehydroxylation of Al-/Fe-(hydr)oxides due to thermal treatments, is followed by a release and oxidation of SOC in Oxisols.